Non-equilibrium behavior in self-driven systems

by

Santanu Das

February 2020

A thesis submitted to the
Jawaharlal Nehru University
for the degree of
Doctor of Philosophy

Dedicated to My Parents

Declaration:

I, hereby, declare that the work reported in this thesis is entirely original. This thesis is composed independently by me at Raman Research Institute under the supervision of Dr. Sanjib Sabhapandit. I further declare that the subject matter presented in this thesis has not previously formed the basis for the award of any degree, diploma, membership, associateship, fellowship or any other similar title of any university or institution. I also declare that I have run it through the **Turnitin** plagiarism software.

Prof. Sanjib Sabhapandit

Santanu Das

Theoretical Physics Group
Raman Research Institute
Bangalore 560 080
India

Certificate:

This is to certify that the thesis entitled **Non-equilibrium behavior in self-driven systems** submitted by **Mr. Santanu Das** for the award of the degree of Doctor of Philosophy of Jawaharlal Nehru University is his original work. This has not been published or submitted to any other University for any other Degree or Diploma.

Prof. Ravi Subrahmanyan
(Director)
Raman Research Institute,
Bangalore 560 080, India.

Prof. Sanjib Sabhapandit
(Thesis Supervisor)
Raman Research Institute,
Bangalore 560 080, India.

Acknowledgements

Firstly, I would like to express my sincere gratitude to my supervisor Prof. Sanjib Sabhapandit for giving me opportunity to work with him and patiently guiding me during the tenure of my PhD.

I would like to thank my collaborators Prof. Deepak Dhar and Dr. Anupam Kundu, for their advice and support. I am also thankful to the rest of my thesis committee members Prof. Joseph Samuel and Prof. Abhishek Dhar for their useful comments and suggestions. I am also greatful to all faculty members in the Theoretical physics group, especially to Dr. Urna Basu for her help, encouragement, and useful discussion on several occasions.

I express my deepest gratitude towards Prof. Narendra Kumar to whom I got an opportunity to work during visiting student program at RRI. His passion for science has always been a constant source of motivation for me.

I would like to acknowledge all the teachers for providing me excellent courses. In particular, I wish to mention the coursework I attended in Bangalore School on Statistical Physics at RRI & ICTS. I also acknowledge the organizing committee of the Spring College on the Physics of Complex systems (2019, ICTP) for selecting me as a participant and also for their hospitability.

I wish to acknowledge the RRI administrative staff for their help in official works. In particular, I would like to mention Manju, Gayathri, Mahadev, Radha, and Vidya. I also thankful to all the library staff for their help whenever I needed. Thanks to Jacob Rajan and Krishnamurthy for resolving my computer, laptop, RRI internet, and RRIHPC related issues. Special acknowledgement should be goes for RRIHPC for accomplishing numerical simulation in my reserach work.

My heartfelt thanks to my beloved seniors Sujit, Arnab, Prasad, Anjan, Chaitra, Suman, Mriganko for many beautiful moments at RRI. I would remain thankful to Meera, Rajib da, Debasish da & co. for learning me cooking at RMV hostel.

I also praise my batch-mates Amit, Alkesh, Sanjay, Aswath, Simanraj, Sreeja, Deepshikha, Asutosh, and Rajarshi for their wonderful companion. My heartiest thanks to Anindya, Sagar, Deepak, Niranjan, Shivam, Sushil, Mari, Surya, Rahul, Shafi, Rangaraj and others for wonderful and joyous moments I spent with them. Thanks to my current colleague Nomaan, Abhishek, Atul, and Ion for providing me a cheerful and friendly environment at TP. I don't forget to thank people to whom I interacted while playing football and vollyball at RRI.

Special thanks to Rituparno for his constant help in different academic and non-academic aspects. My heartfelt thanks to my friends Raj, Debadrita, Sumit, Tanujit, Saintan, Debsankar, Tathagata, Raja Da, Jyotiprasad for everything they have done for me. Undoubtedly, I can say, I am fortunate to have friends like them.

Lastly, and most importantly, my sincere gratitude to my family members, especially to my parents. Without their moral and emotional support this journey would have remained incomplete. I also thank my uncle's and maternal uncle's families for their support, love, and encouragement.

Publications

- Statistics of overtake events by a tagged agent
  Santanu Das, Deepak Dhar, and Sanjib Sabhapandit
  Phys. Rev. E **98**, 052122(2018)

- Finite system-size effects on overtaking
  Santanu Das, and Sanjib Sabhapandit
  Manuscript under preparation

Synopsis

The primary objective of statistical physics is to explain the behaviors of a macroscopic system by starting its description from the microscopic level. Undoubtedly, the most successful branch of this subject is its equilibrium counterpart, which is quite old and well-established with its foundations and formalisms. It is well known that the equilibrium of a macroscopic system is ensured by the principle of the detailed balance. It states that the net current between any two points in the configuration space is zero if the system is in equilibrium. If the net current is non-zero in the same case, then the system is in non-equilibrium for which there is no widely-accepted framework like equilibrium exist in the literature. Besides that, the variety of non-equilibrium systems and the richness of emergent phenomena therein makes the subject interest growing in time.

Among varieties of non-equilibrium systems, in recent years, there has been a growing interest in a particular kind of system, namely the self-driven interacting many particles. The main feature of these types of systems is that its driving force is not external in origin, but are produced by each particle (agent). The self-driven character of individual agent and the complex interactions among them emerge different new phenomena, which are usually not observed in equilibrium systems. Example of such systems includes swarming bacteria, school of fish, flocking of birds, animal herds, pedestrian movements, including traffic and traffic-related flows.

Among a plethora of phenomena in self-driven interacting particle systems, we mainly focus on the problem of overtaking. Studying this phenomenon in detail is the goal of this thesis. Notably, this phenomenon usually appears in traffic or traffic-related flows where a fast-moving agent from behind can go in front of an agent moving slowly in the same direction. Although, the phenomena is quite widespread, surprisingly, statistics related to it has not been studied much in the literature. It motivates us to investigate this problem by making logic-based interactions among

the agents, including the non-interacting case of the Jepsen gas. In addition to the infinite number of agents in a system, we also studied the same problem by considering a finite number of agents in a periodic system to understand the finite-size effects on overtaking statistics. Keeping all these points in mind, the organization of this thesis has been made as follows:

Chapter 1: Introduction

In this chapter, starting with a brief description of foundations of equilibrium system, we shortly give an introduction of non-equilibrium systems with a particular emphasis on interacting particle systems and on self-driven many particles. As an example of a simple non-equilibrium system as well as a prototype of a single self-driven particle, we discuss a problem of a biased random walker on a periodic lattice. Next, as a paradigmatic model of interacting many particles, we briefly discuss the totally asymmetric simple exclusion process (TASEP). Note that the TASEP can be thought of as an example of self-driven (interacting) many particles without any overtaking. Finally, in the end, we briefly survey the literature of TASEP and TASEP related models in a particular direction where one may see *overtakings* among the particles to justify the relevance of our thesis in the context of interacting many particles.

Chapter 2: Statistics of overtakes by a tagged agent in Jepsen gas

In this chapter, we begin with a simple non-interacting model of self-driven agents, namely the Jepsen gas, to get an introductory essence of overtaking by a tagged agent. The model we consider is non-interacting in the sense that all the point-like constituents or agents in this system can pass each other without any obstacles. The self-driven character of each agent is assigned by random but constant initial velocity. For simplicity, we have chosen all these velocities independently from a common distribution. We consider two different initializations depending on how the agents are distributed in space. They are respectively the uniform distribution of agents and a constant gap between all neighboring agents. Starting with these set-up, each agent moves with its constant velocity in time. In this system, as a quantity of

interest, we investigate the net overtaking number $m(t)$ by a tagged agent at time t. By definition, it is the total number of agents that the tagged agent overtakes minus the total number of agents that overtake the tagged agent in a given duration of time. Two different probability distributions associated with the net overtaking number by a tagged agent have been studied. They are namely the conditional and the unconditional distributions. In case of conditional distribution, we exactly know the tagged velocity where we calculate and identify it as the Skellam distribution in case of randomly distributed agent in space. In case of unconditional distribution, we pick an agent in random, and find out that the distribution of the net overtaking rate m/t converges to the initial velocity distribution with a Galilean shift by the mean of the distribution in the limit $t \to \infty$. We have also studied the finite time behavior of this distribution by considering the four different velocity distributions, namely uniform, Gaussian, exponential, and power-law distribution.

Chapter 3: Statistics of overtakes by a tagged agent in a system of interacting agents

In this chapter, we consider a simple model of interacting self-driven agents to study the statistics of net overtaking number by a tagged agent. Our model is an infinite lattice with entirely occupied of singly-seated agents with their constant but random initial velocities which are taken independently for each agent from an identical distribution. With time, each neighboring pair in this system are exchanged their sites with a specified rate that depends on their respective velocities. Three different cases depending on these exchange rates are studied. In the first case, for simplicity, we consider the exchange process is independent of velocities and occurs at a unit rate. In this case, the net overtaking number $m(t) \propto \sqrt{t}$ at large time t and $m/\sqrt{t}$, in the limit $t \to \infty$, is distributed according to the Gaussian distribution. In the next case, the left and the right velocities, v_L and v_R, of an adjacent pair are exchanged their sites at the rate one if the velocity at the left is higher than the same at the right, i.e., $v_L > v_R$. In this case, the mean $m(t|v_0)$ of a tagged agent of velocity v_0 grows linearly with time whereas the corresponding variance $\langle m^2(t|v_0)\rangle_c$ shows a linear increment $\propto t$ followed by a super-diffusive growth $\propto t^{4/3}$ with a velocity dependent transition time $t_1^*(v_0)$. The scaled distribution of $p(m, t|v_0)$ we have found

in the limits $t << t_1^*(v_0)$ and $t >> t_1^*(v_0)$. In the same case, we have also found the distribution of m/t of a randomly chosen agent, in the limit of $t \to \infty$, is distributed uniformly on $[-1 : 1]$ which is independent of the initial velocity distribution. We also discuss the large time approach to this limiting behavior before moving to the third case, where we consider the rate of exchange of a neighboring pair is equal to their relative velocity $v_L - v_R$ in addition to the condition of $v_L > v_R$. The qualitative behavior of $\langle m(t|v_0)\rangle$, $\langle m^2(t|v_0)\rangle_c$, and $p(m, t|v_0)$, in this case, remain same as that of the earlier one except a new super-diffusive behavior of $\langle m^2(t|v_0)\rangle_c$ and the Gaussian scaling function of $p(m, t|v_0)$ appears above the velocity dependent transition time $t_1^{\#}(v_0)$. Although the exact nature of the super-diffusion is unclear in this case, we have found this behavior and the corresponding scaling distribution is quite robust in a sense that, it seems, it is independent of the initial velocity distribution. In case of a randomly chosen agent the distribution of m/t, in the limit $t \to \infty$, converges to the distribution of velocity itself, with a Galilean shift by the mean velocity. The finite but large time behavior of the same is also discussed in case of four different initial velocity distributions.

Chapter 4: Finite-size effects on overtaking in case of Jepsen gas on a ring

In this chapter, we consider a Jepsen gas on a ring to the study finite-size effects on the statistics of net overtaking number by a tagged agent. We discuss the problem with two different ensembles. In the first, we take a fixed number of particles distributed randomly within the system whereas, in the next, the number of randomly distributed particles in different ensembles are chosen according to the Poisson distribution. With a fixed number of agents, we first derive an approximate result of the net overtaking number by a tagged agent of known velocity. By using this result, we calculate all the corresponding cumulants, and hence, the conditional probability distribution in case of four different initial velocity distributions, namely, uniform, Gaussian, exponential, and power-law distributions. In addition to that the unconditional probability distribution of the net overtaking number by a randomly chosen tagged agent is also calculated. We revise all these quantities of interest in case of 2nd ensemble including a brief introduction of finite size scaling analysis and

the dynamical exponent. Exact or approximate analytical results are presented in all cases with the support of the numerical simulation.

Chapter 5: Finite-size effects on overtaking in case of interacting agents on a ring

In this chapter we consider a periodic one-dimensional lattice with each site occupied by a singly-seated, self-driven agent to study how the finite system size affects the statistics of the net overtaking number by a tagged agent. The self-driven character of the agents is assigned by constant but random initial velocities by drawing them independently from a common distribution. In time, each pair of agents at adjacent sites exchange their positions with a specified rate while retaining their respective velocities. Depending on this exchange rate we discuss three different cases: in the 1st case a pair of agents exchange their positions at the rate 1, independent of their velocities. The velocity independent exchange makes the net overtaking number by a tagged agent to execute a simple random walk on the lattice without being affected by the finite system size. In the next two cases, exchange of position occurs only if the velocity of the "left" is higher with the rate 1 and equal to the modulus of their relative velocity, respectively. The effects of the finite system size are obtained in both cases while we are studying the conditional and the unconditional distribution of the net overtaking number by a tagged agent. Besides that, in case II, we compute the dynamical exponent $z = 3/2$ using the finite-size scaling analysis. Taking cues from this case, we compute the golden mean $z = (1+\sqrt{5})/2 \simeq 1.618$ in case III. Finally, in the end, we summarize our results with possible future directions.

Prof. Sanjib Sabhapandit Santanu Das

Theoretical Physics
Raman Research Institute
Bangalore 560 080, India

Chapter 1

Introduction

The aim and objective of this thesis is to study one particular kind of non-equilibrium system, namely, the self-driven many particles. Before going into description of this system, first, we briefly explore the statistical mechanics and its equilibrium counterpart followed by the non-equilibrium statistical mechanics with an emphasis on interacting particle systems.

The primary goal of statistical mechanics is to study behavior of a macroscopic system by starting its description from the microscopic level [1–5]. Macroscopic systems essentially consist of a large number of components like atoms, molecules, particles, spins, agents, etc. Statistical mechanics aims to describe how local interactions among these components at the microscopic level give rise to emergent phenomena at the macroscopic level. This subject can be seen as collections of tools and techniques which are constructed on the basis of statistics and probability theory to solve a wide range of problems.

Broadly, one can divide statistical physics into two classes. They are respectively, the statistical physics of systems in equilibrium and the same for systems out-of-equilibrium. A well-known example of a system in equilibrium is an ideal gas coupled with a heat reservoir. Out-of-equilibrium systems can attain a stationary state at late time. A canonical example of a system in a non-equilibrium stationary state is a metal bar with two ends in contact with two heat reservoirs maintained at two different temperatures. In the steady-state, there exists a constant heat current throughout this system, which is determined by the coefficient of heat conductivity. Notably, all the macroscopic behavior of this system in the linear response regime is encoded in this transport coefficient. Unlike non-equilibrium systems, no average

steady state current exists in a system which is in equilibrium. The average macroscopic properties of a system in equilibrium or in non-equilibrium stationary state are independent of time. But at the microscopic level, the system evolves through different microstates. The distinction between them can be made from the microscopic level. For that, we consider a classical Markov process which is fully specified by a set of microstates $\{\mathcal{C}_1, \mathcal{C}_2, \mathcal{C}_3, ..\}$. During the time evolution, the system goes through different microstates. Within time t to $t + dt$ the transition rate from $\mathcal{C}_i$ to $\mathcal{C}_j$ is $\mathcal{M}(\mathcal{C}_j, \mathcal{C}_i)\ dt$. According to the Markov hypothesis, it is assumed that these transition rates are independent of all previous history of the system. In addition, we assume these rates to be independent of time also. The time evolution of the probability distribution of a given microstate $\mathcal{C}_i$ is governed by the Master equation

$$\frac{d}{dt}P_t(\mathcal{C}_i) = \sum_{\mathcal{C}_j \neq \mathcal{C}_i} \mathcal{M}(\mathcal{C}_i, \mathcal{C}_j)\ P_t(\mathcal{C}_j) - \sum_{\mathcal{C}_j \neq \mathcal{C}_i} \mathcal{M}(\mathcal{C}_j, \mathcal{C}_i)\ P_t(\mathcal{C}_i). \tag{1.1}$$

The first term on the right hand side counts all incoming flux to state $\mathcal{C}_i$ whereas the second term counts the outgoing flux from $\mathcal{C}_i$. One can further write it as

$$\frac{d}{dt}P_t(\mathcal{C}_i) = \sum_{\mathcal{C}_j \neq \mathcal{C}_i} \left(\mathcal{M}(\mathcal{C}_i, \mathcal{C}_j)\ P_t(\mathcal{C}_j) - \mathcal{M}(\mathcal{C}_j, \mathcal{C}_i)\ P_t(\mathcal{C}_i)\right) = \sum_{\mathcal{C}_j \neq \mathcal{C}_i} J_t(\mathcal{C}_i, \mathcal{C}_j)$$

with $J_t(\mathcal{C}_i, \mathcal{C}_j)$ denotes for the net probability current between $\mathcal{C}_i$ and $\mathcal{C}_j$. When a system reach in a stationary state, it means $\frac{d}{dt}P_t(\mathcal{C}_i) = 0$, or $\sum_{\mathcal{C}_j \neq \mathcal{C}_i} J_t(\mathcal{C}_i, \mathcal{C}_j) = 0$ for all $\mathcal{C}_i$. Notably, equilibrium is a special case for which $J_t(\mathcal{C}_i, \mathcal{C}_j) = 0$ for any $\mathcal{C}_i$ and $\mathcal{C}_j$. This is well-known principle of the *detailed balance*. It states that if the net current between any two points in the configurational space is zero, then the system is in equilibrium, otherwise it is out of equilibrium.

1.1 Equilibrium statistical mechanics

Equilibrium statistical mechanics and thermodynamics are closely related to each other. Thermodynamics is a phenomenological description of a macroscopic system in equilibrium [6, 7]. The basic principles and laws in this discipline were established on the basis of empirical observations and summarized by the laws of thermodynamics. It does not require any knowledge of microscopic interactions

among the constituents. Rather it describes the system in terms of a few macroscopic parameters, called state functions like pressure (P), volume (V), temperature (T), chemical potential (μ).

Equilibrium statistical mechanics on the other hand, formulates a theoretical framework from the microscopic level to justify those empirical observations of thermodynamics. The micro-macro connection in this discipline was first found by Boltzmann about a century ago. He hypothesized that all the microstates of an isolated system in equilibrium are equiprobable. By definition, an isolated system does not exchange any heat, particles, or mechanical energy with the environment. Collection of its all the microstates named as *microcanonical ensemble*. The computations of a macroscopic observable in this ensemble reduces into a counting problem through the relation

$$S = k_B \log \Omega \tag{1.2}$$

which bridges entropy S (macroscopic) and the number of microstates Ω (microscopic) of a given system via the Boltzmann constant k_B.

This complete isolation is quite rare in nature, and one can think of it as an idealized case. Equilibrium statistical physics, in fact, goes beyond the isolated system by setting up couplings with the external reservoirs and allows the system to exchange heat, particles, and mechanical work. Depending on the exchange of different quantities, one can construct different ensembles. Of them, one is the *canonical ensemble*. This ensemble allows the system to exchange energy with its external reservoir which is maintained at a constant temperature T. The micro-macro connection in this case is expressed in terms of free energy F and the *partition function* Z as

$$F = -k_B T \log Z. \tag{1.3}$$

In fact, in this case, one can obtain the time-independent probability of a given microstate $\mathcal{C}$ as $\mathcal{P}_{eq}(\mathcal{C}) \propto e^{-E(\mathcal{C})/k_B T}$, with $E(\mathcal{C})$, the energy associated with $\mathcal{C}$ and the normalization constant Z.

1.2 Non-equilibrium statistical mechanics

Unlike equilibrium, the time-independent weight of a microstate in a system in nonequilibrium stationary state is not known in principle. Such systems are defined by the dynamics that violates the principle of the *detailed balance* at the microscopic level and the rules reflect every details present in the system like the nature of interaction of the system with the surroundings. These kind of systems are widespread in nature. Examples include living organisms, financial markets, social networks, traffic and traffic related movements, reaction-diffusion system, growing interface etc.

Broadly, one can divide non-equilibrium systems into two classes. They are, respectively, systems that are slightly away from equilibrium and systems that are far away from equilibrium. For systems slightly away from the equilibrium there exists an efficient framework, namely, the linear response theory [8]. However, unlike equilibrium and near equilibrium systems, we are yet to have a unified framework for systems far away from equilibrium.

Although there is no general framework, substantial progresses have been made in recent years. In the next subsection, we discuss a theoretical framework which has been extensively studied in the context of systems far away from equilibrium. We also include a brief description of a particular kind of non-equilibrium system, namely, the self-driven many particles which we are going to deal with in this thesis.

1.2.1 Interacting particle system

Interacting particle system (IPC) [9–13] offers a theoretical framework to study collective phenomena in complex systems which involve interaction among its components. The basic principle of this framework is as follows: first, it presents all the components of a complex system as particles on a lattice or some discrete geometry. The individual dynamics of the particles and the interactions among them are formulated by local rules which reflects the micrscopic details of the original complex system. These rules are logic-based which can violate the principle of *detailed balance* at the microscopic level. Some extensively studied models which are built on the basis of this framework are asymmetric simple exclusion processes, random

average processes, zero range processes, voter model etc.

1.2.2 Self-driven many particles

Among various non-equilibrium systems, in recent years, there has been a growing interest in a particular kind of system, namely self-driven many particles [14, 15]. The main feature of these type of systems is that the driving forces acting on each constituting particles are not external in origin, but are produced by the particles themselves. Examples of such systems include swarming bacteria, school of fish, flocking of birds, animal herds, pedestrian movements, including the vehicular traffic and traffic-related flows. From the self-driven character of individual constituents and their complex interactions emerge different new phenomena. Examples include collective movements and phase transition [17], phase separation [16], intermittency and clustering [18] etc.

In this thesis we aim to deal with these kinds of systems. Hence to get an introductory idea and essence, in the next two sections, we aim to discuss two paradigmatic models of self-driven agent(s).

1.3 Single self-driven agent: Biased random walk

As an example of a simple non-equilibrium system, and also as a prototype of a single self-driven agent, in this section, we briefly discuss the biased random walk (BRW) on a periodic one-dimensional (1D) lattice. Historically, the problem of random walk was first introduced by Karl Pearson in 1905 [19]. Since then, numerous variants of this model were proposed and studied in the context of different complex systems [20–24]. For convenience, here we discuss the continuous-time, discrete space (lattice) variant of the BRW.

Consider a 1D lattice of N sites ($j = 0, 1, 2, ..., N-1$) with periodic boundary conditions (PBC): $N + j = j$. We consider a walker on this lattice at position $j = 0$ at time $t = 0$. The time evolution rule is: the walker jumps to the right (r) and the left (l) neighboring sites with the rates p_r and p_l respectively (see FIG. 1.1). It implies that within a small interval of time dt the walker jumps to the right with

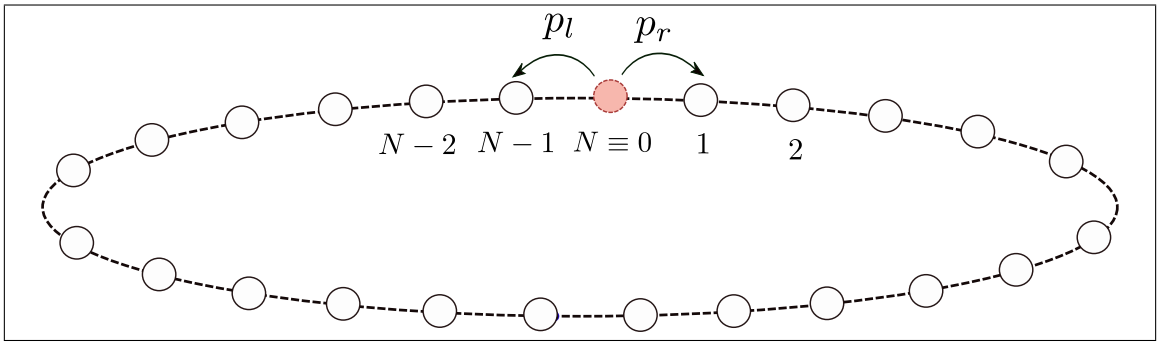

Figure 1.1: Schematic of biased random walk on a periodic one dimensional lattice. The walker can hop to the right and the left neighboring sites with the rates p_r and p_l respectively.

probability $p_r dt$, to the left with probability $p_l dt$, and is at the same position with probability $1-(p_r+p_l)dt$. Notably, "biased" means the walker has a preference of movement in a given direction. For example, for $p_r > p_l$, the bias is on the right. For $p_r = p_l$ it becomes simple random walk.

The time evolution of the probability distribution $P(j,t)$ of the walker of being at site j at time t is governed by the Master equation [25] which can be written by taking $dt \to 0$ as

$$\frac{d}{dt}P(j,t) = p_r\ P(j-1,t) + p_l\ P(j+1,t) - (p_r+p_l)\ P(j,t). \tag{1.4}$$

Now, to solve this equation with the initial condition $P(j,0) = \delta_{j,0}$, we first recall the discrete Fourier transform

$$\widetilde{P}(\kappa,t) = \sum_{j=0}^{N-1} P(j,t)\ \mathrm{Exp}\left[\frac{2\pi i j\kappa}{N}\right] \tag{1.5}$$

with $i=\sqrt{-1}$. By using this on Eq. (1.4) we can get

$$\frac{d}{dt}\widetilde{P}(\kappa,t) = \lambda_\kappa\ \widetilde{P}(\kappa,t) \tag{1.6a}$$

$$\text{with} \qquad \lambda_\kappa = p_r\left(\mathrm{Exp}\left[\frac{2\pi i\kappa}{N}\right]-1\right) + p_l\left(\mathrm{Exp}\left[-\frac{2\pi i\kappa}{N}\right]-1\right). \tag{1.6b}$$

Employing the initial condition $P(j,0) = \delta_{j,0}$ in Eq. (1.6a) we can obtain

$$\widetilde{P}(\kappa,t) = \widetilde{P}(\kappa,0)\; e^{\lambda_\kappa t} = e^{\lambda_\kappa t}. \tag{1.7}$$

Now, the inverse Fourier transform yields

$$P(j,t) = \frac{1}{N}\sum_{\kappa=0}^{N-1} \widetilde{P}(\kappa,t)\; \mathrm{Exp}\left[-\frac{2\pi i j\kappa}{N}\right] = \frac{1}{N}\sum_{\kappa=0}^{N-1} e^{\lambda_\kappa t}\; \mathrm{Exp}\left[-\frac{2\pi i j\kappa}{N}\right]. \tag{1.8}$$

In the next Section we discuss the behavior of the displacement distribution in two different limits. Of them one is transient and other is stationary. The transient limit is obtained by taking $N \to \infty$ first, and then $t \to \infty$, whereas the other by taking $t \to \infty$ first, and then $N \to \infty$. In the transient limit all the results are independent of the system-size N, whereas in the opposite limit it depends on N.

1.3.1 Taking $N \to \infty$ first, then $t \to \infty$

In the limit of $N \to \infty$, considering $k \equiv 2\pi\kappa/N$ as a continuum variable within $-\pi$ to π, one can write Eq. (1.8) as

$$P(j,t) = \frac{1}{2\pi}\int_{-\pi}^{\pi} dk\; e^{\lambda_k t}\; e^{-ijk} \tag{1.9a}$$

$$\text{with} \qquad \lambda_k = p_r\left(e^{ik}-1\right) + p_l\left(e^{-ik}-1\right). \tag{1.9b}$$

By defining $c = j/t$, we can express the distribution as

$$P(c,t) = \frac{t}{2\pi}\int_{-\pi}^{\pi} dk\; e^{-t\;\lambda(c,k)} \tag{1.10a}$$

$$\text{with} \qquad \lambda(c,k) = ick - \lambda_k. \tag{1.10b}$$

At any finite but large time t, the dominant contribution to this integration comes from the saddle point, i.e., the point (k^*) which can be obtained by solving

$$\frac{d}{dk}\lambda(c,k) = 0 \qquad \text{or,} \qquad p_r e^{ik^*} - p_l e^{-ik^*} - c = 0. \tag{1.11a}$$

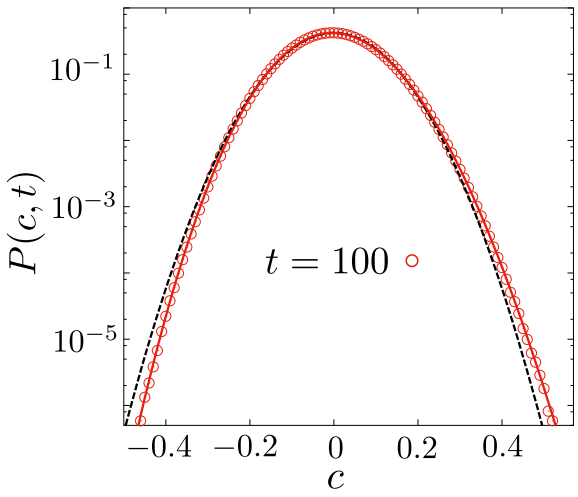

Figure 1.2: Probability distribution function $P(c,t)$ is plotted versus $c - \langle c \rangle$ at time $t = 100$ by considering the right and the left jumping rates $p_r = 0.8$ and $p_l = 0.1$ respectively. The bold (red) line in the plot results from Eq. (1.14) which is showing good agreements with the numerical simulation result. A Gaussian approximated result is also plotted which matches well around the mean but shows clear deviations at the tails of the distribution.

By solving this equation one can find the saddle point

$$k^* = -i \log \left[\frac{c \pm \sqrt{c^2 + 4p_r p_l}}{2p_r} \right]. \tag{1.11b}$$

As $\sqrt{c^2 + 4p_r p_l} \geq c$, we can say that +ve would be the relevant solution of k^*. Now, replacing k^* in the expression of $\lambda(c,k)$ in Eq. (1.10b) we can calculate

$$\phi(c) \equiv \lambda(c,k^*) = c \log \left[\frac{c + \sqrt{c^2 + 4p_r p_l}}{2p} \right] + (p_r + p_l) - \sqrt{c^2 + 4p_r p_l}, \tag{1.12a}$$

$$\text{and} \quad \phi''(c) \equiv \lambda''(c,k^*) = \sqrt{c^2 + 4p_r p_l}. \tag{1.12b}$$

Now, by expanding $\lambda(c,k)$ around k^* we can write

$$\lambda(c,k) \simeq \lambda(c,k^*) + \frac{1}{2}(k-k^*)^2 \, \lambda''(c,k^*) + \mathcal{O}((k-k^*)^3). \tag{1.13}$$

It further allows us to calculate the distribution as follows

$$\begin{aligned} P(c,t) &\simeq \frac{t}{2\pi} \, e^{-t\,\phi(c)} \int_{-\pi}^{\pi} dk \; e^{-\frac{1}{2}(k-k^*)^2 t\,\phi''(c) + \mathcal{O}((k-k^*)^3)} \\ &\simeq \frac{\sqrt{t}}{2\pi} \, \frac{e^{-t\,\phi(c)}}{\sqrt{|\phi''(c)|}} \int_{-\infty}^{\infty} dy \; e^{-\frac{1}{2}y^2 + \mathcal{O}\left((y/\sqrt{t})^3\right)} \simeq \sqrt{\frac{t}{2\pi}} \, \frac{e^{-t\,\phi(c)}}{\sqrt{|\phi''(c)|}} + \mathcal{O}(t^{-3/2}). \end{aligned} \tag{1.14}$$

Note that, the Gaussian integrand in the 1st line of the above expression is sharply peaked at 0 with a variance inversely proportional to t which goes to zero in the limit of large t. It allows us to approximate and compute the integration. Here, $\phi(c)$ is called the *large deviation function* [26] as it encodes rarely probable, atypical fluctuations of the distribution as illustrated in FIG. 1.2. Notably, by expanding c around its mean $\langle c\rangle = p_r - p_l$, we can also get the typical Gaussian fluctuation with a variance $\langle c^2\rangle_c = \langle c^2\rangle - \langle c\rangle^2 = (p_r + p_l)/t$. Clearly, this Gaussian fluctuation is the outcome of the well-known *central limit theorem* [21, 22].

1.3.2 Taking $t \to \infty$ first, then $N \to \infty$

In the limit of $t \to \infty$ first, then $N \to \infty$, one can expect the system to reach in a stationary state. It implies that the distribution in this limit becomes time independent, i.e., $\frac{d}{dt}P(j,t) = 0$. Using Eq. (1.8) we can say $\lambda_\kappa = 0$. From Eq. (1.6a) we can say $\lambda_\kappa = 0$ corresponds $\kappa = 0$. It makes the stationary state probability distribution

$$P(j, t \to \infty) = \frac{1}{N}\widetilde{P}(0, t \to \infty) = \frac{1}{N}. \tag{1.15}$$

It implies the position of the random walker is distributed uniformly throughtout the system in the stationary state. Note that the decay time of the mode $\kappa = 0$ is infinite. To find out the same for the next slowest mode, we can expand Eq. (1.6a) in the limit $\kappa/N \to 0$ as

$$\lambda_\kappa \simeq (p_r - p_l)\frac{2\pi i\kappa}{N} - (p_r + p_l)\frac{4\pi^2\kappa^2}{N^2} + \mathcal{O}((\kappa/N)^3). \tag{1.16}$$

From here we can get the system size dependent decay time as:

$$\frac{1}{|\mathrm{Re}(\lambda_\kappa)|} \approx (p_r + p_l)^{-1}\frac{N^2}{4\pi^2\kappa^2} \propto N^z \tag{1.17}$$

with the dynamical exponent $z = 2$. This exponent alternatively says that the underlying dynamics is diffusive. Finally, we can also calculate a constant current $J = (p_r - p_l)$ which flows through the system in the steady state.

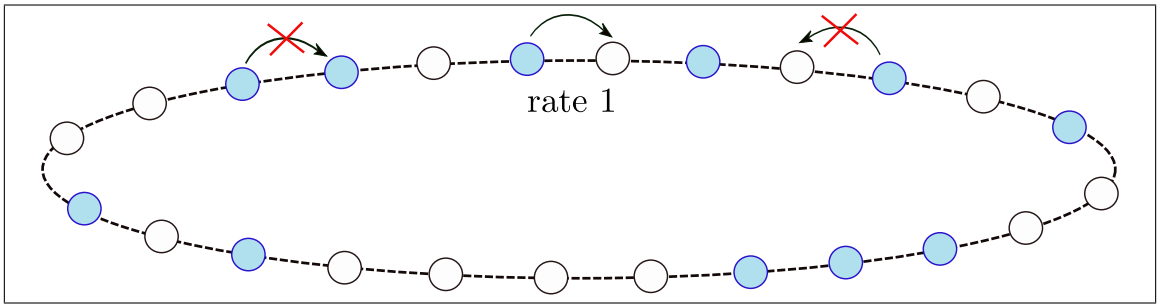

Figure 1.3: Schematic of TASEP on a periodic one-dimensional lattice. Each site on the lattice is occupied atmost by one particle. A typical configuration is presented by making all particles blue. Each particle can hop to the right neighboring site at the rate 1 if the corresponding site remains empty. Movement to the left and to an already occupied site is forbidden.

1.4 Interacting self-driven agents : TASEP

As a paradigmatic model of a non-equilibrium system, in this section, we briefly discuss totally asymmetric simple exclusion process (TASEP). Historically, the model asymmetric simple exclusion process (ASEP) was proposed to describe the protein synthesis on RNA [27, 28]. In the mathematical literature, the same model was introduced independently by Spitzer [29]. Over the years the model has been studied extensively both in mathematics and in physics [9–12, 30–33]. The model can be seen as a collection of identical biased random walkers or self-driven agents on a lattice which are interacting via simple exclusion. The term "exclusion" was coined by Splizer [29]. By exclusion it is meant that a walker can't jump to an already occupied site. In a particular limit, when all the particles in ASEP are allowed to jump in a given direction, say to the right, the process is known as TASEP. In the next, for convenience, we discuss TASEP with periodic boundary condition.

Consider a 1D lattice of N sites ($i = -N/2+1, -1, 0, 1, .., N/2$) with periodic boundary conditions $N + i \equiv i$. Initially, each site on this lattice is either empty or occupied atmost by a particle with probabilities $(1 - \rho_0)$ and ρ_0 respectively. As a dynamics each identical particle can hop to its right at the rate 1 with the restriction of hard-core exclusion (illustrated in FIG. 1.3). The exclusion condition prohibits the double occupancy of particles at any site and also maintains the order of the particles in time.

With this setup, any configuration of this system can be presented by specifying

the positions of all particles. One can do it by defining an occupation variable $\eta(i)$ for each site. These occupation variables take values 0 or 1 if the corresponding site is empty or occupied by a particle respectively. A complete set of $\{\eta(i)\}$ can present a possible configuration of this system.

Starting from any arbitrary configuration, 1D TASEP on a ring attains a non-equilibrium stationary state in the limit of large asymptotic time [34]. This stationary state is completely characterized by occupation probability density of particles i.e.,

$$\mathcal{P}(\eta(i) = 1) = \rho_0 \quad \text{for } 0 \leq \rho_0 \leq 1. \tag{1.18}$$

In this stationary state all the $\mathcal{P}(\eta(i))$'s become independent which makes the joint distribution of occupation probability $P(\{\eta(i)\})$ to follow the product measure rule

$$P(\{\eta(i)\}) = \prod_{i=1}^{N} \mathcal{P}(\eta(i)). \tag{1.19}$$

Moreover, it also implies that any arbitrary configuration in the stationary state with density ρ_0 can be generated by drawing individual $\eta(i)$'s independently from the equidistribution $\mathcal{P}(\eta(i)) \equiv \mathcal{P}(\eta)$. Note that the product measure rule corresponds to a grand-canonical ensemble of fluctuating particle numbers. It makes the density of the system equal to

$$\langle \psi \rangle = \frac{\langle m \rangle}{N} = \frac{1}{N} \sum_{m=0}^{N} \binom{N}{m} \rho_0^m (1-\rho_0)^{N-m}\, m = \rho_0. \tag{1.20}$$

The variance associated with this quantity can be calculated as

$$\langle \psi^2 \rangle_c = \frac{1}{N^2} \left[\sum_{m=0}^{N} \binom{N}{m} \rho_0^m (1-\rho_0)^{N-m}\, m^2 - \left(\sum_{m=0}^{N} \binom{N}{m} \rho_0^m (1-\rho_0)^{N-m}\, m \right)^2 \right]$$
$$= \frac{\rho_0(1-\rho_0)}{N}. \tag{1.21}$$

In the stationary state, one can calculate the current flowing through a bond $(i, i+1)$

as follows

$$J(i \to i+1) = \langle \mathcal{P}(\eta(i)=1)\ \mathcal{P}(\eta(i+1)=0)\rangle_{\rho_0} \\ = \langle \mathcal{P}(\eta(i)=1)\rangle\ \langle \mathcal{P}(\eta(i+1)=0)\rangle_{\rho_0} = \rho_0(1-\rho_0). \quad (1.22)$$

Notably, the angular brackets denote the average over different ensembles in the stationary state.

1.4.1 Kinematic wave in TASEP

To obtain finer information of how the local density in TASEP evolves in time, it is convenient to describe the system in terms of coarse-grained hydrodynamic observables. The relevant hydrodynamic observables in TASEP are density $\psi(x,t)$ and current $J(x,t)$ around a point x at time t. Now the rate at which the particle number within a region Δx around point x changes in time can be written as

$$\Delta x\ \partial_t \psi(x,t) = J(x,t) - J(x+\Delta x, t) \quad (1.23)$$

with $J(x,t)$ and $J(x+\Delta x,t)$ denoting the incoming and outgoing particle current at x and $x+\Delta x$ respectively. By assuming the current as a slowly varying observable in the hydrodynamic limit, the Taylor series expansion of $J(x+\Delta x,t)$ around x simplifies the above equation to the well-known *continuity equation* [10]

$$\partial_t \psi(x,t) + \partial_x J(x,t) = 0. \quad (1.24)$$

To provide a more detailed description about how the local density field evolves in time, we recall the idea of *kinematic wave* used in the context of the traffic flow by Lighthill and Whitham [36, 37]. The idea is to consider the spatio-temporal dependence of current $J(x,t)$ coming through the density $\psi(x,t)$ i.e., $J(x,t) \equiv J(\psi(x,t))$, then

$$\partial_t \psi(x,t) + \frac{dJ(x,t)}{d\psi(x,t)}\ \partial_x \psi(x,t) = 0. \quad (1.25)$$

If one considers the leading order contribution in $\frac{dJ(x,t)}{d\psi(x,t)}$ is coming from the average, then it yields

$$\frac{dJ(x,t)}{d\psi(x,t)} \approx \frac{dJ(\rho_0)}{d\rho_0} = J'(\rho_0) = (1-2\rho_0). \tag{1.26}$$

Now, if we expand $\psi(x,t)$ around the uniform background density ρ_0 as

$$\psi(x,t) = \rho_0 + \widetilde{\psi}(x,t) \tag{1.27}$$

with $\widetilde{\psi}(x,t)$ denoting the density fluctuation around the mean, then combining Eq. (1.25), (1.26), and (1.27) we finally get

$$\partial_t \widetilde{\psi}(x,t) + J'(\rho_0)\ \partial_x \widetilde{\psi}(x,t) = 0. \tag{1.28}$$

The solution of this equation is of the form

$$\widetilde{\psi}(x,t) = f(x - J'(\rho_0)\ t) \tag{1.29}$$

where f is an arbitrary function which we can find from the initial condition $\widetilde{\psi}(x,0) = f(x)$. The solution implies that the coarse-grained density fluctuation $\widetilde{\psi}(x,t)$ propagetes through the medium in the form of a travelling wave of velocity $J'(\rho_0) = (1-2\rho_0)$.

1.4.2 NLFH equation for TASEP

Product measure stationary initial condition alongside the periodicity makes the density of particles a conserved quantity in TASEP. The time evolution of the coarse-grained local density fluctuation $\widetilde{\psi}(x,t)$ of this conserved quantity can be obtained by using the formalism of nonlinear fluctuating hydrodynamics (NLFH) [39, 40]. NLFH has recently emerged as a powerful tool to study the space-time fluctuations of conserved quntities in the context of transport processes. Using this formalism one can express $J(x,t) \equiv J(\psi(x,t)) = J(\rho_0 + \widetilde{\psi}(x,t))$. Next, expanding the current around the uniform background density ρ_0 upto the second order in $\widetilde{\psi}(x,t)$, and then adding phenomenological dissipation and noise terms with it, one can write

$$J(x,t) = J(\rho_0) + J'(\rho_0)\ \widetilde{\psi}(x,t) + \frac{1}{2}J''(\rho_0)\ \widetilde{\psi}^2(x,t) - D(\rho_0)\ \partial_x \widetilde{\psi}(x,t) + \sqrt{\sigma(\rho_0)}\ \eta(x,t). \tag{1.30}$$

The strength of the dissipative and the noise terms are respectively characterized by the diffusivity $D(\rho_0)$ and the mobility $\sigma(\rho_0)$. $D(\rho_0)$ and $\sigma(\rho_0)$ are model dependent parameters which are related in this case to each other by $\sigma(\rho_0) = 2\ D(\rho_0)\ \rho_0\ (1-\rho_0)$. The noise $\eta(x,t)$ is characterized by its zero mean and variance $\langle \eta(x,t)\eta(x',t')\rangle = \delta(x-x')\delta(t-t')$. As the background density ρ_0 and the corresponding current $J(\rho_0) = \rho_0(1-\rho_0)$ are space-time invariant quantities, the continuity equation in Eq. (1.24) becomes

$$\partial_t \widetilde{\psi}(x,t) = -\partial_x \left(J'(\rho_0)\ \widetilde{\psi}(x,t) + \frac{1}{2} J''(\rho_0)\ \widetilde{\psi}^2(x,t) - D(\rho_0)\ \partial_x \widetilde{\psi}(x,t) + \sqrt{\sigma(\rho_0)}\ \eta(x,t) \right). \tag{1.31}$$

It is the non-linear fluctuating hydrodynamic equation for $\widetilde{\psi}(x,t)$ which is also known as the noisey Burger equation [39]. Using a Galilean shift $x - J'(\rho_0)t \to x$ one can further reduce it to

$$\partial_t \widetilde{\psi}(x,t) + \partial_x \left(\frac{1}{2} J''(\rho_0)\ \widetilde{\psi}^2(x,t) - D(\rho_0)\ \partial_x \widetilde{\psi}(x,t) + \sqrt{\sigma(\rho_0)}\ \eta(x,t) \right) = 0. \tag{1.32}$$

1.4.3 KPZ universality class

Universality is one of the central concepts in statistical physics [43]. It groups a wide range of systems with different dynamical rules and interactions at the microscopic level into a small number of universality classes. Each class is characterized by some critical exponents and certain scaling functions (e.g., correlation function). The concept of universality is well-established in the case of equilibrium systems around the critical point [44,45]. In the context of non-equilibrium systems, the concept of universality is quite familiar. For example, different universality classes in the context of interface growth model [48]. It includes well-established Edwards-Wilkilson [46] and Kardar-Parisi-Zhang (KPZ) [38] universality classes. Interestingly, it was found that 1D TASEP belongs to Kardar–Parisi–Zhang (KPZ) universality class [38–42]. 1D TASEP can be mapped to the KPZ interface growth model [38] which we discuss in the next.

The mapping between TASEP and the (1+1) dimensional interface growth model, which belongs to the KPZ universality class, is as follows [47,48]. Each site $i \in [1:N]$ on the lattice is associated with a discrete height variable $h(i,t)$ at time t. The height

variable satisfies the following recursive relation

$$h(i,t) = h(i-1,t) + 1 - 2\eta(i,t) \tag{1.33}$$

with the condition $h(0,t) = 0$ for all t. As we know, $\eta(i,t)$ can take values 0 (1) if the site is occupied by a hole (particle) at time t. It further implies that the presence of a hole (particle) at the i-th site produces a positive (negative) unit slope with respect to the $(i-1)$-th site. The resultant line connecting all the neighboring slopes represents a TASEP equivalent interface. The stochastic dynamics of the particles along the lattice corresponds to an evolution of the height variable. For example, when a particle jumps from site i to site $(i+1)$, the height variable $h(i,t)$ is decreased by 2 units. As an initial condition in TASEP if one considers the product measure stationary initial distribution of particles with density ρ_0, the average height at the N-th site would be

$$\langle h(N,t)\rangle = \langle h(0,t)\rangle + \sum_{i=1}^{N}[1 - 2\langle\eta(i,t)\rangle] = \langle h(0,t)\rangle + (1-2\rho_0)N. \tag{1.34}$$

Now, to maintain the equivalence between 0 and N-th sites in a periodic system, instead of $h(i,t)$, a scaled variable $\widetilde{h}(i,t)$ can be defined as

$$\widetilde{h}(i,t) = h(i,t) - (1-2\rho_0)i. \tag{1.35}$$

It is easy to see that this scaled variable removes the tilted boundary condition i.e., $\langle\widetilde{h}(N,t)\rangle = \langle\widetilde{h}(0,t)\rangle = 0$. Now, coarse-graining the discrete height by a continuum variable x, Eq. (1.33) can be written as $h(x,t) = h(x-\delta x,t) + (1-2\psi(x,t))\delta x$. In the hydrodynamic limit considering $h(x,t)$ as a slowly varying observable one can get $\frac{\partial}{\partial x}h(x,t) = 1 - 2\psi(x,t)$. Similarly, the coarse-graining of Eq. (1.35) yields $\widetilde{h}(x,t) = h(x,t) - (1-2\rho_0)x$. Now, using the relation $\psi(x,t) = \rho_0 + \widetilde{\psi}(x,t)$ in the above two equations it is easy to obtain

$$\widetilde{\psi}(x,t) = -\frac{1}{2}\frac{\partial}{\partial x}\widetilde{h}(x,t). \tag{1.36}$$

By replacing the relation into Eq. (1.32), the time evolution equation of the fluctu-

ating height variable can be written as

$$\partial_t \widetilde{h}(x,t) = \nu_0 \, \partial_x^2 \widetilde{h}(x,t) + \frac{\xi_0}{2} \, [\partial_x \widetilde{h}(x,t)]^2 + \sigma_0 \, \eta(x,t) \tag{1.37}$$

which is the well-known Kardar-Parasi-Zhang (KPZ) equation of non-equilibrium interface growth [38]. The coefficient $\nu_0 = D(\rho_0)$ is an effective surface tension, $\sigma_0 = 2\sqrt{\sigma(\rho_0)}$ and $\xi_0 = J''(\rho_0)/2$ to denote the strength of noise and nonlinearity, respectively.

1.4.4 Two-point correlation function

The stochastic dynamics with the above-mentioned stationary initial condition defines a space-time stationary process $\eta(i,t)$ [35]. In the stationary TASEP, the main quantity of interest is a two-point density-density correlation function which is defined by

$$S(j,t) = \langle \eta(j,t)\eta(0,0) \rangle_{\rho_0} - \rho_0^2. \tag{1.38}$$

The index j denotes the relative difference in the spatial coordinate. In a periodic system of size N, it can take interger values between $-\frac{N}{2} + 1 \leq j \leq \frac{N}{2}$. The susceptibility $\chi(\rho_0)$ of this process can be defined and calculated as follows

$$\chi(\rho_0) = \sum_{j=-N/2+1}^{N/2} S(j,0) = \sum_{j=-N/2+1}^{N/2} S(j,t) = \rho_0(1-\rho_0). \tag{1.39}$$

In fact, one can also find [49]

$$\frac{1}{\chi(\rho_0)} \sum_{j=1}^{N} j \; S(j,t) = (1-2\rho_0) \; t = J'(\rho_0) \; t. \tag{1.40}$$

From Eq. (1.39) and Eq. (1.40) it can be said that $S(j,t)$ has a total weight $\chi(\rho_0)$ centered around $J'(\rho_0)t$. The full solution of $S(j,t)$ for 1D TASEP can be written as [35, 49–51]

$$S(j,t) \simeq \chi(\rho_0) \; (\lambda_0 t)^{-2/3} \; g''[(\lambda_0 t)^{-2/3} \; (j - J'(\rho_0)t)] \tag{1.41}$$

with non-universal coefficient $\lambda_0 = \sqrt{2\chi}|J''(\rho_0)|$ and universal scaling function $g''(x)$ Notably, $S(j,t)/\chi(\rho_0)$ can be treated as a normalized PDF with mean $J'(\rho_0)t$.

Note that, with the aid of universality, one can express the correlation function in TASEP in terms of critical exponents and a scaling function in the interface growth model. To show this, we first write the two-point spatio-temporal correlation function in the interface growth model [48]

$$C(x,t) = \langle [h(x+x',t) - h(x',0)]^2 \rangle - \langle [h(x+x',t) - h(x',0)] \rangle^2.$$

For a stationary process it can be written as

$$C(x,t) = \langle [h(x,t) - h(0,0)]^2 \rangle - \langle [h(x,t) - h(0,0)] \rangle^2. \tag{1.42}$$

Here, $\langle h(x,t) - h(0,0) \rangle = (1-2\rho_0)x$, can be obtained from the definition of average interface slope. Now, taking the second derivative of $C(x,t)$ with respect to x, and using the periodicity of the translationally invariant system we can obtain

$$\begin{aligned} \partial_x^2 C(x,t) &= \partial_x \left(2\langle [h(x,t) - h(0,0)][1 - 2\psi(x,t)] \rangle\right) - 2(1-2\rho_0)^2 \\ &= 8\left(\langle \psi(0,0)\psi(x,t) \rangle - \rho_0^2\right) = 8\,\langle \widetilde{\psi}(0,0)\widetilde{\psi}(x,t) \rangle = 8S(x,t). \end{aligned} \tag{1.43}$$

The correlation function in the interface growth model follows the scaling relation [48]

$$C(x,t) \sim t^{2\beta} g\left(\frac{x}{t^{1/z}}\right) \tag{1.44}$$

with the growth and the dynamical exponents β and z respectively. In case of the KPZ interface $z = 3/2$. The roughening exponent α of the same interface satisfies $\alpha + z = 2$ and $\alpha = \beta z$. Using these two relations in Eq. (1.43) we get

$$S(x,t) \sim t^{2\beta - 2/z} g''\left(\frac{x}{t^{1/z}}\right) \sim t^{2/z-2} g''\left(\frac{x}{t^{1/z}}\right) \sim t^{-2/3} g''\left(\frac{x}{t^{2/3}}\right) \tag{1.45}$$

which is consistent with Eq. (1.41).

1.4.5 Variants of TASEP with overtakings

The variants of TASEP are still providing excellent set of models that can show rich and interesting non-equilibrium phenomena [15, 52]. But the extensive literature on this subject is too vast to cover here. Hence, for convenience, in this section, we briefly survey the literature of TASEP and TASEP related models in a particular direction where one may see *overtakings* among the particles.

Starting with TASEP, one can say it mimics single-lane traffic movements where *overtakings* among the particles are not allowed. The exclusion condition in this process maintains the relative order of the particles in time. If one denotes the particles and holes by 1 and 0 respectively, the allowed transition in TASEP can be represented by

$$1\ 0 \to 0\ 1 \qquad \text{at the rate} \quad 1.$$

In recent years different variants of the TASEP have been studied [12, 31, 52–59] which allow overtaking among the particles, i.e., where the relative order among the particles changes in time. As a first and simple case, one may think of a second class particle in TASEP [53]. It has been introduced to locate the position of the shock profile in TASEP [31, 53–55]. The dynamics of this particle is different from normal particles. It can hop like particles but is treated as a hole by the particles. Denoting the particle, hole, and the 2nd class particle by 1, 0 and 2 respectively, the allowed transitions can be written as:

$$1\ 0 \to 0\ 1,\ 2\ 0 \to 0\ 2, \text{ and } 1\ 2 \to 2\ 1 \quad \text{at the equal rate 1.}$$

The position exchange between the particles (holes) and the second class particle can alternatively be described in the language of overtaking. In this language, the particles overtake (holes are overtaken by) the second class particle at the rate one in the right direction.

A straightforward generalization of a single second class particle comes through the multi-species version of the TASEP [56–58]. Instead of one, this process deals with multiple species or classes of particles. Following the earlier thread, one can define this case by labeling the different classes with different numbers. The process can also include holes as a distinct class [57]. Interaction wise the process has a

hierarchical structure among the different classes. The process allows a higher class particle to overtake all the lower ones with an equal rate, say one for simplicity. For a neighboring pair of classes α and β, the allowed transitions are represented by

$$\alpha\beta \to \beta\alpha \quad \text{at the rate 1} \quad \text{if} \quad \alpha > \beta.$$

Notion wise this interaction provides a partial sense of velocity. It tells that the higher-class particles have higher velocities with respect to all lower classes in the right direction. Note that all the rates associated with the allowed transition are equal and independent of the species-identifying numbers.

As a generalization of multi-species TASEP, one can think of randomness in the hopping rates. The idea of randomness has extensively been studied in the literature from the cellular automata model [60,61] to the periodic 1D ASEP [62–64]. However, hardcore exclusion in most of the cases left behind the issues of overtaking.

Finally, in the context of overtaking that includes randomness in the particle hopping rates, an efficient extension has been made by Karimpour *et al.* [65]. The model considers a particle with faster (f) hopping rate v_f to stochastically overtake a slower (s) one of hopping rate v_s at the rate $(v_f - v_s)$ i.e.,

$$v_f\, v_s \to v_s\, v_f \quad \text{at rate } (v_f - v_s) \quad \text{if} \quad v_f > v_s.$$

Although, one finds different variants of TASEP where one can allow overtaking (or the change in relative orders) among the particles in time, there is no systematic study of this phenomenon in literature. It sets the main goal of this thesis.

1.5 Objective and Outline of this thesis

The phenomenon of overtaking is ubiquitous in nature. It occurs naturally in all sorts of traffic, ranging from the vehicular traffic on highways [66] to the transport at the molecular scale by motor proteins [67, 68]. Animals in groups, overtake each other to move to a less risky position at the center of the group [69]. Overtaking also takes place in sedimentation or electrophoresis of mixtures with polydisperse (different sizes, densities) particles falling (or rising) through a fluid under gravity or electric field [70]. In biological evolution, the population sizes of different genotypes

overtake each other depending on their fitness [71–74]. In spite of this ubiquity, there is no systematic study of this phenomenon in literature. Keeping this aspect in mind, we organized our thesis as follows:

In the next chapter, we begin with a simple non-interacting model of self-driven agents, namely the Jepsen gas, to get an introductory essence of overtaking by a tagged agent. The model we consider is non-interacting in the sense that all the point-like constituents or agents in Jepsen gas can pass each other without any obstacles. We consider two different initializations depending on how the agents are distributed in space. They are respectively the uniform distribution of agents and a constant gap between all neighboring agents. The self-driven character of each agent is assigned by random but constant initial velocity. For simplicity, we have chosen all these velocities independently from a common distribution. Starting with this set-up, each agent moves with its constant velocity in time. In this system, as a quantity of interest, we investigate the net overtaking number $m(t)$ by a tagged agent at time t. By definition, it is the total number of agents that the tagged agent overtakes minus the total number of agents that overtakes the tagged agent in a given duration of time. Notably, this is a stochastic observable. The stochasticity comes from the randomness in initial positions and velocities. Two different probability distributions associated with the net overtaking number by a tagged agent has been studied. They are namely the conditional and the unconditional distributions. In case of the conditional distribution, we exactly know the tagged velocity where we calculate and identify it as the Skellam distribution in case of a randomly distributed agent in space. In case of the unconditional distribution, we pick an agent in random and find out that the distribution of the net overtaking rate m/t converges to the initial velocity distribution with a Galilean shift by the mean of the distribution in the limit $t \to \infty$. We have also studied the finite time behavior of this distribution by considering the four different velocity distributions, namely uniform, Gaussian, exponential, and power-law distribution.

In the third chapter, we consider a simple model of interacting self-driven agents to study the statistics of net overtaking number by a tagged agent. Our model is an infinite lattice with entirely occupied of singly-seated agents with their constant

but random initial velocities which are taken independently for each agent from an identical distribution. With time, each neighboring pair in this system exchange their sites with a specified rate that depends on their respective velocities. Three different cases depending on these exchange rates are studied. In the first case, for simplicity, we consider the exchange process is independent of velocities and occurs at a unit rate. In this case, the net overtaking number $m(t) \propto \sqrt{t}$ at large time t and $m/\sqrt{t}$, in the limit $t \to \infty$, is distributed according to the Gaussian distribution. In the next case, the left and the right velocities, v_L and v_R, of an adjacent pair are exchanged their sites at the rate one if the velocity at the left is higher than the same at the right, i.e., $v_L > v_R$. In this case, the mean $m(t|v_0)$ of a tagged agent of velocity v_0 grows linearly with time whereas the corresponding variance $\langle m^2(t|v_0)\rangle_c$ shows a linear increment $\propto t$ followed by a super-diffusive growth $\propto t^{4/3}$ with a velocity dependent transition time $t_1^*(v_0)$. The scaled distribution of $p(m, t|v_0)$ we have found in the limits $t << t_1^*(v_0)$ and $t >> t_1^*(v_0)$. In the same case, we have also found the distribution of m/t of a randomly chosen agent, in the limit of $t \to \infty$, is distributed uniformly on $[-1 : 1]$ which is independent of the initial velocity distribution. We also discuss the large time approach to this limiting behavior before moving to the third case, where we consider the rate of exchange of a neighboring pair is equal to their relative velocity $v_L - v_R$ in addition to the condition of $v_L > v_R$. The qualitative behavior of $\langle m(t|v_0)\rangle$, $\langle m^2(t|v_0)\rangle_c$, and $p(m, t|v_0)$, in this case, remain same as that of the earlier one except a new super-diffusive behavior of $\langle m^2(t|v_0)\rangle_c$ and the Gaussian scaling function of $p(m, t|v_0)$ appears above the velocity dependent transition time $t_1^{\#}(v_0)$. Although the exact nature of the super-diffusion is unclear in this case, we have found this behavior, and the corresponding scaling distribution is quite robust in the sense that, it seems, it is independent of the initial velocity distribution. In case of a randomly chosen agent the distribution of m/t, in the limit $t \to \infty$, converges to the distribution of velocity itself, with a Galilean shift by the mean velocity. The finite but large time behavior of the same is also discussed in cases of four different initial velocity distributions.

In the fourth chapter, we consider a Jepsen gas on a ring to the study finite-size effects on the statistics of net overtaking number by a tagged agent. We discuss the problem with two different ensembles. In the first, we take a fixed number

of particles distributed randomly within the system whereas, in the next, the randomly distributed particle numbers in different ensembles are chosen according to the Poisson distribution. With a fixed number of agents, we first derive an approximate result of the net overtaking number by a tagged agent of known velocity. By using this result, we calculate all the corresponding cumulants, and hence, the conditional probability distribution in case of four different initial velocity distributions, namely, uniform, Gaussian, exponential, and power-law distributions. In addition to that the unconditional probability distribution of the net overtaking number by a randomly chosen tagged agent is also calculated. We revise all these quantities of interest in case of 2nd ensemble including a brief introduction of finite size scaling analysis and the dynamical exponent. Exact or approximate analytical results are presented in all cases with the support of the numerical simulation.

In the final chapter, we consider a periodic one-dimensional lattice with each site occupied by a singly-seated, self-driven agent to study how the finite system size affects the statistics of the net overtaking number by a tagged agent. The self-driven character of the agents is assigned by constant but random initial velocities by drawing them independently from a common distribution. In time, each pair of agents at adjacent sites exchange their positions with a specified rate while retaining their respective velocities. Depending on this exchange rate we discuss three different cases: in the 1st case a pair of agents exchange their positions at the rate 1, independent of their velocities. The velocity-independent exchange makes the net overtaking number by a tagged agent to execute a simple random walk on the lattice without being affected by the finite system size. In the next two cases, exchange of position occurs only if the velocity of the "left" is higher with the rate 1 and equal to the modulus of their relative velocity, respectively. The effects of the finite system size are obtained in both cases while we are studying the conditional and the unconditional distribution of the net overtaking number by a tagged agent. Besides that, in case II, we compute the dynamical exponent $z = 3/2$ using the finite-size scaling analysis. Taking cues from this case, we have found the golden mean $z = (1 + \sqrt{5})/2 \simeq 1.618$ in case III. Finally, in the end, we summarize our results with possible future directions.

Bibliography

[1] L. D. Landau, and E. M. Lifshits, *Statistical Physics, Volume 5,* (Butterworth-Heinemann, Oxford, 1999).

[2] Huang Kerson. *Introduction to statistical physics.* CRC Press, 2001.

[3] Reif Frederick. *Fundamentals of statistical and thermal physics.* Waveland Press, 2009.

[4] Plischke Michael and Bergersen Michael. *Equilibrium statistical physics.* World Scientific,2006.

[5] Kardar, M., *Statistical Physics of Particles,* (Cambridge University Press, Cambridge, 2008).

[6] Callen Herbert B. *Thermodynamic and an introduction to thermo-statistics.* John Wiley Sons, 2006.

[7] Zemansky Mark Waldo. *Heat and thermodynamics.* McGraw-Hill, 1957.

[8] Kubo, R. (1966) Rep. Prog. Phys. **29**, 255284.

[9] T.M. Liggett, Interacting Particle Systems (New York: Springer-Verlag, 1985).

[10] H. Spohn, Large scale dynamics of Interacting Particles (Springer-Verlag, New York, 1991).

[11] T. M. Liggett, Stochastic Models of Interacting Systems:Contact, Voter and Exclusion Processes, Springer-Verlag New-York, (1999).

[12] Kipnis C and Landim C 1999 Scaling Limits of Interacting Particle Systems (Berlin: Springer).

[13] L. Bertini, A. De Sole, D. Gabrielli, G. Jona-Lasinio,and C. Landim, J. Stat. Mech. (2007) P07014.

[14] D. Helbing, Rev. Mod. Phys. **73**, 1067(2001).

[15] A. Schadschneider, D. Chowdhury, K. Nishinari, Stochastic Transport in Complex Systems (Elsevier, 2010).

[16] J. Krug. Boundary-induced phase transitions in driven diffusive systems. *Phys. Rev. Lett.*, 67:1882, 1991.

[17] T. Vicsek, A. Czirok, E. Ben-Jacob, I. Cohen, and O. Shochet, Noveltype of phase transition in a system of self-driven particles, Phys. Rev. Lett., vol. 675, no. 6, pp. 12261229, Aug. 1995.

[18] C. Huepe and M. Aldana, Phys. Rev. Lett. **92**, 168701 (2004).

[19] K. Pearson Nature. **72**, 294 (1905).

[20] Chandrasekhar S (1943) Stochastic problems in physics and astronomy *Rev. Mod. Phys.* **15** 1.

[21] Weiss G H (1994) *Aspects and Applications of the Random Walk* (Amsterdam: North-Holland).

[22] Hughes B D (1995) *Random Walks and Random Environments* (Oxford: Clarendon Press).

[23] J. W. Haus and K. W. Kehr, Phys. Rep. **150**, 263 (1987).

[24] J.P. Bouchaud and A. Georges, Phys. Rep., **195** (1990), 127.

[25] N. G. VanKampen, *Stochastic Processes in Physics and Chemistry* (North-Holland, Amsterdam, 1992).

[26] H. Touchette, Phys. Rep. **478**, 1 (2009).

[27] C. T. MacDonald, J. H. Gibbs, and A. C. Pipkin. Kinetics of biopolymerization on nucleic acid templates. *Biopolymers*, 6(1), 1968.

[28] C. T. MacDonald and J. H. Gibbs. Concerning the kinetics of polypeptidesynthesis on polyribosomes. *Biopolymers*, 7:707, 1969.

[29] F Spitzer. Interaction of markov processes. *Adv. Math.*, 5:246, 1970.

[30] S. Katz, J. L. Lebowitz and H. Spohn, Nonequilibrium steady states of stochastic lattice gas models of fast ionic conductors, J. Stat. Phys. 34, 497 (1984).

[31] B. Derrida, S.A. Janowski, J. L. Lebowitz and E. R. Speer, Exact solution of the totally asymmetric exclusion process: shock profiles, J. Stat. Phys. 73, 813 (1993).

[32] B. Derrida, An exactly soluble non-equilibrium system: the asymmetric simple exclusion process, Phys. Rep. 301, 65 (1998).

[33] B. Schmittmann and R.K.P. Zia, *Statistical Mechanics of Driven Diffusive Systems* (Academic Press, 1995).

[34] P.L. Krapivsky, S. Redner and E. Ben-Naim, A Kinetic View of Statistical Physics, Cambridge University Press, New York, 2010.

[35] P.L. Ferrari and H. Spohn, Scaling limit for the space-time covariance of the stationary totally asymmetric simple exclusion process, Comm. Math. Phys. 265 (2006), 144.

[36] Lighthill M J and Whitham G B 1955 On kinematic waves: II. A theory of traffic flow on long crowded roads, Proc. R. Soc. A **229** 317.

[37] G. B. Whitham, Linear and Nonlinear Waves (John Wiley & Sons, New York, 1974).

[38] M. Kardar, G. Parisi, and Y.-C. Zhang,Phys. Rev. Lett. 56, 889 (1986).

[39] Spohn, H.: Nonlinear fluctuating hydrodynamics for anharmonic chains. J. Stat. Phys. 154(5), 11911227 (2014).

[40] Spohn, H.: The Kardar–Parisi–Zhang equation-a statistical physics perspective. arXiv preprintarXiv:1601. 00499 (2016).

[41] Corwin, I.: The Kardar–Parisi–Zhang equation and universality class. Random Matrices Theory Appl1, 113001 (2012).

[42] Kriecherbauer, T., Krug, J.: A pedestrians view on interacting particle systems, KPZ universality, andrandom matrices. J. Phys. A43, 403001 (2010).

[43] H. E. Stanley, *Scaling, universality, and renormalization: three pillars of modern critical phenomena*, Rev. Mod. Phys.*71*, S358 (1999).

[44] Goldenfeld N 1992 Lectures on phase transitions and the renormalization group (Reading: Addison-Wesley).

[45] H. E. Stanley, Introduction to Phase Transitions and Critical Phenomena (Oxford University Press, Oxford, 1971).

[46] S. Edwards, Proc. R. Soc. London, Ser. A **381**, 17 (1982).

[47] M. Plischke, Z. Racz, and D. Liu, Phys. Rev. B 35, 3485 (1987).

[48] A. L. Barabasi and H.E. Stanley, Fractal Concepts in Surface Growth (Cambridge University Press, Cambridge, 1995).

[49] Prhofer, M., Spohn, H.: Current fluctuations for the totally asymmetric simple exclusion process. In: In and out of equilibrium (V. Sidoravicius, ed.), Progress in Probability, Boston Basel: Birkhuser, 2002.

[50] See M. Prhofer and H. Spohn (2003). https://www-m5.ma.tum.de/KPZ to numerically obtain $G_{scaling}(x)$.

[51] J. Baik, P.L. Ferrari, and S. Pch, Convergence of the two-point function of the stationary TASEP, arXiv:1209.0116 (2012).

[52] R.A. Blythe and M.R. Evans, *Nonequilibrium Steady States of Matrix Product Form: A Solver's Guide*, J. Phys. **A40** (2007) R333-R441.

[53] P. A. Ferrari, Shock fluctuations in the asymmetric simple exclusion, Prob. Theor. Rel. Fields 91, 81 (1992).

[54] P. A. Ferrari, L. R. G. Fontes, Current fluctuations for the asymmetric exclusion process, Ann. Prob. 22, 1 (1994).

[55] P. A. Ferrari, C. Kipnis, Second class particle in the rarefaction fan, Inst. H. Poincare **31** 143-154 (1995).

[56] Ferrari, P. A. and Martin, J. B. (2007). Stationary distributions of multi-type totally asymmetric exclusion processes. Ann. Probab. 35 807832. MR2319708

[57] M. Evans, P. Ferrari, and K. Mallick *Matrix representation of the stationary measure for the multispecies TASEP*, J. Stat. Phys., 135:217, (2009).

[58] C. Arita, A. Ayyer, K. Mallick and S. Prolhac, *Recursive structures in the multispecies TASEP*, J. Phys. **A44** (2011) 335004.

[59] Amir,G., Angel,O. and Valko, B. (2011). The TASEP speed process. *Ann.Probab.* **39** 12051242. MR2857238.

[60] K. Nagel and M. Schreckenberg: J. Physique I, **2**, 2221 (1992).

[61] O. Bihem, A. A. Middleton, and D. Levine, Phys. Rev. A **46**, R6124 (1992).

[62] Benjamini I, Ferrari P A and Landim C *Asymmetric conservative processes with random rates* 1996 Stoch. Proc. Appl. 61 181.

[63] Krug J and Ferrari P A *Phase transitions in driven diffusive systems with random rates* 1996 J. Phys. A: Math. Gen. 29 L465.

[64] Evans M R *bose-einstein condensation in disordered exclusion models and relation to traffic flow* 1996 Europhys. Lett. 36 13.

[65] Karimipour V 1999 Multispecies asymmetric simple exclusion process and its relation to traffic flow Phys.Rev. E 59 20512.

[66] D. Chowdhury, L. Santen, and A. Schadschneider, Phys. Rep. **329**, 199 (2000).

[67] M. Schliwa and G. Woehlke, Nature **422**, 759 (2003).

[68] R. Lipowsky, Y. Chai, S. Klumpp, S. Liepelt, and M. J. I. Müller, Physica A **372**, 34 (2006).

[69] A. Ward and M. Webster, *Sociality: The Behaviour of Group-Living Animals* (Springer 2016).

[70] R H Davis and A Acrivos, Ann. Rev. Fluid Mech. **17**, 91 (1985).

[71] J. A. G. M. de Visser and J. Krug, Nat. Rev, Genet. **15**, 480 (2014).

[72] J. Krug and C. Karl, Physica A **318**, 137 (2003).

[73] K. Jain and J. Krug, J. Stat. Mech. P04008 (2005).

[74] C. Sire, S. N. Majumdar, D. S. Dean, J. Stat. Mech., L07001 (2006).

Chapter 2

Statistics of overtakes by a tagged agent in Jepsen gas

2.1 Introduction

Jepsen gas is named after Jepsen for his work [1] in the discipline of interacting many particles [2, 3]. In his work, Jepsen considers a collection of equal-mass point particles distributed on a line. All these particles are assigned constant but random velocities at the beginning. This system evolves via elastic collisions between the neighboring pairs. Notably, an elastic collision between two equal-mass particles can only exchange their velocities. These elastic collisions alongside the equal-mass condition allow us to redefine the model as a collection of non-interacting point particles moving with their constant but random initial velocities. With this representation, the system becomes a prototype of non-interacting self-driven [4, 5] particle system. The primary feature of this kind of system is the persistent motion of individual agents in a given direction.

One particular phenomenon commonly seen in self-driven particle systems is overtaking. In an overtaking event, an agent with a higher degree of persistence can go ahead of an agent with a lower degree of persistence. In this chapter, our goal is to study this phenomenon in this simple non-interacting particle system. Notably, our model is quite similar to the real system of multilane vehicular traffic flow in the low-density limit. It is because, in that condition, each vehicle moves on an average with a constant velocity without any traffic jam (which may cause interaction and may bring a drastic change in velocity).

The rest of the chapter is organized as follows. First, in Sec. 2.2, we introduce our

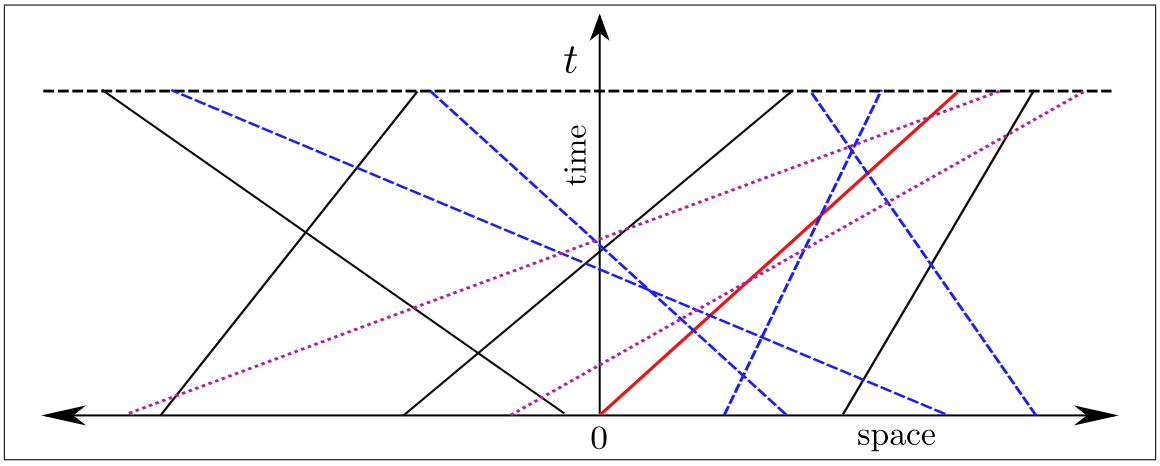

Figure 2.1: Space-time trajectories of particles in a Jepsen gas is presented. The red line starting at the origin depicts the trajectory of a tagged particle. The four blue lines represent the trajectories of particles which cross the red line from right to left in time t and the two magenta lines depicts the trajectory of the particles that cross the red line from left to right in time t. In other words, the red line overtakes the blue lines, whereas the magenta lines overtake the red line. Therefore, the net number of overtakes for the red line in the figure is $4 - 2 = 2$.

model with our quantities of interest. In Sec. 2.2.3 we briefly discuss the four initial velocity distributions which we are going to use repeatedly in this chapter as well as throughout the thesis. After that, in Sec. 2.3 we study the distribution of net overtaking number by a tagged agent of known velocity followed by a discussion of the same for a randomly chosen tagged agent without knowing its exact velocity by considering a constant density of agents. Instead of the constant density of agents, similar quantities of interest are investigated by fixing a constant gap between all neighboring agents in Sec. 2.4.

2.2 Model and necessary ingredients

2.2.1 The model

Consider a collection of non-interacting point particles distributed on a line. All these particles are moving with their constant velocities which are taken independently for each particle from an identical distribution $\rho(v)$ at the beginning. The space-time trajectories of the particles are given by slanted straight lines where the

slopes with respect to the time-axis represent the velocities (see FIG. 2.1). Notably, any two lines in this system can cross each other at the most once. We investigate here the net number of overtaking by a tagged agent in a given duration of time. It is given by the number of lines crossing the tagged line from the right minus the number of lines crossing it from the left within a given duration of time (as illustrated in FIG. 2.1).

Two different initialization : Constant density and constant gap

Now depending on the arrangement of particles on the line, in this chapter, we study two different cases. In the 1st case, we consider a fixed (or constant) initial density of particles, whereas in the next we set a constant initial gap between all neighboring particles.

2.2.2 Quantities of interest

Net overtaking number :

Our goal here is to investigate the net number of overtakings by a tagged particle in a given duration of time. Let us denote this number by $m(t|v_0)$ for a tagged agent of velocity v_0 at time t. This number is equal to the number of lines intersecting the tagged line from the right ($m_R(t|v_0)$) minus the number of lines intersecting it from the left ($m_L(t|v_0)$), in a given duration t, *i.e.,*

$$m(t|v_0) = m_R(t|v_0) - m_L(t|v_0) \tag{2.1}$$

(see illustration in FIG. 2.1). First, we study the mean and the variance of $m(t|v_0)$. We denote them by $\langle m(t|v_0)\rangle$ and $\langle m^2(t|v_0)\rangle_c$ respectively.

Two different distributions : Conditional and Unconditional distributions

Apart from the mean and the variance, we extend our studies for the n-th order cumulants $\langle m^n(t|v_0)\rangle_c$, and hence, for the complete probability distribution $p(m, t|v_0)$. For convenience, we call $p(m, t|v_0)$ the conditional distribution of $m(t|v_0)$. Alongside

that, we also study the probability distribution of a randomly chosen tagged agent. We name this distribution as unconditional distribution and denote it by $P(m,t)$. Clearly, $P(m,t)$ can be obtained by integrating $p(m,t|v_0)$ over all v_0 with the weight of $\rho(v_0)$ i.e.,

$$P(m,t) = \int_{-\infty}^{\infty} dv_0 \; \rho(v_0) \; p(m,t|v_0). \tag{2.2}$$

2.2.3 Four different velocity distributions

Throughout the thesis, we mainly discuss our results by considering four different velocity distributions. In this section, we introduce their explicit form with some essential features. The distributions are respectively

$$(i) \;\; \text{Gaussian} : \rho(v) = \frac{e^{-\frac{v^2}{2}}}{\sqrt{2\pi}} \; ; \; v \in (-\infty : \infty), \tag{2.3}$$

$$(ii) \;\; \text{Uniform} : \;\; \rho(v) = \frac{1}{2} \; ; \; v \in [-1 : 1], \tag{2.4}$$

$$(iii) \;\; \text{Exponential} : \;\; \rho(v) = e^{-v} \; ; \;\; v \in [0 : \infty), \tag{2.5}$$

$$(iv) \;\; \text{Power-law} : \;\; \rho(v) = \frac{\nu}{v^{1+\nu}} \; ; \; v \in [1 : \infty), \; \nu > 0 \; . \tag{2.6}$$

First two distributions are symmetric while the last two are asymmetric with respect to the mean of the distribution $\langle v \rangle$. From another viewpoint, the first three distributions have all finite moments while the last one has diverging moments. The behavior of the last, namely the power-law distribution, is entirely characterized by its exponent ν. Notably, it is a simple version of the Pareto distribution [6]. If we consider ν lying within $0 < \nu \leq 1$, the distribution has diverging moments. Following the thread, for $1 < \nu \leq 2$, only the first moment $\langle v \rangle = \nu/(\nu - 1)$ exist with all diverging higher moments. Similarly, for $2 < \nu \leq 3$, only the first two moments, $\langle v \rangle = \nu/(\nu-1)$ and $\langle v^2 \rangle = \nu/(\nu-2)$ exist, and so on. Note that the integer values of $\nu = 1, 2, 3, ...$ correspond the logarithmic divergence of the lowest diverging moment. Now, for further convenience, we summarize the n-th order moment or cumulant of

the above distributions as follows:

$$\langle v^n \rangle_c = \begin{cases} 1 & \text{for } n = 2 \\ 0 & \text{otherwise} \end{cases} \text{ (Gaussian)}, \tag{2.7}$$

$$\langle v^n \rangle = \begin{cases} 1/(n+1) & \text{for even n} \\ 0 & \text{for odd n} \end{cases} \text{ (Uniform)}, \tag{2.8}$$

$$\langle v^n \rangle_c = (n-1)! \text{ (Exponential)}, \tag{2.9}$$

$$\langle v^n \rangle = \begin{cases} \nu/(\nu - n) & \text{for } n < \nu \\ \infty & \text{for } n \geq \nu \end{cases} \text{ (Power law)}. \tag{2.10}$$

The subscript c in Eq. (2.7) and (2.9) denotes for the cumulant.

2.3 Constant density of agents

In this section, we discuss the statistics of the net overtaking number by fixing the density of the agents. For convenience, we denote this density by ϱ. It implies that within a large segment N on the line the distribution of the total number of particles would be the Poisson distribution with the mean number ϱN. Now, we calculate the rate of overtaking by a tagged velocity followed by our quantities of interest.

2.3.1 Rate of overtaking

Since, the initial positions as well as the velocities of the particles chosen independently, all the crossings in this case are mutually independent. For a particle starting at a position $x > 0$ with velocity v to cross the tagged particle that starts at the origin with velocity v_0, between time t and $t+dt$, one must have $t < x/(v_0 - v) < t + dt$ with $v_0 > v$. Since, x can be anywhere in $(0, \infty)$ with a probability density ϱ and v drawn from $\rho(v)$, the probability of the two particles crossing between t to $t + dt$ is

$$\rho_R(v_0)dt = \varrho \int_0^\infty dx \int_{-\infty}^{v_0} dv\ \rho(v) \left[\delta \left(t - \frac{x}{v_0 - v} \right) dt \right]. \tag{2.11}$$

Using, $\delta\left(t-\frac{x}{v_0-v}\right)=(v_0-v)\delta(x-(v_0-v)t)$ and then carrying out the integration over x, gives the rate of crossing the tagged particle from the right at time t as follows

$$\begin{aligned}\rho_R(v_0) &= \varrho \int_{-\infty}^{v_0} dv\ \rho(v)\ (v_0-v) \int_0^{\infty} dx\ \delta\left(x-t(v_0-v)\right) \\ &= \varrho \int_{-\infty}^{v_0} (v_0-v)\ \rho(v)\ dv.\end{aligned} \tag{2.12}$$

Similarly, in case of the rate of crossing the tagged particle from the left between t to $t+dt$ we can proceed as follows

$$\begin{aligned}\rho_L(v_0)\ dt &= \int_{-\infty}^{0} \varrho\ dx \int_{v_0}^{\infty} dv\ \rho(v) \left[\delta\left(t-\frac{-x}{(v-v_0)}\right) dt\right] \\ &= \varrho\ dt \int_{v_0}^{\infty} dv\ \rho(v)\ (v-v_0) \int_{-\infty}^{0} dx\ \delta\left(x+t(v-v_0)\right).\end{aligned} \tag{2.13}$$

It further simplifies the corresponding rate as

$$\rho_L(v_0) = \varrho \int_{v_0}^{\infty} (v-v_0)\ \rho(v)\ dv. \tag{2.14}$$

Note that the stochasticity in the problem arises from the randomness of initial positions as well as from the velocity of agents. It is quite clear from Eq. (2.12) and (2.14) that the randomness in positions come out from initial density ϱ whereas the same for the velocity arise from velocity distribution the $\rho(v)$. Note that, instead of constant density of agents if we fix the gap between all neighboring agents, then the initial position of the particles no longer remain independent of each other. Hence, in that case, it is not possible to apply the similar formalism to find out the underlying rates.

2.3.2 Cumulants of net overtaking number

In this case we can decompose the net number of overtaking events of v_0 upto time t as $m(t|v_0) = m_R(t|v_0) - m_L(t|v_0)$ where $m_R(t|v_0)$ ($m_L(t|v_0)$) is the number of agents that were on the right (left) of v_0 at time $t=0$ and reach to the left (right) of the same before time t. Since we know, the intersecting rates from the right and the

left of a given tagged v_0, we can find out the average number of overtake events, i.e., $\langle m(t|v_0)\rangle$ in a given duration of time t. To do so, we first note that the average number of agents that were on the right of v_0 at time $t = 0$ and reach to the left of the same at time t is $\langle m_R(t|v_0)\rangle = \rho_R(v_0)t$. Similarly, $\langle m_L(t|v_0)\rangle = \rho_L(v_0)t$. By using Eq. (2.12) and (2.14) we can get

$$\langle m(t|v_0)\rangle = (\rho_R(v_0) - \rho_L(v_0))t = \varrho(v_0 - \langle v\rangle)t. \tag{2.15}$$

Note that the angular brackets from here onwards denote the ensemble average.

Now, to find out the higher-order cumulants of $m(t|v_0)$ we first identify that the process associated with the intersecting rates are Poissonian. It implies that the n-th order cumulant of $m_R(t|v_0)$ and $m_L(t|v_0)$ are respectively $\langle m_R^n(t|v_0)\rangle_c = \rho_R(v_0)t$ and $\langle m_L^n(t|v_0)\rangle_c = \rho_L(v_0)t$. Using these results we find

$$\begin{aligned}\langle m^n(t|v_0)\rangle_c &= \left[\frac{d^n}{ds^n}\ln\left\langle e^{sm(t|v_0)}\right\rangle\right]_{s=0} = \left[\frac{d^n}{ds^n}\left(\ln\left\langle e^{sm_R(t|v_0)}\right\rangle + \ln\left\langle e^{-sm_L(t|v_0)}\right\rangle\right)\right]_{s=0} \\ &= \langle m_R^n(t|v_0)\rangle_c + (-1)^n\,\langle m_L^n(t|v_0)\rangle_c = (\rho_R(v_0) + (-1)^n\rho_L(v_0))\,t. \end{aligned} \tag{2.16}$$

2.3.3 Conditional Distribution

As the initial positions and the velocities of the particles are chosen independently, all the crossings in this case are mutually independent. It makes the rate of overtaking the trajectory of the tagged agent of velocity v_0 from the left and right are also independent. As all the crossings from a given direction, say from the right, are point events and thay are independent to each other, we can say these crossings constitute a Poisson process of rate $\rho_R(v_0)$. It allows us to write the probability of $m_R(t|v_0)$ number of crossings the trajectory of the tagged agent of velocity v_0 from the right (R) of the form:

$$p_+(m_R, t|v_0) = e^{-\rho_R(v_0)\,t}\,\frac{[\rho_R(v_0)t]^{m_R}}{m_R!}. \tag{2.17a}$$

Similarly, the probability of $m_L(t|v_0)$ number of crossings the trajectory of the tagged agent of velocity v_0 from the left (L) can be written as

$$p_-(m_L, t|v_0) = e^{-\rho_L(v_0)\, t}\ \frac{[\rho_L(v_0)t]^{m_L}}{m_L!}. \tag{2.17b}$$

It enable us to write the probability $p(m, t|v_0)$ that there are $m \geq 0$ more crossings from the right than from the left [7] as

$$\begin{aligned} p(m \geq 0, t|v_0) &= \sum_{l\geq 0} p_+(l+m, t|v_0)\ p_-(l, t|v_0) \\ &= e^{-[\rho_R(v_0)\, +\rho_L(v_0)]t}\ \{\rho_R(v_0)t\}^m \sum_{l\geq 0}\ \frac{\{\rho_R(v_0)\ \rho_L(v_0)t^2\}^l}{(l+m)!\ l!} \\ &= e^{-[\rho_R(v_0)\, +\rho_L(v_0)]t}\ \left(\frac{\rho_R(v_0)}{\rho_L(v_0)}\right)^{m/2}\ \mathcal{I}_m(u) \end{aligned} \tag{2.18a}$$

where $u = 2t\sqrt{\rho_R(v_0)\ \rho_L(v_0)}$ and

$$\mathcal{I}_m(u) = \left(\frac{u}{2}\right)^m \sum_{l\geq 0}\ \frac{1}{(l+m)!\ l!}\ \left(\frac{u}{2}\right)^{2l} \tag{2.18b}$$

is the modified Bessel function of the first kind. Similarly, the probability that there are $m \leq 0$ more crossings from the left than from the right can be written as follows

$$\begin{aligned} p(m \leq 0, t|v_0) &= \sum_{l\geq 0} p_-(l-m, t|v_0)\ p_+(l, t|v_0) \\ &= e^{-[\rho_R(v_0)\, +\rho_L(v_0)]t}\ \left(\frac{\rho_R(v_0)}{\rho_L(v_0)}\right)^{m/2}\ \mathcal{I}_{-m}(u). \end{aligned} \tag{2.19}$$

Combining Eq. (2.18a) and (2.19) one can write the distribution for any integer m as

$$p(m, t|v_0) = e^{-[\rho_R(v_0)\, +\rho_L(v_0)]t}\ \left(\frac{\rho_R(v_0)}{\rho_L(v_0)}\right)^{m/2}\ \mathcal{I}_{|m|}(u). \tag{2.20}$$

This final distribution is known as Skellam distribution [8].

Now, using Eq. (2.12) and (2.14) we can easily calculate the intersecting rates

associated with v_0 in case of each velocity distribution as follows

$$\text{Uniform}: \quad \rho_R(v_0) = \tfrac{1}{4}\varrho(1+v_0)^2, \tag{2.21a}$$
$$\rho_L(v_0) = \tfrac{1}{4}\varrho(1-v_0)^2, \tag{2.21b}$$

$$\text{Gaussian}: \quad \rho_R(v_0) = \tfrac{1}{\sqrt{2\pi}}\varrho\, e^{-v_0^2/2} + \tfrac{1}{2}\varrho v_0\left(1+\text{Erf}\left[\tfrac{v_0}{\sqrt{2}}\right]\right), \tag{2.22a}$$
$$\rho_L(v_0) = \tfrac{1}{\sqrt{2\pi}}\varrho\, e^{-v_0^2/2} - \tfrac{1}{2}\varrho v_0\left(1-\text{Erf}\left[\tfrac{v_0}{\sqrt{2}}\right]\right), \tag{2.22b}$$

$$\text{Exponential}: \quad \rho_R(v_0) = \varrho\left(v_0 - 1 + e^{-v_0}\right), \tag{2.23a}$$
$$\rho_L(v_0) = \varrho\, e^{-v_0}, \tag{2.23b}$$

$$\text{Power-law}: \quad \rho_R(v_0) = \varrho\left(v_0 - \tfrac{\nu}{\nu-1}\right) + \varrho\tfrac{v_0^{1-\nu}}{\nu-1}, \tag{2.24a}$$
$$\rho_L(v_0) = \varrho\tfrac{v_0^{1-\nu}}{\nu-1}. \tag{2.24b}$$

Note that in case of power-law distribution it is clear from Eq. (2.24) the exponent ν must be greater than 1. Now, by plugging these intersecting rates of each velocity distribution in Eq. (2.20) we obtain $p(m,t|v_0)$ which we have plotted in terms of a scaled variable $y = (m(t|v_0) - \langle m(t|v_0)\rangle)/\sqrt{\langle m^2(t|v_0)\rangle_c}$ and verified by numerical simulation in FIG. 2.2. A Gaussian approximated result, obtained by truncating the contribution of higher than 2nd order cumulants of $m(t|v_0)$, is also plotted in each case for comparison.

2.3.4 Unconditional Distribution

In the case of unconditional distribution, we find that it is convenient to discuss it in terms of scaling variable $c = m/t\varrho$. From Eq. (2.16) it is clear that $\langle c^n(t|v_0)\rangle_c \propto t^{1-n}$. It implies that all the higher order cumulants except the first one $\langle c(t|v_0)\rangle = v_0 - \langle v\rangle$ converges to zero in the limit $t \to \infty$. It allows us to write the conditional distribution of c as $p(c, t\to\infty|v_0) = \delta(c - v_0 + \langle v\rangle)$. Now, using Eq. (2.2) we can get

$$P(c, t\to\infty) = \int_{-\infty}^{\infty} dv_0\ \rho(v_0)\ \delta(c - v_0 + \langle v\rangle) = \rho(c + \langle v\rangle). \tag{2.25}$$

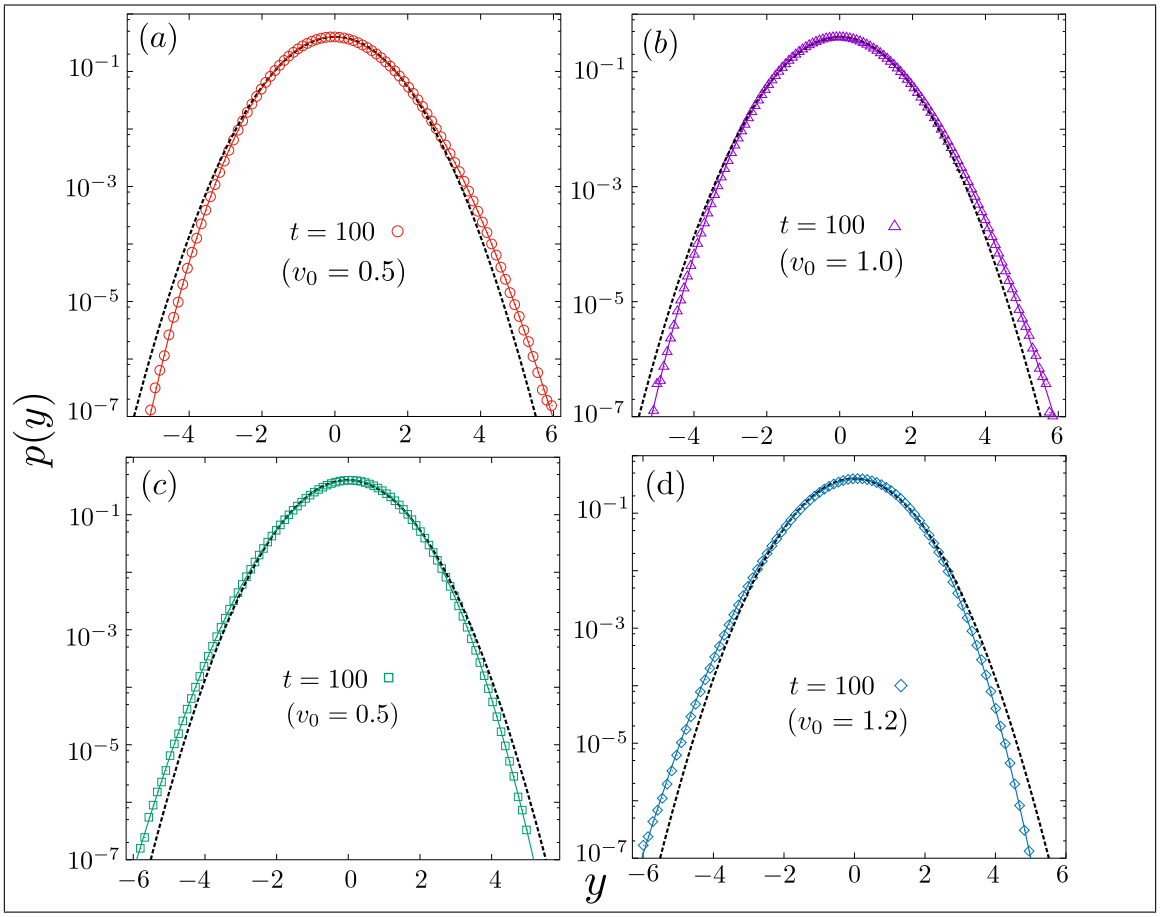

Figure 2.2: Probability distribution function $p(y)$ of the scaled net overtakings $y = (m(t|v_0) - \langle m(t|v_0)\rangle)/\sqrt{\langle m^2(t|v_0)\rangle_c}$ are plotted for a given v_0 at time $t = 100$, for the Jepsen gas, with four different choices of the initial velocity distribution, namely, (a) uniform (b) Gaussian (c) exponential and (d) power-law ($\nu = 5/2$) distributions. The discrete points in each plot are the simulation results which show good agreements with the results coming from Eq. (2.20) including Gaussian approximated results shown by the dotted line in each case.

It implies that the distribution of the net overtaking number of a randomly picked agent while rescaled with time and density converges to the initial velocity distribution with a Galilean shift by the mean of the distribution in the limit of $t \to \infty$.

Now, we focus on finite but large time behavior of $P(c, t)$. The exact analytical result is challenging to find out. However, writing down Eq. (2.2) in terms of c, we can numerically integrate it and find out the result that shows a good agreement with the numerical simulation result as displayed in FIG. 2.3. Although the exact analytical result is hard to find out, one can estimate the tail behaviors of $P(c, t)$.

Hence, in the next, we consider each one of four $\rho(v)$ one by one to discuss the behavior of the tails.

Uniform $\rho(v)$:

First, for uniform distribution, it is clear from the simulation result that at any finite time the distribution has two different tails, namely the right (R) and the left (L) around $c \gtrsim 1$ and $c \lesssim -1$ respectively. For the right, we can say that its contribution comes from all Poissonian processes with rates $\rho_R(v_0) = \varrho(1+v_0)^2/4$ over all possible values of v_0 i.e., $v_0 \in [-1:1]$. It allows us to approximately write

$$P_R(c \gtrsim 1, t) \simeq \varrho t \int_{-1}^{1} dv_0 \; \rho(v_0) \; p_+(c\varrho t, t|v_0)$$

$$\simeq \frac{\varrho t}{2(c\varrho t)!} \int_{-1}^{1} dv_0 \; \mathrm{Exp}\left[-\frac{\varrho t}{4}(1+v_0)^2\right] \left(\frac{\varrho t}{4}(1+v_0)^2\right)^{c\varrho t}.$$

First, by using the Stirling's approximation $x! \simeq \sqrt{2\pi x}\; (x/e)^x$, and then, carrying out intergration, we can obtain

$$P_R(c \gtrsim 1, t) \simeq \frac{1}{2}\sqrt{\frac{\varrho t}{2\pi c}} \left(\frac{e}{4c}\right)^{c\varrho t} \int_{-1}^{1} dv_0 \; \mathrm{Exp}\left[-\frac{\varrho t}{4}(1+v_0)^2\right] \; (1+v_0)^{2c\varrho t}$$

$$\simeq \frac{1}{2\sqrt{2\pi c}} \left(\frac{e}{c\varrho t}\right)^{c\varrho t} \; \gamma\left(c\varrho t + \frac{1}{2}, \varrho t\right) \tag{2.26}$$

where $\gamma(s,t) = \int_0^t dx \; e^{-x} x^{s-1}$ is the lower incomplete gamma function. Similarly, for the left tail (L) we can argue that its contribution comes from all Poissonian processes with rates $\rho_L(v_0) = \varrho(1-v_0)^2/4$ over all possible values of v_0. Following similar arguments like above, we can derive the result in this case also. The left-right symmetry of the result allow us to write

$$P_{\mathrm{tail}}(|c| \gtrsim 1, t) \simeq \frac{1}{2\sqrt{2\pi|c|}} \left(\frac{e}{|c|\varrho t}\right)^{|c|\varrho t} \; \gamma\left(|c|\varrho t + \frac{1}{2}, t\varrho\right). \tag{2.27}$$

The result we obtain here is showing a good agreement with the numerical simulation result as shown in the inset of FIG. 2.3 (a).

Gaussian $\rho(v)$:

Next, in case of the Gaussian distribution, we can argue that the contribution of its right tail comes mostly from large values of v_0, i.e., $v_0 >> 0$. It allows us to approximate $\rho_R(v_0)$ in Eq. (2.22) as $\rho_R(v_0) \simeq \varrho v_0$. Now using the above formalism we can write and proceed as follows

$$P_R(c >> 0, t) \simeq \frac{\varrho t}{(c\varrho t)!} \int_0^\infty dv_0 \, \frac{e^{-v_0^2/2}}{\sqrt{2\pi}} \, e^{-\varrho v_0 t} (\varrho v_0 t)^{c\varrho t}$$

$$\simeq \sqrt{\frac{\varrho t}{2\pi c}} \left(\frac{e}{c}\right)^{c\varrho t} \int_0^\infty dv_0 \, \frac{e^{-v_0^2/2}}{\sqrt{2\pi}} \, e^{-\varrho t \, \phi_0(v_0, c)}$$

where $\phi_0(v_0, c) = v_0 - c \log(v_0)$. In the limit of large t using the Saddle point method of asymptotic expansion we can get

$$\simeq \sqrt{\frac{\varrho t}{2\pi c}} \int_{-\infty}^\infty dv_0 \, \frac{e^{-v_0^2/2}}{\sqrt{2\pi}} \, \mathrm{Exp}\left[-\frac{t\varrho}{2c}(v_0 - c)^2\right] \simeq \frac{1}{\sqrt{2\pi(1 + \frac{c}{\varrho t})}} \mathrm{Exp}\left[-\frac{c^2 \varrho t}{2(c + \varrho t)}\right]$$

$$\simeq \frac{e^{-c^2/2}}{\sqrt{2\pi}} \left(1 + \frac{c(c^2 - 1)}{2\varrho t}\right) + \mathcal{O}(t^{-2}). \tag{2.28}$$

From the symmetry of the problem in this case also we can write

$$P_{\text{tail}}(|c| >> 0, t) \simeq \frac{e^{-c^2/2}}{\sqrt{2\pi}} \left(1 + \frac{|c|(c^2 - 1)}{2\varrho t}\right) + \mathcal{O}(t^{-2}). \tag{2.29}$$

The obtained result is showing a good agreement with the numerical simulation result as shown in the inset of FIG. 2.3(b).

Exponential $\rho(v)$:

Now, for exponential distribution, we can argue that the contribution of $P_R(c, t)$ comes from all Poissonian processes with rates $\rho_R(v_0) = \varrho(v_0 - 1 - e^{-v_0}) \simeq \varrho(v_0 - 1)$ over all possible $v_0 >> 1$. To obtain the behavior we proceed as follows

$$P_R(c >> -1, t) \simeq \varrho t \int_0^\infty dv_0 \, e^{-v_0} \, p_+(c\varrho t, t | v_0)$$

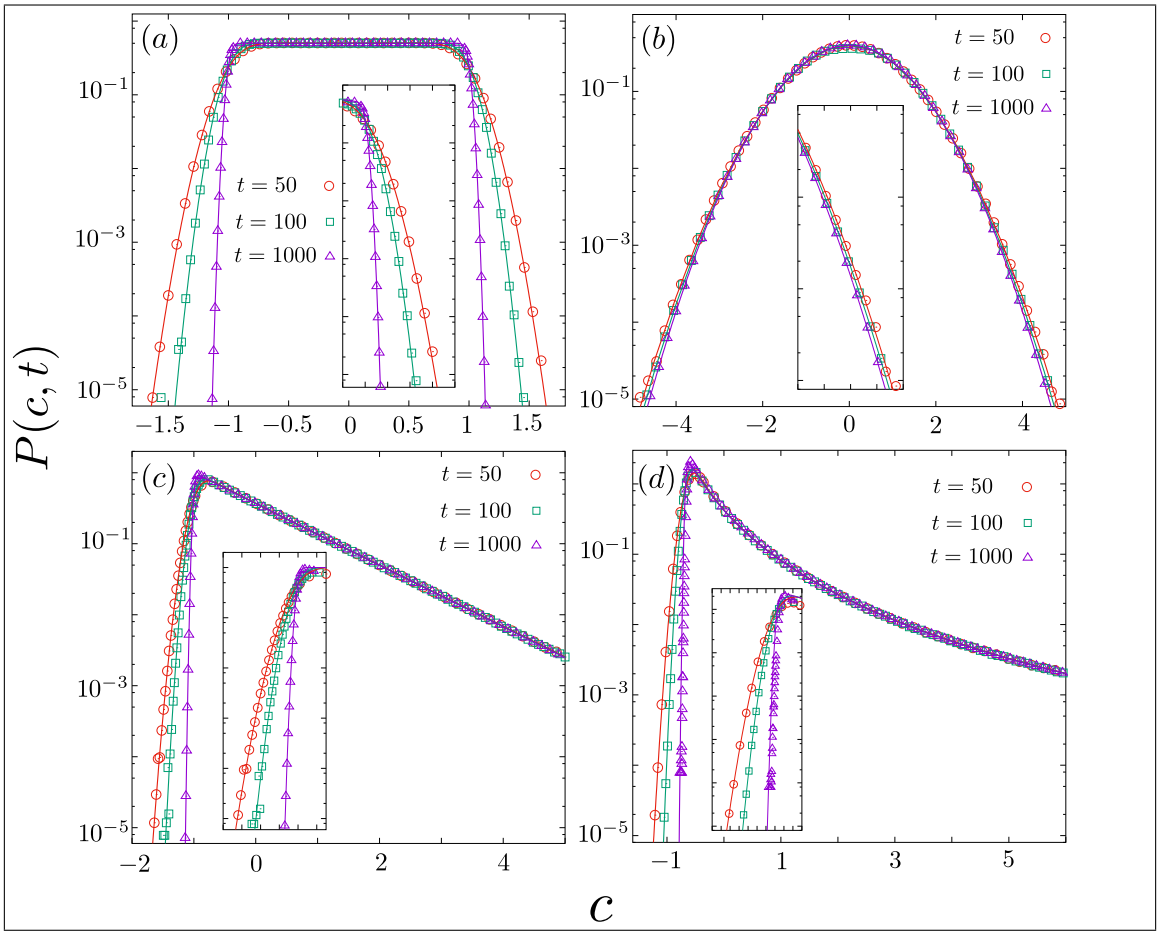

Figure 2.3: Probability distribution function $P(c,t)$ of the scaled net overtakings $c = m(t)/\varrho t$ are plotted at three different times, for the Jepsen gas, with four different choices of the initial velocity distribution, namely, (a) uniform (b) Gaussian (c) exponential and (d) power-law ($\nu = 5/2$) distributions by considering $\varrho = 1$. The discrete points in each plot are the simulation results, which are showing a good agreement with the results coming from the numerical integration of Eq. (2.2). In the inset of each scenario, we have found a good matching between the simulation result and the approximate analytical result valid for the tails.

$$\simeq \frac{\varrho t}{(c\varrho t)!}\int_0^\infty dv_0\; e^{-v_0}\,(\varrho t(v_0-1))^{c\varrho t}\;\; e^{-\varrho t\,(v_0-1)}$$

$$\simeq \sqrt{\frac{\varrho t}{2\pi c}}\left(\frac{e}{c}\right)^{c\varrho t}\;\int_0^\infty dv_0\; e^{-v_0\,-\,\varrho t\;\phi_1(v_0,\,c)}$$

with $\phi_1(v_0,\ c) = (v_0 - 1) - c\,\log(v_0 - 1)$. In the limit of large t making the saddle point integration we can get

$$P_R(c >> -1, t) \simeq e^{-(1+c)} \left(1 - \frac{c}{2\varrho t}\right) + \mathcal{O}(t^{-2}). \tag{2.30}$$

The obtained result in the limit of $t \to \infty$ is consistent with the result Eq. (2.25). Now, for $P_L(c,t)$ the contribution comes from all Poissonian processes owith rates $\rho_L(v_0) = \varrho e^{-v_0}$ over all possible values of v_0. It allows us to write and progress as follows

$$\begin{aligned} P_L(c \lesssim -1, t) &\simeq \varrho t \int_0^\infty dv_0\ \rho(v_0)\ p_-(c\varrho t, t|v_0) \\ &\simeq \frac{\varrho t}{(|c|\varrho t)!} \int_0^\infty dv_0\ e^{-v_0} \left(\varrho t\ e^{-v_0}\right)^{|c|\varrho t}\ \mathrm{Exp}\left[-\varrho t\ e^{-v_0}\right] \\ &\simeq \sqrt{\frac{\varrho t}{2\pi|c|}} \left(\frac{e}{|c|}\right)^{|c|\varrho t} \sum_{n=0}^{\infty} \frac{(-\varrho t)^n}{n!}\ \frac{1}{(1 + n + |c|\varrho t)} \\ &\simeq \frac{1}{\sqrt{2\pi|c|\varrho t}} \left(\frac{e}{|c|\varrho t}\right)^{|c|\varrho t}\ \gamma\left(1 + |c|\varrho t, \varrho t\right). \end{aligned} \tag{2.31}$$

The obtained result is showing a good agreement with the numerical simulation result as displayed in the inset of FIG. 2.3(c).

Power-law $\rho(v)$:

Finally, for the power-law distribution of the form Eq. (2.6), following similar arguments like the right tail of the exponential distribution above, we can estimate the behavior of the same in this case. Here we integrate over all possible right jumping rates $\rho_R(v_0) = \varrho(v_0 - \nu/(\nu-1) - v_0^{1-\nu}/(\nu-1)) \simeq \varrho(v_0 - \nu/(\nu-1))$ with the assumption that $v_0 >> \nu/(\nu-1)$. It allows us to advance as follows

$$P_R\left(c >> -\frac{\nu}{\nu-1}, t\right) \simeq \varrho t \int_1^\infty dv_0\ \frac{\nu}{v_0^{\nu+1}}\ p_+(c\varrho t, t|v_0)$$

$$\simeq \frac{\varrho t}{(c\varrho t)!} \int_1^\infty dv_0\ \frac{\nu}{v_0^{\nu+1}} \left(\varrho t \left(v_0 - \frac{\nu}{\nu-1}\right)\right)^{c\varrho t}\ \mathrm{Exp}\left[-\varrho t\ \left(v_0 - \frac{\nu}{\nu-1}\right)\right]$$

$$\simeq \sqrt{\frac{\varrho t}{2\pi c}}\left(\frac{e}{c}\right)^{c\varrho t}\int_1^\infty dv_0 \frac{\nu}{v_0^{\nu+1}}\, e^{-\varrho t\, \phi_2(v_0,c,\nu)}$$

with $\phi_2(v_0, c, \nu) = v_0 - \nu/(\nu-1) - c\log(v_0 - \nu/(\nu-1))$. Now, in the limit of large t making the saddle point integration we can get

$$P_R\left(c >> -\frac{\nu}{\nu-1}, t\right) \simeq \int_{-\infty}^\infty dv_0 \frac{\nu}{v_0^{\nu+1}}\sqrt{\frac{\varrho t}{2\pi c}}\text{Exp}\left[-\frac{\varrho t}{2c}\left(v_0 - c - \frac{\nu}{\nu-1}\right)^2\right]$$
$$\simeq \int_{-\infty}^\infty dv_0 \frac{\nu}{v_0^{\nu+1}}\delta\left(v_0 - c - \frac{\nu}{\nu-1}\right) \simeq \nu\left(c + \frac{\nu}{\nu-1}\right)^{-1-\nu} \quad (2.32)$$

in the limit of $t \to \infty$. In case of $P_L(c,t)$, employing Eq. (2.12) and (2.14) we can get $\rho_L(v_0) = \varrho\ v_0^{1-\nu}/(\nu-1)$. The behavior of the left tail, in this case, can be obtained by integrating all the Poissonian process with rate $\rho_L(v_0)$ over all possible v_0. Following the similar path like earlier we can proceed as follows

$$P_L(c \lesssim -1/(\nu-1), t) \simeq \frac{\varrho t}{(|c|\varrho t)!}\int_1^\infty dv_0\ \frac{\nu}{v_0^{1+\nu}}\ \text{Exp}\left[-\frac{t\varrho\ v_0^{1-\nu}}{\nu-1}\right]\ \left(\frac{t\varrho\ v_0^{1-\nu}}{\nu-1}\right)^{|c|\varrho t}$$

$$\simeq \sqrt{\frac{\varrho t}{2\pi|c|}}\left(\frac{e}{|c|(\nu-1)}\right)^{|c|\varrho t}\int_1^\infty dv_0\ \frac{\nu}{v_0^{1+\nu}}\ v_0^{-(\nu-1)|c|\varrho t}\ \text{Exp}\left[-\frac{t\varrho\ v_0^{1-\nu}}{\nu-1}\right]$$

$$\simeq \sqrt{\frac{\varrho t}{2\pi|c|}}\ \frac{\nu}{\varrho t}\ \left(\frac{\nu-1}{\varrho t}\right)^{1/(\nu-1)}\ \left(\frac{e}{|c|\varrho t}\right)^{|c|\varrho t}\ \gamma\left(\frac{\nu}{\nu-1} + |c|\varrho t, \frac{\varrho t}{\nu-1}\right). \quad (2.33)$$

The obtained result is showing a good agreement with the numerical simulation result as displayed in the inset of FIG. 2.3(d).

2.4 Constant gap between all neighboring agents

In this section, we investigate the same problem by slightly modifying the above system. Instead of the constant density of agents here, we consider a constant gap between all the neighboring agents. For convenience, we set this gap equal to one and shift the origin of the system at the initial position of the tagged agent. It implies that the initial position of the agents takes all possible integer values from $-\infty$ to $+\infty$. The shift of the origin ensures that $m_R(t|v_0)$ and $m_L(t|v_0)$ are contributed by the agents seated initially at the +ve and the −ve sides of the origin respectively.

These simplifications allow us to write the net overtaking number of v_0 upto t as

$$m(t|v_0) = \underbrace{\sum_{i=1}^{\lfloor (v_0-v_{\min})t \rfloor} \Theta\left(v_0 - v_i - \frac{i}{t}\right)}_{m_R(t|v_0)} - \underbrace{\sum_{i=-1}^{-\lfloor (v_{\max}-v_0)t \rfloor} \Theta\left(v_i - v_0 + \frac{i}{t}\right)}_{m_L(t|v_0)}. \tag{2.34}$$

Here $v_{\max}$ and $v_{\min}$ are respectively the upper and lower bound of $\rho(v)$ with the heaviside theta function $\Theta(x)$ which yields 0 and 1 for $x < 0$ and $x \geq 1$ respectively. Note that in the upper limit of both summation we use the floor function $\lfloor u \rfloor$ which yields the largest integer less than or equal to a real number u. Now, using Eq. (2.34) we can write the average of $m(t|v_0)$ in the limit of large t as follows

$$\begin{aligned} \langle m(t|v_0)\rangle &\simeq t\int_{v_{\min}}^{v_0} dv\ \rho(v) \int_0^{v_0-v_{\min}} dx\ \Theta(v_0 - v - x) \\ -t\int_{v_0}^{v_{\max}} dv\ \rho(v) \int_0^{v_{\max}-v_0} dx\ \Theta(v - v_0 - x) &\simeq t\int_{v_{\min}}^{v_0} dv\ \rho(v)\ (v_0 - v) \\ -t\int_{v_0}^{v_{\max}} dv\ \rho(v)\ (v - v_0) &\simeq (v_0 - \langle v\rangle)t. \end{aligned} \tag{2.35}$$

In above we first consider $x = i/t$ as a continuous variable in the limit of $t >> 1$ and replace the summation by integration. We also use $\int_0^a dx\ \Theta(b-x) = \min(a,b)$ to obtain the final result. Now, we can comment on the behavior of the higher order cumulants at large time with the following result: if $X = \sum_{j=1}^{l} \pm x_j$, then n-th order cumulant of X can be written as $\langle X^n\rangle_c = \sum_{j=1}^{l} (\pm 1)^n \langle x_j^n\rangle_c$. With the help of it we can write

$$\begin{aligned} \langle m^n(t|v_0)\rangle_c = &\sum_{i=1}^{\lfloor (v_0-v_{\min})t \rfloor} \left\langle \Theta^n\left(v_0 - v_i - \frac{i}{t}\right)\right\rangle_c \\ + (-1)^n &\sum_{i=-1}^{-\lfloor (v_{\max}-v_0)t \rfloor} \left\langle \Theta^n\left(v_i - v_0 + \frac{i}{t}\right)\right\rangle_c \simeq t\int_0^{(v_0-v_{\min})} dx\ \langle \Theta^n\left(v_0 - v_x - x\right)\rangle_c \\ &+ (-1)^n\, t\int_0^{-(v_{\max}-v_0)} dx\ \langle \Theta^n\left(v_x - v_0 + x\right)\rangle_c \propto t. \end{aligned} \tag{2.36}$$

That is all the higher order cumulants at large time would be proportional to t. With these leads, now we study the conditional distribution $p(m, t|v_0)$ followed by

the unconditional distribution $P(m,t)$ for each case of $\rho(v)$ one by one.

2.4.1 Conditional Distribution

To study the conditional PDF we first write it down in terms of a scaling function $y = (m(t|v_0) - \langle m(t|v_0)\rangle)/\sqrt{\langle m^2(t|v_0)\rangle_c}$ as

$$p(y|v_0) = \frac{1}{2\pi}\int_{-\infty}^{\infty} dk\; e^{-iky}\;\mathrm{Exp}\left[\sum_{n=2}^{\infty}\frac{(ik)^n}{n!}\frac{\langle m^n(t|v_0)\rangle_c}{\langle m^2(t|v_0)\rangle_c^{n/2}}\right]. \tag{2.37}$$

Uniform $\rho(v)$:

Now, with this result we start from uniform distribution. For uniform $\rho(v)$, using $v_{\max} = 1$ and $v_{\min} = -1$ and following the same procedure like Eq. (2.35) and (2.36) we can calculate the variance, 3rd, and 4th cumulants as follows:

$$\langle m^2(t|v_0)\rangle_c \simeq \frac{t}{3}, \tag{2.38a}$$

$$\langle m^3(t|v_0)\rangle_c \simeq 0, \tag{2.38b}$$

$$\langle m^4(t|v_0)\rangle_c \simeq -\frac{t}{15}. \tag{2.38c}$$

Note that the the dominant contribution of the variance turns out v_0 independent in the limit of large t. This result is entirely different from the same in the case of Jespen gas (see Eq. (2.16)). In addition to that the skewness $\langle m^3\rangle_c/\langle m^2\rangle_c^{3/2} \sim \mathcal{O}(t^{-3/2})$ and the excess kurtosis $\langle m^4\rangle_c/\langle m^2\rangle_c^2 \sim \mathcal{O}(t^{-1})$ tend to zero in the limit of large t. In fact, by using Eq. (2.36) we can say all the higher order terms in Eq. (2.37) like $\langle m^5\rangle_c/\langle m^2\rangle_c^{5/2}$, $\langle m^6\rangle_c/\langle m^2\rangle_c^3$, and so on decay faster than t^{-1}. It allows us to write the PDF considering the minute correction of the 4th cumulant in terms of a scaling function y as

$$p(y) = \frac{1}{2\pi}\int_{-\infty}^{\infty} dk\; e^{-iky}\;\mathrm{Exp}\left[-\frac{k^2}{2} - \frac{3}{5t}\frac{k^4}{4!}\right] \simeq \frac{1}{2\pi}\int_{-\infty}^{\infty} dk\; e^{-iky}\;\mathrm{Exp}\left[-\frac{k^2}{2}\right] \times\left(1 - \frac{3}{5t}\frac{k^4}{4!}\right) \simeq \frac{e^{-y^2/2}}{\sqrt{2\pi}}\left(1 - \frac{y^4 - 6y^2 + 3}{40\;t}\right) \simeq \frac{e^{-y^2/2}}{\sqrt{2\pi}} + \mathcal{O}(t^{-1}). \tag{2.39}$$

The obtained result is showing a good agreement with the numerical simulation result as shown in FIG. 2.4(a).

Gaussian $\rho(v)$:

Now for Gaussian $\rho(v)$, using $v_{\max} = \infty$ and $v_{\min} = -\infty$, and following the above procedure we can calculate the variance, 3rd, and 4th cumulants as follows

$$\begin{aligned}\langle m^2(t|v_0)\rangle_c \simeq t\int_0^\infty dx\left\{\frac{1}{2}\,\mathrm{Erfc}\left[\frac{x-v_0}{\sqrt{2}}\right]-\left(\frac{1}{2}\,\mathrm{Erfc}\left[\frac{x-v_0}{\sqrt{2}}\right]\right)^2\right\}\\ +\,t\int_0^\infty dx\left\{\frac{1}{2}\,\mathrm{Erfc}\left[\frac{x+v_0}{\sqrt{2}}\right]-\left(\frac{1}{2}\,\mathrm{Erfc}\left[\frac{x+v_0}{\sqrt{2}}\right]\right)^2\right\}\simeq\frac{t}{\sqrt{\pi}},\end{aligned} \tag{2.40a}$$

$$\langle m^3(t|v_0)\rangle_c \simeq \frac{t}{2\sqrt{2}}\int_{-v_0/\sqrt{2}}^{v_0/\sqrt{2}} dx\ \left(\mathrm{Erf}(x)-(\mathrm{Erf}(x))^3\right)\simeq 0, \tag{2.40b}$$

$$\langle m^4(t|v_0)\rangle_c \simeq \frac{t}{2\sqrt{2}}\int_0^\infty dx\ \left(-1+4\,(\mathrm{Erf}(x))^2-3\,(\mathrm{Erf}(x))^4\right)\simeq -0.0298\,t. \tag{2.40c}$$

Note that the variance in this case also comes out v_0 independent. More importantly, the skewness $\langle m^3\rangle_c/\langle m^2\rangle_c^{3/2}\simeq 0$ and the excess kurtosis $\langle m^4\rangle_c/\langle m^2\rangle_c^2\sim\mathcal{O}(t^{-1})$ tend to zero in the limit of large t. Like uniform $\rho(v)$ in this case also we can find out the conditional distribution in terms of $y=\pi^{1/4}(m-v_0t)/t^{1/2}$ as

$$p(y)\simeq\frac{e^{-y^2/2}}{\sqrt{2\pi}}\left(1-0.0298\,\pi\,\frac{y^4-6y^2+3}{24\,t}\right)\simeq\frac{e^{-y^2/2}}{\sqrt{2\pi}}+\mathcal{O}(t^{-1}) \tag{2.41}$$

which we have shown in FIG. 2.4(b) including the numerical simulation result.

Exponential $\rho(v)$:

Now, for exponential $\rho(v)$, using $v_{\max}=\infty$ and $v_{\min}=0$ we can calculate the variance, 3rd, and 4th cumulants as follows

$$\langle m^2(t|v_0)\rangle_c \simeq \frac{t}{2}, \tag{2.42a}$$

$$\langle m^3(t|v_0)\rangle_c \simeq -\frac{t}{6}, \tag{2.42b}$$

$$\langle m^4(t|v_0)\rangle_c \simeq 0. \tag{2.42c}$$

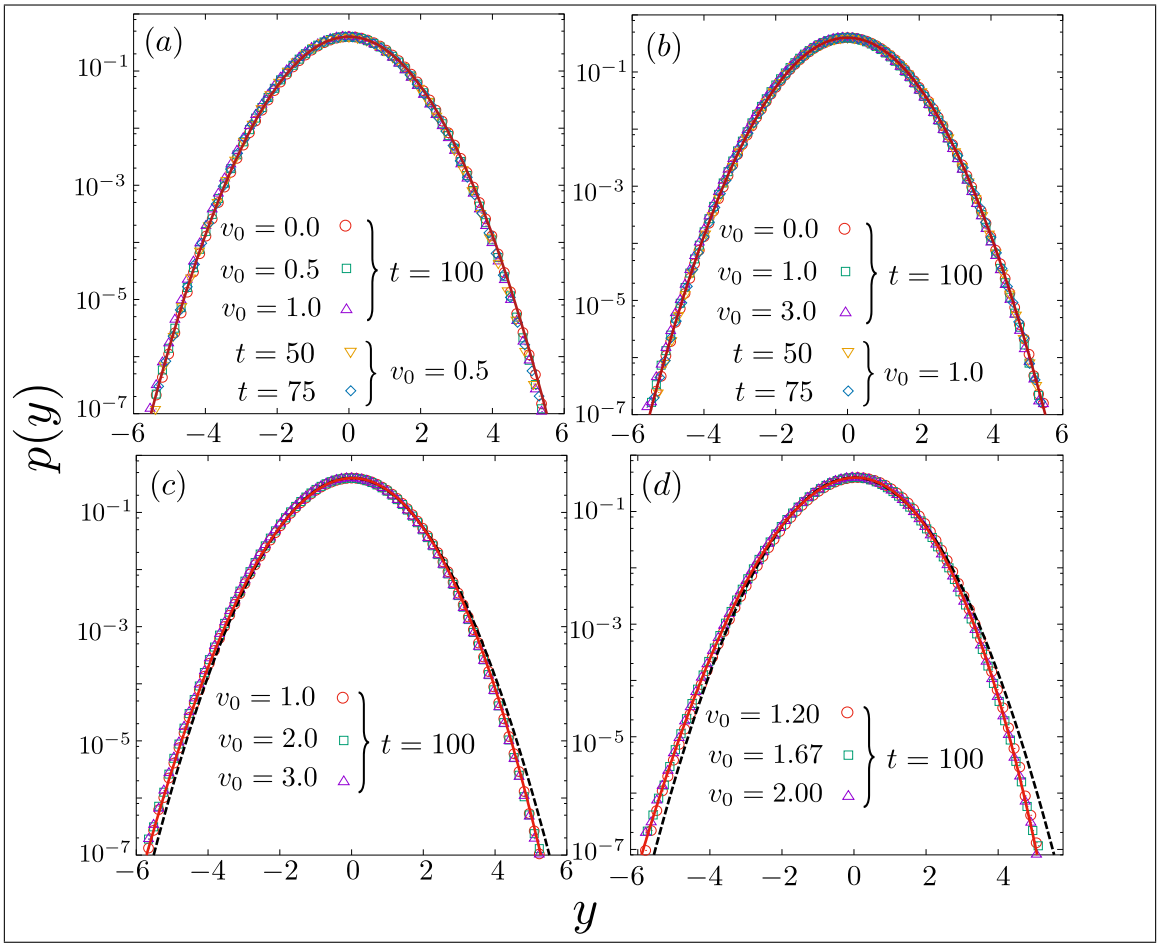

Figure 2.4: Probability distribution function $p(y)$ of the scaled net overtakings $y = (m(t|v_0) - \langle m(t|v_0)\rangle)/\sqrt{\langle m^2(t|v_0)\rangle_c}$ are plotted for a given v_0 at time $t = 100$, in case of constant gap between all neighboring agents, with four different choices of the initial velocity distribution, namely, (a) uniform (b) Gaussian (c) exponential and (d) power-law ($\nu = 5/2$) distributions. The discrete points in each plot are the simulation results which are showing a good agreement with the analytical or numerical results including a Gaussian approximated results shown by the dashed line in last two cases.

Note that the dominant contribution of the variance in this case also comes out v_0 independent. Like earlier cases, the skewness $\langle m^3\rangle_c/\langle m^2\rangle_c^{3/2} \sim \mathcal{O}(t^{-1/2})$ and the excess kurtosis $\langle m^4\rangle_c/\langle m^2\rangle_c^2 \sim 0$ converge to zero in the limit of large t. Following

the arguments of earlier two cases here we can write Eq. (2.37) as

$$p(y) \simeq \frac{1}{2\pi}\int_{-\infty}^{\infty} dk\; e^{-iky}\,\mathrm{Exp}\left[-\frac{k^2}{2}+\frac{ik^3}{9\sqrt{2t}}\right] \simeq \frac{1}{\pi}\int_{0}^{\infty} dk\; e^{-k^2/2}\,\mathrm{Cos}\left[ky-\frac{k^3}{9\sqrt{2t}}\right]. \tag{2.43}$$

Solving numerically the above integration we can find out result which is showing a good agreement with the numerical simulation result as shown in FIG. 2.4(c).

Power-law $\rho(v)$:

Finally, for power-law distribution, using $v_{\max} = \infty$ and $v_{\min} = 1$ we can calculate its variance, 3rd, and 4th cumulants as follows

$$\langle m^2(t)\rangle_c \simeq \left(\frac{1}{\nu-1}-\frac{1}{2\nu-1}\right)t, \tag{2.44a}$$

$$\langle m^3(t)\rangle_c \simeq -\left(\frac{1}{\nu-1}-\frac{3}{2\nu-1}+\frac{2}{3\nu-1}\right)t, \tag{2.44b}$$

$$\langle m^4(t)\rangle_c \simeq \left(\frac{1}{\nu-1}-\frac{7}{2\nu-1}+\frac{12}{3\nu-1}-\frac{6}{4\nu-1}\right)t. \tag{2.44c}$$

In this case also we have found these cumulants are v_0 independent. Now, considering the contribution of 3rd and 4th cumulants we can approximately write Eq. (2.37) as

$$p(y) \simeq \frac{1}{\pi}\int_{0}^{\infty} dk\; e^{-k^2/2}\,\mathrm{Cos}\left[ky+\frac{k^3}{3!}\frac{\langle m^3(t)\rangle_c}{\langle m^2(t)\rangle_c^{3/2}}\right]\left(1+\frac{k^4}{4!}\frac{\langle m^4(t)\rangle_c}{\langle m^2(t)\rangle_c^2}\right). \tag{2.45}$$

The numerically obtained result from the above Eq. (2.45) matches quite well with the numerical simulation result as shown in FIG. 2.4(d).

2.4.2 Unconditional Distribution

In this case, we can see that it is convenient to discuss the distribution in terms of scaling variable $c = m/t$. From Eq. (2.35) and (2.36) it is clear that all the higher order cumulants of c except the first one $\langle c(t|v_0)\rangle = v_0 - \langle v\rangle$ converges to zero in the limit of $t \to \infty$. It allows us to write the conditional distribution of c as $p(c, t\to\infty|v_0) = \delta(c - v_0 + \langle v\rangle)$. Now, using Eq. (2.2) we can get $P(c, t\to\infty) =$

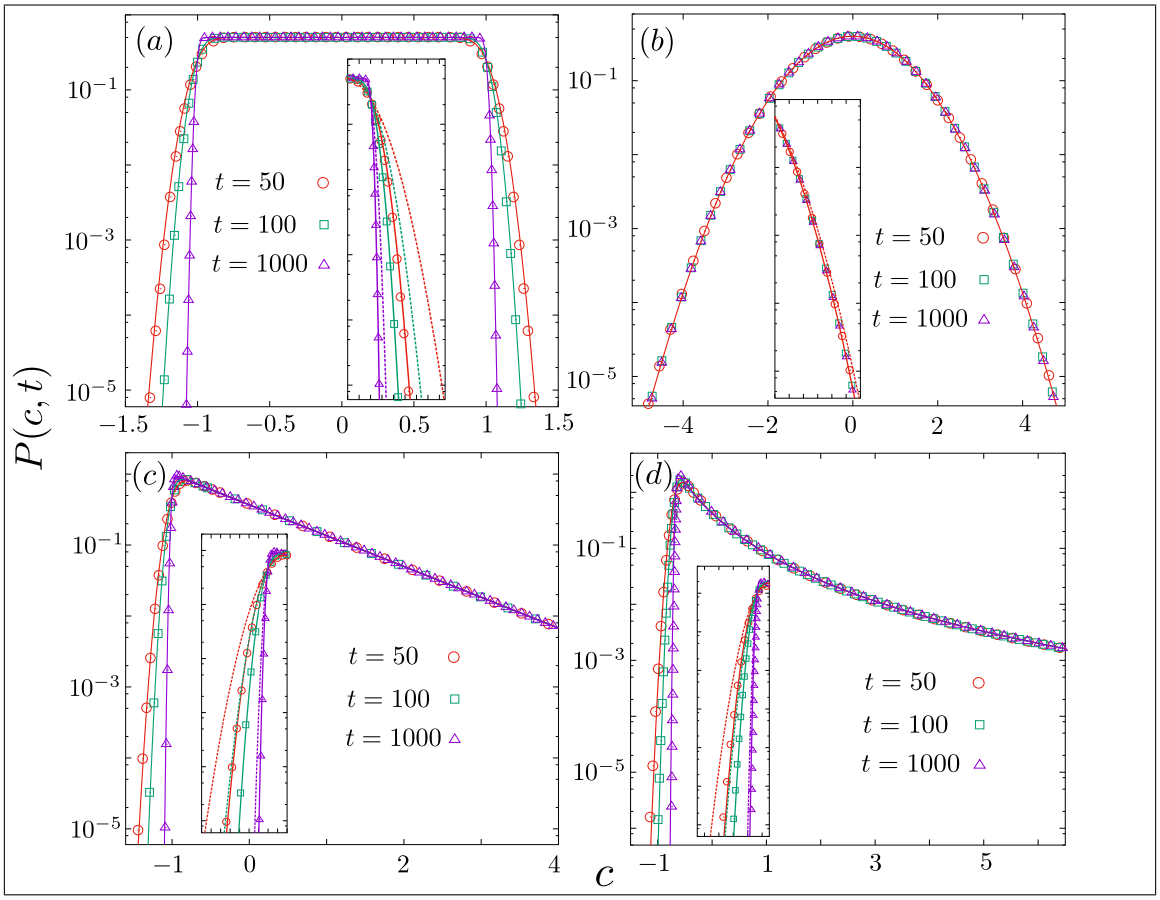

Figure 2.5: Probability distribution function $P(c,t)$ of the scaled net overtakings $c = m(t)/t$ are plotted at three different times by fixing the gap between all neighboring agents, with four different choices of the initial velocity distribution, namely, (a) uniform, (b) Gaussian, (c) exponential, and (d) power-law ($\nu = 5/2$) distributions. The discrete points in each plot are the simulation results which are showing a good agreement with the analytical or numerical (in case of power-law distribution) as shown by the bold lines. In the inset of each plot, we zoomed the tail-behavior of the respective distribution. We include the result of the same in case of the Jepsen gas as shown by dotted lines for comparison.

$\int_{-\infty}^{\infty} dv_0\ \rho(v_0)\ \delta(c - v_0 + \langle v \rangle) = \rho(c + \langle v \rangle)$. It implies that the distribution of the net overtaking number of a randomly picked agent while rescaled with time converges to the initial velocity distribution with a Galilean shift by the mean of the same distribution in the limit of $t \to \infty$. Now, to obtain finite but large time behavior of $P(c,t)$ we consider each $\rho(v)$ one by one.

First, for uniform $\rho(v)$, using the Gaussian approximated $p(m,t|v_0)$ in Eq. (2.39)

we can calculate the distribution of c as

$$P(c,t) = \frac{t}{2}\int_{-1}^{1} dv_0\; p(ct,t|v_0) \simeq \frac{1}{2}\sqrt{\frac{3t}{2\pi}}\int_{-1}^{1} dv_0\; \mathrm{Exp}\left[-\frac{3t}{2}(c-v_0)^2\right]$$

$$\simeq \frac{1}{4}\left\{\mathrm{Erf}\left[\sqrt{\frac{3t}{2}}(c+1)\right] - \mathrm{Erf}\left[\sqrt{\frac{3t}{2}}(c-1)\right]\right\}. \tag{2.46}$$

Now, for Gaussian $\rho(v)$ using $p(m,t|v_0)$ from Eq. (2.41) we can obtain

$$P(c,t) = t\int_{-\infty}^{\infty} dv_0\; \rho(v_0)\; p(ct,t|v_0) \simeq \frac{\sqrt{t}}{2\;\pi^{3/4}}\int_{-\infty}^{\infty} dv_0\; \mathrm{Exp}\left[-\frac{v_0^2}{2} - \frac{t\sqrt{\pi}}{2}(c-v_0)^2\right]$$

$$\simeq \frac{e^{-c^2/2}}{\sqrt{2\;\pi}} + \frac{(c^2-1)e^{-c^2/2}}{2\sqrt{2}\;\pi\;t} + \mathcal{O}(t^{-2}). \tag{2.47}$$

Similarly, for exponential $\rho(v)$ using $p(m,t|v_0)$ from Eq. (2.43) we can get

$$P(c,t) \simeq t\int_{0}^{\infty} dv_0\; e^{-v_0}\; p(ct,t|v_0) \simeq \sqrt{\frac{t}{\pi}}\int_{0}^{\infty} dv_0\; e^{-v_0}\; e^{-t(c-v_0+1)^2}$$

$$\simeq \frac{1}{2}\;\mathrm{Exp}\left[-(1+c)+\frac{1}{4t}\right]\left\{1+\mathrm{Erf}\left[\sqrt{t}(c+1)-\frac{1}{2\sqrt{t}}\right]\right\}. \tag{2.48}$$

Finally, in case of power-law $\rho(v)$, using the Gaussian approximated $p(m,t|v_0)$ we can numerically compute $P(c,t)$. All the derived results are showing a good agreement with the numerical simulation result, as shown in FIG. 2.5.

Bibliography

[1] D. W. Jepsen, J. Math. Phys. (N.Y.) **6**, 405 (1965).

[2] T.M. Liggett, Interacting Particle Systems (New York: Springer-Verlag, 1985).

[3] H. Spohn, Large scale dynamics of Interacting Particles (Springer-Verlag, New York, 1991).

[4] D. Helbing, Rev. Mod. Phys. **73**, 1067(2001).

[5] A. Schadschneider, D. Chowdhury, K. Nishinari, Stochastic Transport in Complex Systems (Elsevier, 2010).

[6] A. Clauset, C. R. Shalizi, and M. E. J. Newman. Power-lawdistributions in empirical data. Feb 2009

[7] P.L. Krapivsky, S. Redner and E. Ben-Naim, A Kinetic View of Statistical Physics, Cambridge University Press, New York, 2010.

[8] J. G. Skellam, J. Roy. Stat. Soc. 109, 296 (1946).

Chapter 3

Statistics of overtakes by a tagged agent in a system of interacting agents

3.1 Introduction

The phenomenon of overtaking is widespread in nature. It commonly appears in traffic and traffic-related flows [1], where a fast-moving agent from behind can go in front of an agent moving slowly in the same direction. Despite its widespread appearance, there is no systematic studies of this phenomenon exist in the literature. It motivates us to study this phenomenon by starting it from a simple non-interacting system of self-driven agents in Chapter 2. Following this thread, in this chapter, we study the same problem in a system of interacting self-driven agents.

To construct a simple model of interacting self-driven agents, we assume all the agents distributed homogeneously in real space. This assumption allows us to ignore the actual position of the agents and focus on their relative order. Notably, this relative order can be presented by occupying each site of a 1D lattice by a singly-seated, self-driven agent. The self-driven character of each agent can simply be assigned by a real scalar variable. Note that, as we ignore the actual position of the agents, these scalars serve as the relevant parameters in our model. More accurately, the dynamical rules we formulate depends on those variables. It is also worth to mention that the dynamical rules we aimed to formulate are mainly logic-based and only consider the local interaction among the agents to change the sequence or the relative order of the agents on the lattices in time.

With all the above assumptions and simplifications, in this chapter, we study the statistics of net overtaking numbers by a tagged agent in a given duration of time.

Clearly, for a tagged agent, the net number of overtaking is the total number of agents that it overtakes minus the total number of agents that overtake it, in a given duration of time.

The rest of the chapter is organized as follows. First, in Sec. 3.2, we outline our model with three different dynamical rules and our quantities of interest. Next, in Sec. 3.3, we discuss our problem with the first dynamical rule followed by the same with the second dynamical rule in Sec. 3.4. In Sec. 3.4.1, we show that the tagged dynamics in the second case is equivalent to the dynamics of a second class particle in TASEP. By using this result, we calculate the mean and the variance of the net overtaking number by a tagged agent in Sec. 3.4.2. Next we discuss the corresponding conditional and the unconditional distributions in Sec. 3.4.3 and 3.4.4 respectively. In Sec. 3.5, all the results for the third dynamical rules are presented by following a similar sequence like the earlier section.

3.2 Model

Consider a 1D lattice ranging from $-\infty$ to ∞. Initially, each site i on this lattice is occupied by an agent. We assign each agent with a real scalar variable v_i which one may call its preferred velocity. The velocity of each agent is taken independently from a common distribution $\rho(v)$. The velocity associated with an agent remain unchanged over time. As a dynamical rule each nearest neighboring pair of left (L) and right (R) velocities, v_L and v_R respectively, are exchanged their sites on the lattice at the rate $r(v_L, v_R)$ which depends on their velocities (as illustrated in 3.1). Note that these velocities, v_L and v_R, associated with a pair are time-dependent variables. They instantaneously take the velocities of the agents seated on those sites. The location exchange rule of the neighboring pairs mimics the consequence of overtaking. A successful exchange of a neighboring pair increases (decreases) the net overtaking number by an amount $+1$ (-1) for the left (right) particle of a selected pair as shown in 3.1.

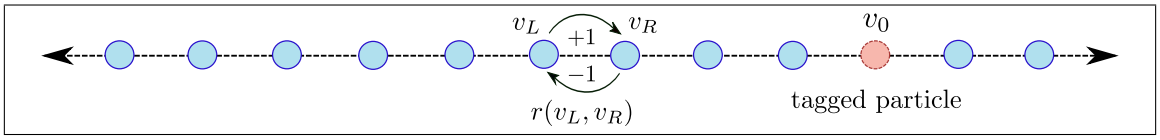

Figure 3.1: Schematic of our model on an infinite one dimensional lattice with singly-seated agent of constant but random velocity in each site. The system evolution is Markovian, where each neighboring pair of left (L) and right (R) velocities, v_L and v_R respectively, are exchanged their site at the rate $r(v_L, v_R)$. For a selected pair, a successful exchange increases (decreases) the net overtaking number by an amount $+1$ (-1) for the left (right) agent. The particle in red is being tagged to study the statistics of its net overtaking number in time.

3.2.1 Three different transition rules

In this subsection, we devise three different cases depending on the exchange (overtaking) rate $r(v_L, v_R)$ of nearest neighboring pairs of velocities v_L and v_R. For a complete and consistent flow in the description, we consider the exchange rate in the first case is velocity independent. All the nearest neighboring pairs, in this case, are exchanged with equal rate, say 1 for simplicity, irrespective of their assigned velocities. In the next case we consider an agent with velocity v_L to exchange with its right-nearest-neighbor of velocity v_R at the rate 1 if $v_L > v_R$. This case is more appropriate for a crowded scenario where what matters is that an agent tries to overtake, but the actual difference in their velocities is less important. In the third case where the overtaking rate between the nearest neighboring pairs is equal to their relative velocity $(v_L - v_R)$ alongside the criteria of $v_L > v_R$. This dynamical rule is appropriate in the low-density limit of the traffic or traffic-related flows where the velocity of the agents plays a vital role. Now, these three different exchange rules can be represented in a compact formalism by

$$r(v_L, v_R) = \begin{cases} 1 & \text{as case I} \\ \Theta(v_L - v_R) & \text{as case II} \\ (v_L - v_R)\Theta(v_L - v_R) & \text{as case III} \end{cases} \tag{3.1}$$

where $\Theta(v) = 1$ for $v > 0$ and 0 for $v \leq 0$, is the Heaviside theta function.

3.2.2 Quantity of interest

In this chapter, we investigate all the quantities we have already studied in the context of Jepsen gas in Chapter 2. Therefore, from Sec. 2.2.2, we first recall our main quantity of interest, namely, the net overtaking number $m(t|v_0)$ by a tagged agent of velocity v_0 upto time t. It is easy to see that this number in our lattice-based model is equivalent to the displacement of the same tagged agent up to the same time. Hence, the primary objective of this work boils down to the statistics of tagged displacement on the lattice. We study its mean $\langle m(t|v_0)\rangle$, variance $\langle m^2(t|v_0)\rangle_c$, and the same two probability distributions which we have defined in Sec. 2.2.2. The distributions are namely the conditional and the unconditional distributions which we have denoted by $p(m,t|v_0)$ and $P(m,t)$ respectively.

3.3 Case I : $r(v_L, v_R) = 1$

The velocity independent stochastic updation rule makes the tracer dynamics simple in this case. Here two bonds associated with any site or equivalently with any particle are independently selected with the rate one. It effectively makes any tagged agent to execute a symmetric random walk (RW) [2] on the lattice with the left (l) and the right (r) hopping rates $p_l = p_r = 1$. Now, by putting these values in Eq. (1.12) we can get the final result from Eq. (1.14). Notably, by expanding the result around its average $\bar{c} = (p_r - p_l)t = 0$, we can get the well-known Gaussian approximated result $p(y) = (1/\sqrt{2\pi})\,\exp(-y^2/2)$ in terms of a scaled variable $y = \sqrt{t/2}\; c = m/\sqrt{2t}$. In fact, this Gaussian approximated result in this case is showing a good agreement with the numerical simulation result as displayed in FIG. 3.2.

3.4 Case II : $r(v_L, v_R) = \Theta(v_L - v_R)$

The velocity dependent constraint, in this case, makes the process entirely different from the earlier one. Here an agent with a velocity higher than it's right neighbor (or lower than it's left neighbor) is only allowed to make an exchange. More importantly, all the allowed exchanges are executed at the equal rate one. These two criteria makes the process similar to the totally asymmetric simple exclusion process

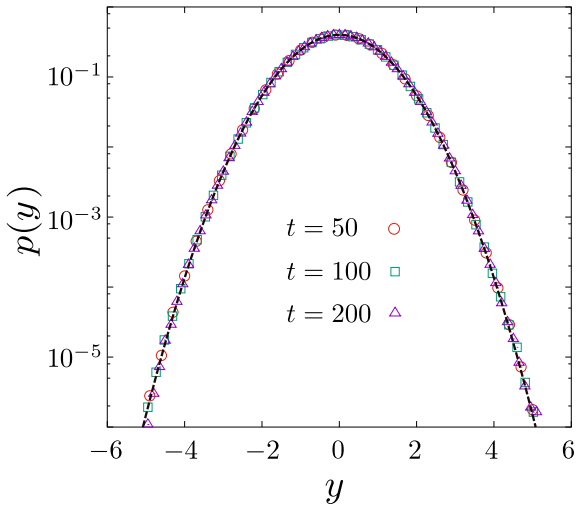

Figure 3.2: PDF of scaled net overtakings $y = m/\sqrt{2t}$ are plotted at three different times which are showing a good agreement with the analytical result as indicated by the dashed line.

(TASEP) with infinitely many classes of particles [3–8]. But, from the viewpoint of a tagged v_0, the process can be reduced to a much simpler one which we are going to describe in the next.

3.4.1 Second class particle in TASEP

By definition, all the fast moving particles ($v > v_0$) overtake the tagged v_0 (from the left) at the equal rate one. It makes them appear identical and indistinguishable to the tracer i.e., any interchange between the two fast moving particles remain invisible to the tracer. Similarly, all the slowly moving particles ($v < v_0$) also appear identical to the tracer as they are overtaken from the left at the equal rate one. Now, by considering all these above-mentioned facts, it is easy to identify the dynamics of v_0 is equivalent to the *2nd class particle* [3] in TASEP. Particles with higher and lower velocities than v_0 are respectively playing the role of particles and holes in TASEP. Being a second class particle, the tracer appears with different dynamical rules than both the particles and the holes. It moves with the same dynamics of other particles (as it can overtake holes) while being treated like a hole by the particles (as it is overtaken by the particles). Denoting the particle, hole, and the 2-nd class particle by 1, 0, and 2 respectively, all the effective transitions with respect to the tracer can be summarized by

$$1\ 0 \to 0\ 1,\ 2\ 0 \to 0\ 2 \ \text{ and } \ 1\ 2 \to 2\ 1 \quad \text{at the equal rate 1.}$$

Now, for a given v_0, the fraction of particles $\rho_+(v_0)$ and holes $\rho_-(v_0) = 1 - \rho_+(v_0)$ can be calculated as

$$\rho_+(v_0) = \int_{v_0}^{\infty} \rho(v)\, dv. \tag{3.2}$$

Note that, as the initial velocities are taken independently from a common distribution, it corresponds a product measure stationary initial distribution of particle in TASEP [9–12]. It implies that the probability of a particle seated at any site at any instant of time remains constant and equal to $\rho_+(v_0)$. Another important aspect here to be noticed that the 2nd class particle could not bring any change in TASEP as it is not affecting any particle dynamics.

3.4.2 Mean and variance of the net overtaking number

Now to calculate the mean and the variance of the net overtaking number by a tagged v_0, first we find out the jumping rates $p_r(v_0)$ and $p_l(v_0)$ to the right (r) and to the left (l) neighboring sites. The relation between the jumping rates $p_r(v_0)$ and $p_l(v_0)$ and the particle density $\rho_+(v_0)$ is coming from the requirement of occupation probability of a hole and a particle on the right and the left neighboring sites respectively, i.e.,

$$p_r(v_0) = 1 - \rho_+(v_0) \;\text{ and }\; p_l(v_0) = \rho_+(v_0). \tag{3.3}$$

Now, by using Eq. (3.2) and (3.3) it is easy to obtain the mean as

$$\langle m(t|v_0))\rangle = (p_r(v_0) - p_l(v_0))t = \bar{c}(v_0)\, t \tag{3.4}$$

$$\text{where}\quad \bar{c}(v_0) = 1 - 2\rho_+(v_0) = 1 - 2\int_{v_0}^{\infty} \rho(v)\, dv. \tag{3.5}$$

the average speed of the second class particle in TASEP [3]. Note that this average speed $\bar{c}(v_0)$ is nothing but the speed associated with the kinematic wave coming out of the local density fluctuation in TASEP (see Sec. 1.4.1).

Now, to find out the behavior of the variance, first we point out that the system initialization we consider produces an uncorrelated background of the particles in TASEP. Initially, in this uncorrelated background, the second class particle, i.e., our tagged particle execute a random walk with the left and the right jumping rates

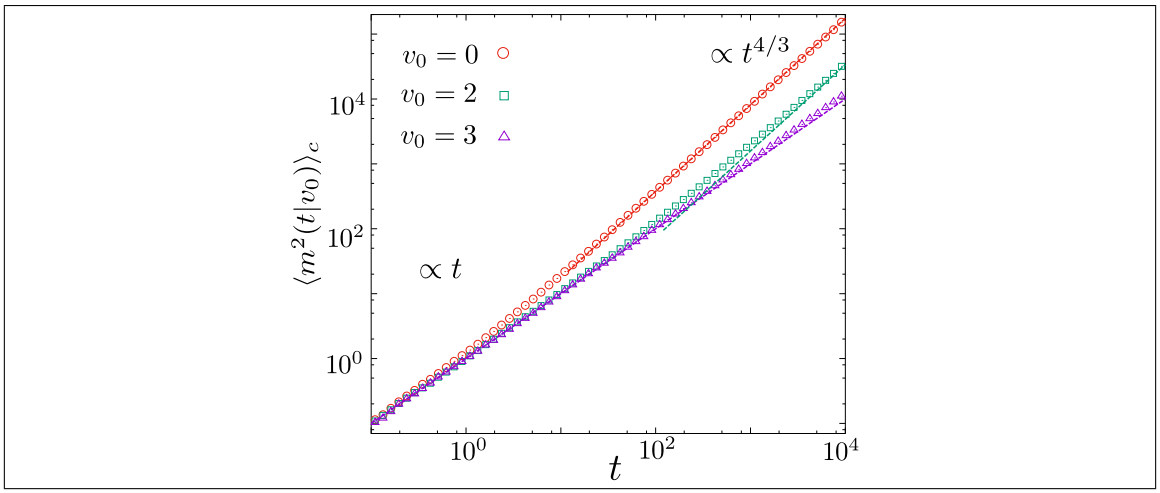

Figure 3.3: Simulation results (shown by discrete points), illustrating the crossover from the initial $\propto t$ behavior to the long-time $\propto t^{4/3}$ behavior, for the variance of the displacement of the tagged particle in case II. Three different values of the tagged velocity $v_0 = 0$, 2, and 3 are considered while the remaining velocities are chosen independently from the Gaussian distribution. The finite size effects do not show up till the final measurement time considered in the simulations, for a system of size $N = 2 \times 10^3$ with periodic boundary condition. For $v_0 = 0$ an anomalous growth $\propto t^{4/3}$ is clearly noticeable. The result for the intermediate velocity $v_0 = 2$ is showing a transition from the initial $\propto t$ behavior to the long-time $\propto t^{4/3}$ behavior. The third one $v_0 = 3$ mostly shows the linear growth $\propto t$, with a hint of the crossover towards the end. The dashed lines plot the analytical results which show a good agreement with the corresponding numerical results.

$p_l(v_0)$ and $p_r(v_0)$ respectively. It makes the displacement variance

$$\langle m^2(t)\rangle_c \;=\; (p_r(v_0) + p_l(v_0))\; t = \; t, \tag{3.6}$$

independent of the tagged velocity.

However, as the time progresses the movements of particles in TASEP get correlated. These correlated dynamics of the particles in the limit of long time and large length scale can be described by the density-density correlation function (see Sec. 1.4.4 for details). It can be argued that variance of the normalized density-density correlation function is equivalent to the variance of the second class particle in TASEP [9, 10, 14]. By using this argument one can find out

$$\langle m^2(t|v_0)\rangle_c \simeq 4 \times 0.51\; \chi^{2/3}(v_0)\; t^{4/3} \tag{3.7a}$$

$$\text{with} \quad \chi(v_0) = \rho_+(v_0)(1-\rho_-(v_0)) = (1-\bar{c}^2(v_0))/4. \tag{3.7b}$$

The prefactor 0.51 is the variance of the scaling function $G_{\text{scaling}}(x)$ associated with the spatio-temporal two-point correlation function of the TASEP with the Bernoulli product measure initial distribution [9–13].

Now comparing Eq. (3.6) and Eq. (3.7a), we can obtain the crossover time $t_1^*(v_0)$ between the initial diffusive behavior to the subsequent super-diffusion as

$$t_1^*(v_0) \propto \chi^{-2}(v_0) \propto (1-\bar{c}^2(v_0))^{-2}. \tag{3.8}$$

Clearly, below the time scale the behavior is simple diffusion and above of it it is superdiffusion. Now, from Eq. (3.5) and (3.8) it is clear that for $v_0 \sim \langle v\rangle$, the behavior at finite but large time is dominated by $t^{4/3}$ as $t_1^*(v_0) \sim \mathcal{O}(1)$. On the other hand, the opposite limit ($v_0 \to \pm\infty$) corresponds $t_1^*(v_0) \to \infty$ which brings out diffusive behavior at any finite time as illustrated in FIG. 3.3.

An alternate argument of the variance

The height-height correlation function in interface growth model follows the corresponding scaling relation [15, 16]

$$C(x,t) \sim t^{2\beta} g(x\, t^{-1/z}) \tag{3.9}$$

where β and z are the growth and the dynamical exponent. It makes the density correlation function associated with TASEP follows the relation (see Sec. 1.4.4 for details)

$$S(x,t) \sim \partial_x^2 C(x,t) \sim t^{2(\beta-\frac{1}{z})}\, g''(x\, t^{-1/z}). \tag{3.10}$$

Here $g''(x)$ denotes for the second derivative of $g(x)$ with respect to x. Now, the variance of $S(x,t)$ can be computed as follows

$$\langle x^2(t)\rangle_c = \int dx\, x^2 S(x,t) \sim t^{2(\beta-\frac{1}{z})} \int dx\, x^2 g''(x\, t^{-\frac{2}{3}}) \sim t^{2\beta+\frac{1}{z}} \int du\, u^2 g''(u). \tag{3.11}$$

As TASEP can be mapped on the KPZ interface growth model, it corresponds $\beta = 1/3$ and $z = 3/2$. It yields the variance $\propto t^{4/3}$.

3.4.3 Conditional distribution

From the above discussion it is clear that $p(m,t|v_0)$ has two different distribution which depends on t and v_0. For a given v_0 and t, if $t << t_1^*(v_0)$, then the distribution can be obtained by the random walk approximation. In this case, for a tagged v_0 we can write $p_r(v_0) = \rho_+(v_0) = (1-\bar{c}(v_0))/2$ and $p_l(v_0) = \rho_-(v_0) = (1+\bar{c}(v_0))/2$. Now, using the PDF of the form of Eq. (1.14), the conditional PDF $p(c,t|\bar{c})$ can be written as:

$$p(c,t|\bar{c}) \simeq \sqrt{\frac{t}{2\pi}} \frac{e^{-t\,\phi(c,\bar{c})}}{\sqrt{|\phi''(c,\bar{c})|}}, \tag{3.12a}$$

$$\text{with } \phi(c,\bar{c}) = c \log\Big[\,(c+\sqrt{c^2+1-\bar{c}^2})/(\bar{c}+1)\Big] + 1 - \sqrt{c^2+1-\bar{c}^2}, \tag{3.12b}$$

$$\text{and } |\phi''(c,\bar{c})| = \sqrt{c^2+1-\bar{c}^2}. \tag{3.12c}$$

We compare this result with the numerical simulation result as shown in FIG. 3.4(a).

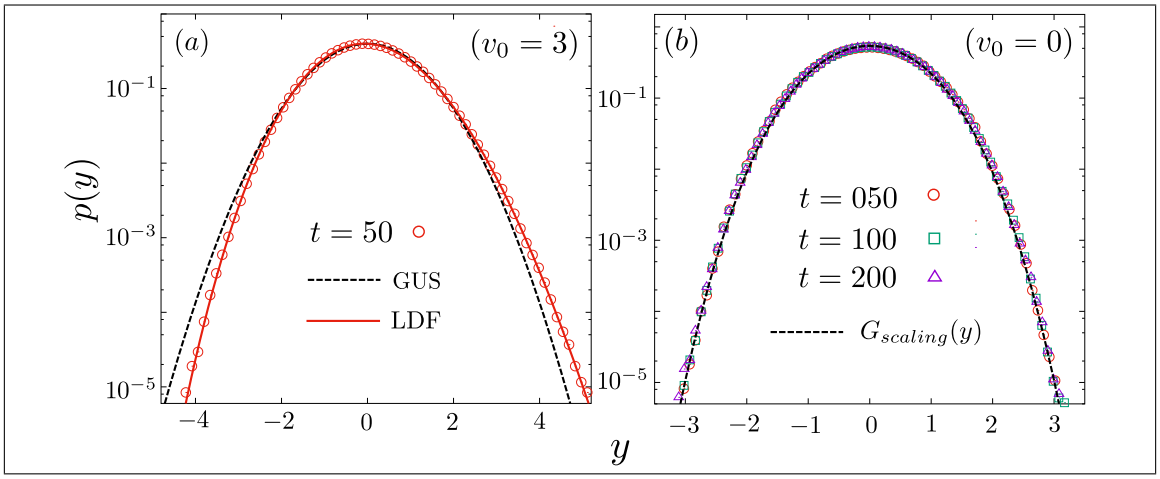

Figure 3.4: Conditional distributions of the net overtaking number $m(t|v_0)$ by a tagged agent of velocity v_0 are plotted in the two different limits (a) $t << t_1^*(v_0)$ and (b) $t >> t_1^*(v_0)$, for case II. To satisfy those limits we have conveniently considered the tagged velocity $v_0 = 3$ and $v_0 = 0$ in figure (a) and (b) respectively while drawing the remaining velocities from the Gaussian distribution. In (a), the simulation results, denoted by points, for the PDF of the scaled displacement $y \propto (m - \bar{c}t)/\sqrt{t}$, are plotted together with a Gaussian distribution (GUS) denoted by the dashed line. Alongside that to show a large fluctuation that deviates from the Gaussian, the large deviation result shown by the bold line. Figure (b) demonstrates that in the opposite limit $t >> t_1^*(v_0)$, with the appropriate scaling $y \propto t^{-2/3}(m - \bar{c}t)$, the PDFs for different times collapse onto the scaling function $G_{scaling}(y)$ (shown by dashed line).

On the other hand in the opposite limit ($t >> t_1^*(v_0)$) the distribution is related to the scaling function $G_{\rm scaling}(x)$ [9, 10] by

$$p(c, t|\bar{c}) \simeq (2\chi^{1/3}t^{-1/3})^{-1}\, G_{scaling}([c - \bar{c}]/2\chi^{1/3}t^{-1/3}) \tag{3.13}$$

which we have illustrated in FIG. 3.4(b). Notably, this $G_{scaling}(u)$ and $g''(u)$ in Eq. (3.11) are same quantity.

3.4.4 Unconditional distribution

In case of unconditional distribution, we first discuss it's behavior in the limit of $t \to \infty$. To do so, using Eq. (3.6) and Eq. (3.7a) we can write

$$c \sim \begin{cases} \bar{c} + \mathcal{O}(t^{-\frac{1}{2}}) & \text{for} \quad t << t_1^*(\bar{c}), \\ \bar{c} + \mathcal{O}(t^{-\frac{1}{3}}) & \text{for} \quad t >> t_1^*(\bar{c}). \end{cases} \tag{3.14}$$

Ignoring fluctuations around $\bar{c}(v_0)$, the variable c is random within $[-1 : 1]$ as $c = \bar{c}(v_0) = 1 - 2\rho_+(v_0)$. Therefore, using $dc/dv_0 = -2\rho'_+(v_0) = 2\rho(v_0)$, we get

$$P(c, \infty) = \frac{\rho(v_0(c))}{|dc/dv_0|} = \frac{1}{2}. \tag{3.15}$$

Thus $c = m(t)/t$, in the limit $t \to \infty$, is uniformly distributed on $[-1 : 1]$, for all continuous distribution $\rho(v)$. A somewhat similar result was obtained earlier for TASEP with the step initial condition, and it was shown that a second class particle starting at the step, acquires a limiting speed that is uniformly distributed on $[-1 : 1]$ [7, 8]. The corresponding result in our case appears when the initial velocities in our model are in the descending order, and an agent picked at random has a limiting speed, uniformly distributed on $[-1 : 1]$.

Now, to obtain the result at finite but large time we first reduce Eq. (2.2) as:

$$P(c, t) = \frac{1}{2} \int_{-1}^{1} d\bar{c} \;\; p(c, t|\bar{c}). \tag{3.16}$$

Now, considering the Gaussian approximated solution of $p(c, t|\bar{c}) = \sqrt{t/2\pi}\ \mathrm{Exp}[-(c - \bar{c})^2/2]$, the solution of the above Eq. (3.16) can be obtained as

$$P(c, t) \simeq \frac{1}{4}\left[\mathrm{Erf}\left(\sqrt{\frac{t}{2}}(c+1)\right) - \mathrm{Erf}\left(\sqrt{\frac{t}{2}}(c-1)\right)\right] \tag{3.17}$$

with the error function defined by $\mathrm{Erf}\,(\mathrm{u}) = \frac{2}{\sqrt{\pi}} \int_0^u e^{-w^2}\, dw$. Using the same procedure we can numerically compute $P(c, t)$ by putting the large deviation solution of $p(c, t|\bar{c})$ from Eq. (3.12) into Eq. (3.16). The obtained numerical solution is show-

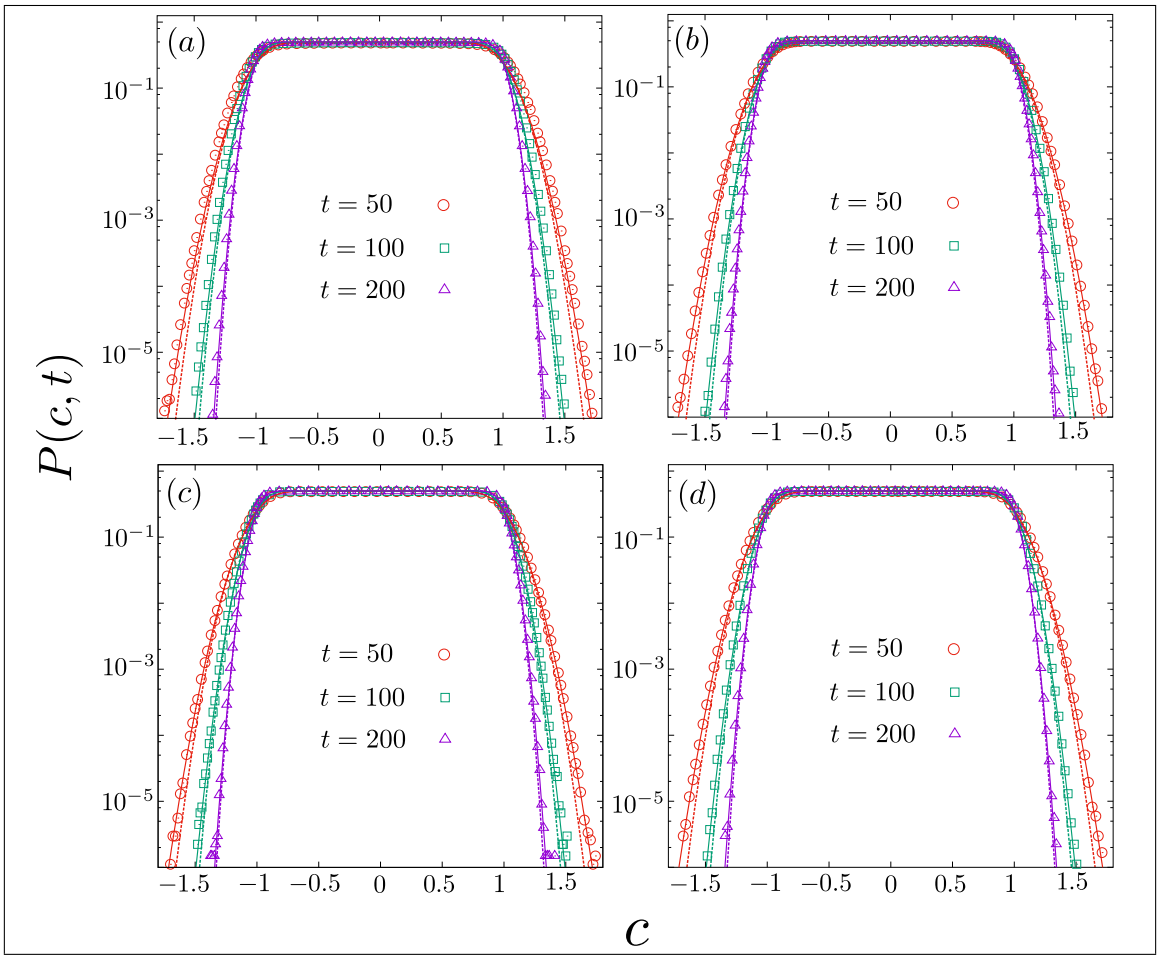

Figure 3.5: (a) Probability density function $P(c,t)$ of the scaled net overtakings $c(t) = m(t)/t$ are plotted at three different times in case II with four different choices of the initial velocity distribution, namely, (a) uniform, (b) Gaussian, (c) exponential, and (d) power-law ($\nu = 2.5$) distributions. The discrete points in the plots are the simulation results, which are showing good agreements with the results coming from the analysis of the large deviation form of the conditional distribution $p(c,t|v_0)$ (as shown by the bold lines). The corresponding results coming from the Gaussian approximation, are plotted by the dashed lines, for which the agreements at the tails improve as t becomes larger.

ing a good agreement with the simulation result as illustrated in FIG. 3.5. Note that this Gaussian approximated solution and the corresponding LDF is valid for $t << t_1^*(v_0)$. For a finite but large time t, this criteria yield the limit $v_0 \to \pm\infty$ which corresponds $c(v_0) \to \pm 1$. It implies the solution $P(c,t)$, in this case, accurate around the tails of the distribution.

To obtain an alternate analytical result at the tails we argue and proceed as follows. The contribution of the right tail of $P(c,t)$, for example, comes from the limit of $v_0 \to \infty$. In this limit, we already know that v_0 executes a biased random walk on the lattice with the right jumping rate $\bar{c}(v_0)$. Alternatively, we can say it becomes a Poissonian process with rate $\bar{c}(v_0)$. Now, integrating over all $\bar{c}(v_0)$ we can approximately write Eq. (3.16) as

$$P_R(c \gtrsim 1, t) \simeq \frac{1}{2}\int_0^1 d\bar{c}\; p(c,t|\bar{c}) \simeq \frac{t}{2}\int_0^1 d\bar{c}\; e^{-\bar{c}t}\frac{(\bar{c}t)^{ct}}{(ct)!}. \tag{3.18}$$

Now, using the Stirling approximation $x! \simeq \sqrt{2\pi x}\;(x/e)^x$ we can further simplify the above expression as

$$P_R(c \gtrsim 1, t) \simeq \frac{1}{\sqrt{8\pi ct}}\left(\frac{e}{ct}\right)^{ct}\;\gamma(ct+1,t) \tag{3.19}$$

with the lower incomplete gamma function $\gamma(s,u) = \int_0^u dx\;\; x^{s-1}\;\; e^{-x}$. From the symmetry of the problem we can say that the behavior of the left tail is identical to the right one. It allows us to write the above expression in a more concrete form as

$$P_{\text{tails}}(|c| \gtrsim 1, t) \simeq \frac{1}{\sqrt{8\pi|c|t}}\left(\frac{e}{|c|t}\right)^{|c|t}\;\gamma(|c|t+1,t). \tag{3.20}$$

The obtained analytical result is showing a good agreement with the numerical simulation result as shown in FIG. 3.6(a). Notably, the above result is similar to the result we obtained by inserting the large deviation solution of $p(c,t|\bar{c})$ from Eq. (3.12) into Eq. (3.16).

Finally, to get the result around the center of $P(c,t)$ (i.e., $c \sim 0$), we use the data of $\mathrm{G}_{\text{scaling}}(x)$ from ref [9] to plug it Eq. (3.16) via Eq. (3.13). The obtained numerical result we plotted in FIG. 3.6(b) which is showing a good agreement with the result

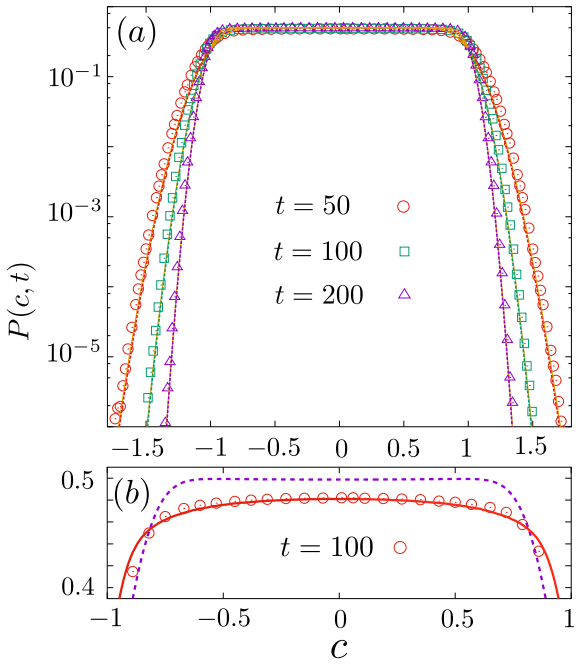

Figure 3.6: Probability density function $P(c,t)$ of the scaled net overtakings $c(t) = m(t)/t$ are plotted for case II. In (a): Discrete points are from a numerical simulation where the initial velocities are chosen from a uniform distribution on $[-1,1]$ with the dashed lines plot Eq. (3.20) with the bold lines computed by putting the large deviation solution of $p(c,t|\bar{c})$ from Eq. (3.12) into Eq. (3.16). In (b): Discrete points are from a numerical simulation where the initial velocities are chosen from a uniform distribution on $[-1,1]$ and t = 100. The solid line plots Eq. (3.16) computed by using Eq. (3.13) and the dashed line plots Eq. (3.17) for t = 100.

coming from simulation.

3.5 Case III : $r(v_L, v_R) = (v_L - v_R)\,\Theta(v_L - v_R)$

The relative velocity-dependent exchange in the updation rule makes this process completely different from the earlier one. The process here, in fact, corresponds to an infinite-species Karimipour model in ref [17]. Unlike case II, here, each particle (with its distinct velocity) exchanges with a distinct rate with the tagged particle of a given velocity. Hence, we expect that the result, in this case, may have a dependence on the initial velocity distribution.

3.5.1 Mean and variance of the net overtaking number

From the numerical simulation, like case II, here also we get a velocity-dependent crossover time $t_1^{\#}(v_0)$ which increases with the absolute value of v_0. Below that time scale ($t << t_1^{\#}(v_0)$), the behavior of v_0 is well approximated by the RW description by ignoring the correlation between jump events. The jumping rates to the right (r)

and the left (l) can be calculated in this limit as

$$p_r(v_0) = \int_{-\infty}^{v_0} (v_0 - v)\ \rho(v)\ dv \tag{3.21a}$$

$$p_l(v_0) = \int_{v_0}^{\infty} (v - v_0)\ \rho(v)\ dv. \tag{3.21b}$$

Notably, these jumping rates are the same as that of Jepsen gas of uniformly distributed particles with density $\varrho = 1$ which we have discussed in Sec. 2.3.1. Hence, by following a similar procedure from Sec. 2.3.2 we can write the mean and the variance as follows:

$$\langle m(t|v_0)\rangle = \bar{c}(v_0)t = (p_r(v_0) - p_l(v_0))t = (v_0 - \langle v\rangle)t \tag{3.22a}$$

$$\langle m^2(t|v_0)\rangle_c = \sigma^2(v_0)t = (p_r(v_0) + p_l(v_0))t. \tag{3.22b}$$

The behavior in the opposite limit ($t >> t_1^{\#}(v_0)$), from the numerical simulation, shows an anomalous growth of the form

$$\langle m^2(t|v_0)\rangle_c \propto t\ s(t) \tag{3.23}$$

where $s(t)$ gives the correction to the standard RW result. The exact behavior of the factor $s(t)$ is difficult to distinguish from our simulation. It may be either a very-small power-law $s(t) \sim t^{0.12..}$ or a logarithmic correction $s(t) \sim (\ln t)^{\gamma}$. It is difficult to distinguish between these two behaviors based on our numerics (as shown in FIG. 3.7) - as it is often appears in the case of marginal corrections [18–21]. Such logarithmic corrections have been found earlier in two dimensional driven diffusive systems [22–24] as well as for 1+1 dimensional interface with cubic nonlinearity [25–27]. Although the nature of the anomalous growth is not clear, it seems, it is quite robust as it is independent of the initial velocity distribution which we have displayed in FIG. 3.7. We come back to this discussion in Chapter 5.

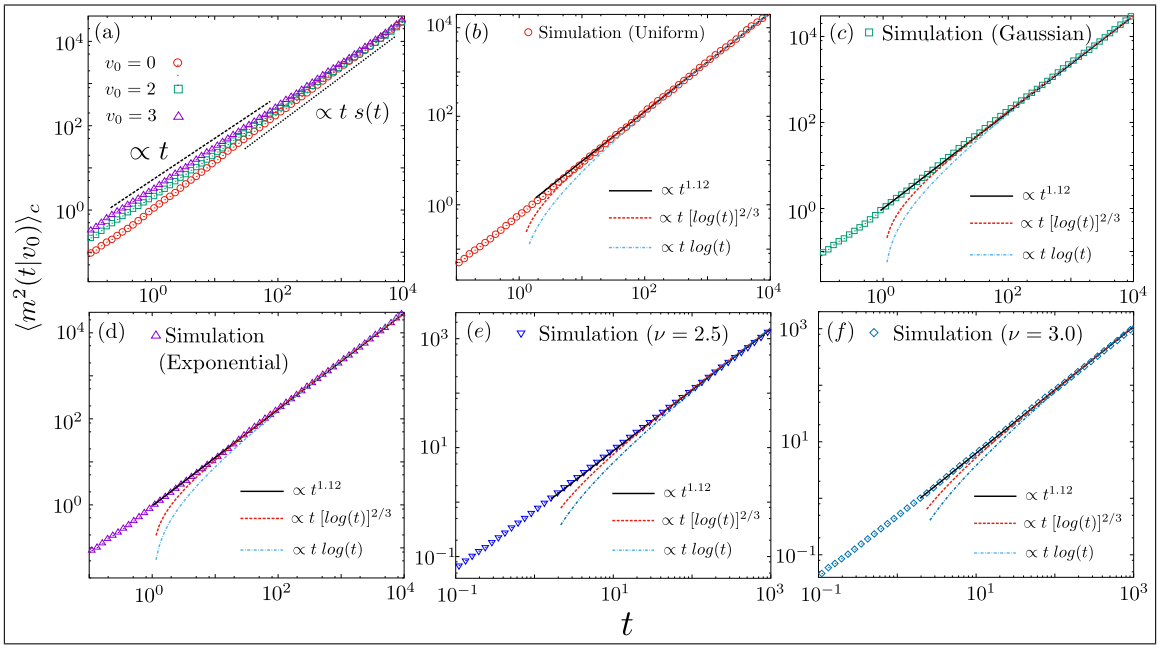

Figure 3.7: Simulation results of the variance of the net overtaking number by a tagged particle in case III are shown by discrete points. In figure (a), we plot the variance for three different values of the tagged velocity by taking the remaining velocities from the Gaussian distribution. The finite size effects do not show up till the final measurement time considered in the simulations, for a system of size $N = 10^4$ with periodic boundary condition. The data for the largest tagged velocity $v_0 = 3$ shows only a linear growth $\propto t$ in time. The data for the intermediate value v_0 is showing a transition from the initial $\propto t$ behavior to an anomalous long time behavior. For $v_0 = 0$ an anomalous growth is clearly noticeable. In the next five figures, we plot the displacement variance of a tagged $v_0 = \langle v \rangle$ by taking the remaining velocities from uniform, Gaussian, exponential, and power-law distributions of exponents $\nu = 2.5$ and 3.0 respectively. In all the five cases we obtain the same anomalous behavior. However, the exact anomalous behavior is not clear as it matches with both $\propto t^{1.12}$ (as shown by bold lines) and $\propto t\ [\log(t)]^{\gamma}$. Our simulation results show a good agreement for both $\gamma = 2/3$ (as shown by dashed lines) and $\gamma = 1$ (as shown by dotdashed lines).

3.5.2 Conditional distribution

In the limit $t << t_1^{\#}(v_0)$, we can write a complete solution of $p(c, t|v_0)$ in terms of $\bar{c}(v_0)$ and $\sigma^2(v_0)$ as

$$p(c,t|v_0) \simeq \sqrt{\frac{t}{2\pi}} \frac{e^{t\ \phi(c,v_0)}}{\sqrt{|\phi''(c,v_0)|}}, \tag{3.24a}$$

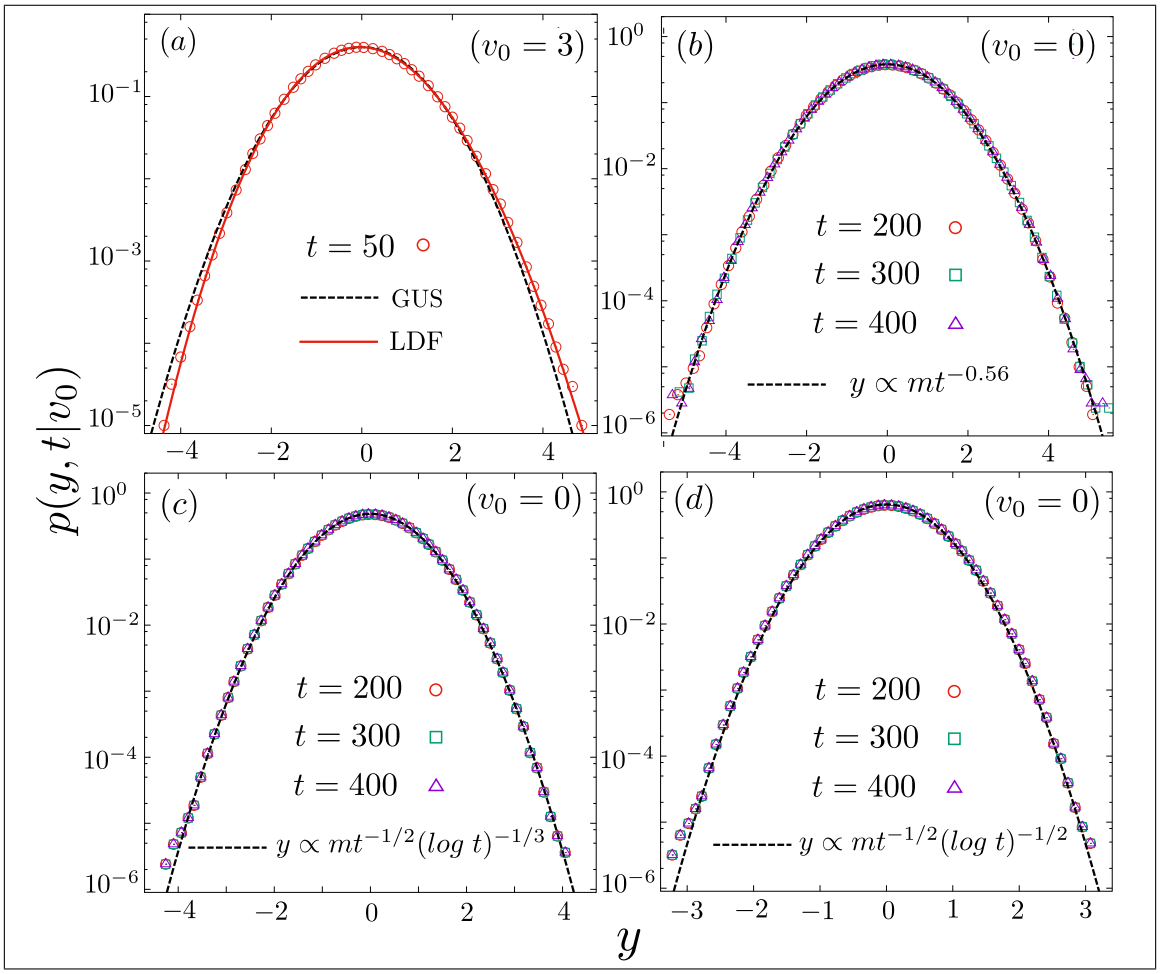

Figure 3.8: Conditional PDF of the displacement of a tagged particle with a given velocity in the two different limits (i) $t << t_1^{\#}(v_0)$ (in figure (a)) and (ii) $t >> t_1^{\#}(v_0)$ (in other figures), for the case III. To satisfy these limits we conveniently consider the tagged velocity $v_0 = 3$ and 0, respectively, while drawing the rest of the velocities independently from a Gaussian distribution. In figure (a), the typical fluctuations of the scaled displacement $y \propto (m - \bar{c}t)/\sqrt{t}$ are Gaussian (shown by the dashed line) with it atypical fluctuations better described by a large deviation result (shown by the bold line). In the next three figures, we consider the opposite limit $t >> t_1^{\#}(v_0)$, where the PDF of the scaled displacement $y \propto (m - \bar{c}t)/\sqrt{t\ s(t)}$ is well described by Gaussian (shown by dashed lines), the exact time dependence of the variance is not clear as it matches equally well with (b) $s(t) \propto t^{0.12}$ as well as $s(t) \propto (\log t)^{\gamma}$ for (c) $\gamma = 2/3$ and (d) $\gamma = 1$.

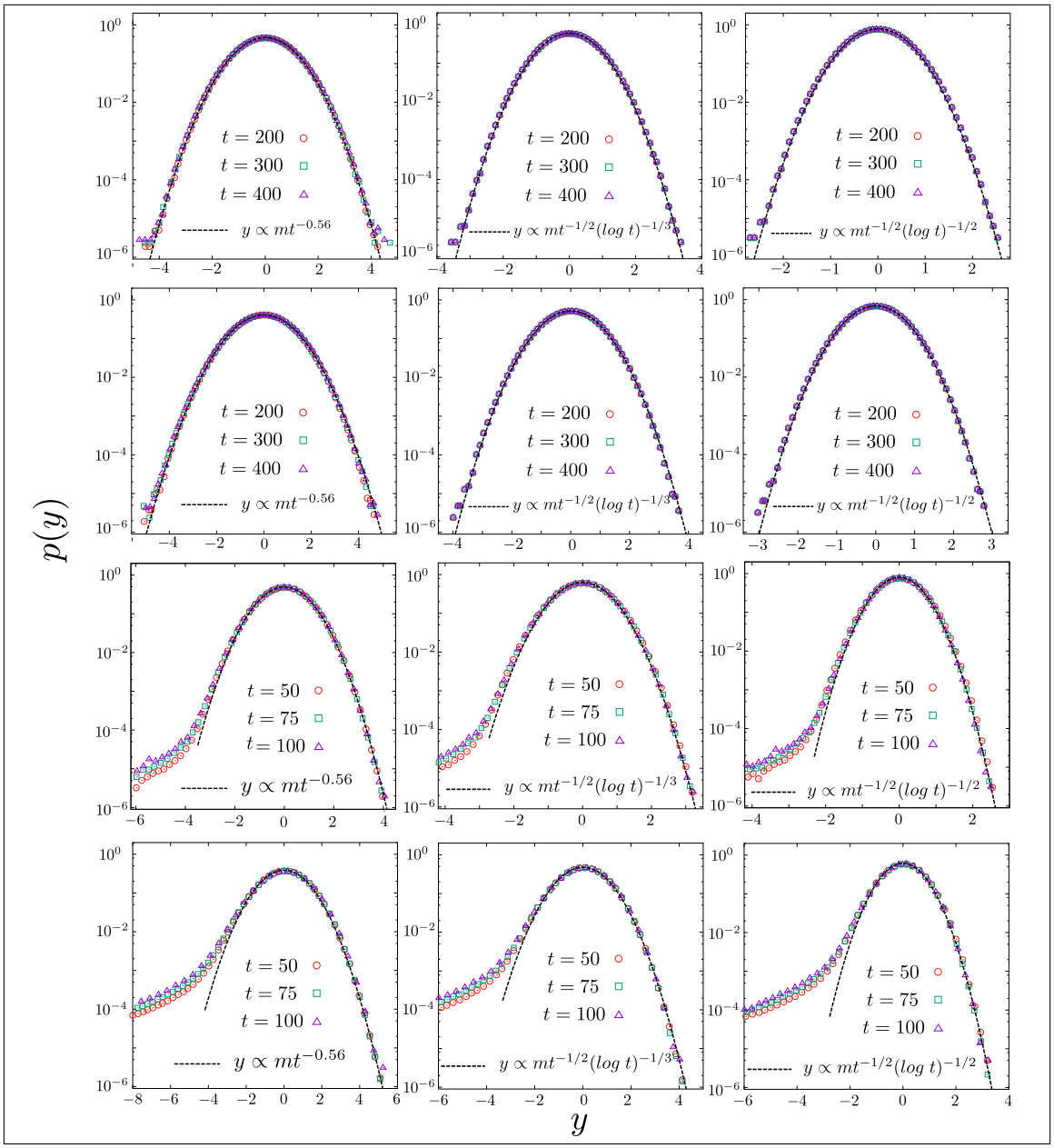

Figure 3.9: Conditional PDF's of the displacement of a tagged particle of velocity $v_0 = \langle v \rangle$ are plotted at times $t \gg t^{\#}(v_0)$, for the case III. The velocities of the remaining particles are drawn from three different distributions: uniform (1st row), exponential (2nd row), and power-law distribution of exponents $\nu = 2.5$ (3rd row) and $\nu = 2.0$ (4th row). While the typical fluctuations of the scaled displacement $y \propto (m - \bar{c}t)/\sqrt{ts(t)}$ is well described by Gaussian (shown by dashed lines), the exact time dependence of the variance is not clear as it matches equally well with $s(t) \propto t^{0.12}$ (figures on the first row) as well as $s(t) \propto [\log(t)]^{\gamma}$ for $\gamma = 2/3$ (figures on the 2nd row) and $\gamma = 1$ (figures on the 3rd row).

$$\text{with the LDF } \phi(c, v_0) = \sqrt{c^2 + \sigma^4(v_0) - \bar{c}^2(v_0)} - \sigma^2(v_0) - c \log \left[\frac{c + \sqrt{c^2 + \sigma^4(v_0) - \bar{c}^2(v_0)}}{\bar{c}(v_0) + \sigma^2(v_0)} \right], \tag{3.24b}$$

$$\text{and } |\phi''(c, v_0)| = \sqrt{c^2 + \sigma^4(v_0) - \bar{c}^2(v_0)}. \tag{3.24c}$$

From here, we can also get the Gaussian approximated solution in terms of scaled variable $y = (\sigma^2(v_0)t)^{-1/2}(m - \bar{c}(v_0)t)$. Both the results are plotted in FIG. 3.8(a) alongside the numerical simulation result.

In the opposite limit $t >> t_1^{\#}(v_0)$, from the numerical simulation, we have found the scaled PDF Gaussian around the mean. Like the variance, this result is also quite robust in the sense that it is independent of all initial velocity distribution as we verified it by numerical simulation and shown in FIG. 3.8 and FIG. 3.9. Notably, in case of power-law $\rho(v)$, the scaled distribution is showing a different behavior at the left tail (see 3rd and 4th columns of FIG. 3.9). The behavior is due to the large velocities present in the system which rotates our periodic system multiple times at any finite but large time. This behavior we describe in details in Chapter 5 while we encounter the finite size effects on the same problem.

3.5.3 Unconditional distribution

To study the unconditional distribution, we first observe that both $\sigma^2(v_0)/t \to 0$ and $s(t)/t \to 0$ in the limit $t \to \infty$. It yields

$$p(c, t \to \infty | v_0) \sim \delta(c - v_0 + \langle v \rangle) \sim \delta(c - \bar{c}(v_0)). \tag{3.25}$$

Now, by using Eq. (2.2) we can easily get

$$P(c, t \to \infty) \sim \rho(c + \langle v \rangle). \tag{3.26}$$

It implies that $P(c, t)$ converges towards the initial velocity distribution $\rho(v)$ with a shifted origin differ by the average $\langle v \rangle$ of the same distribution.

Now, to obtain the approach to this limiting distribution, we will use the explicit

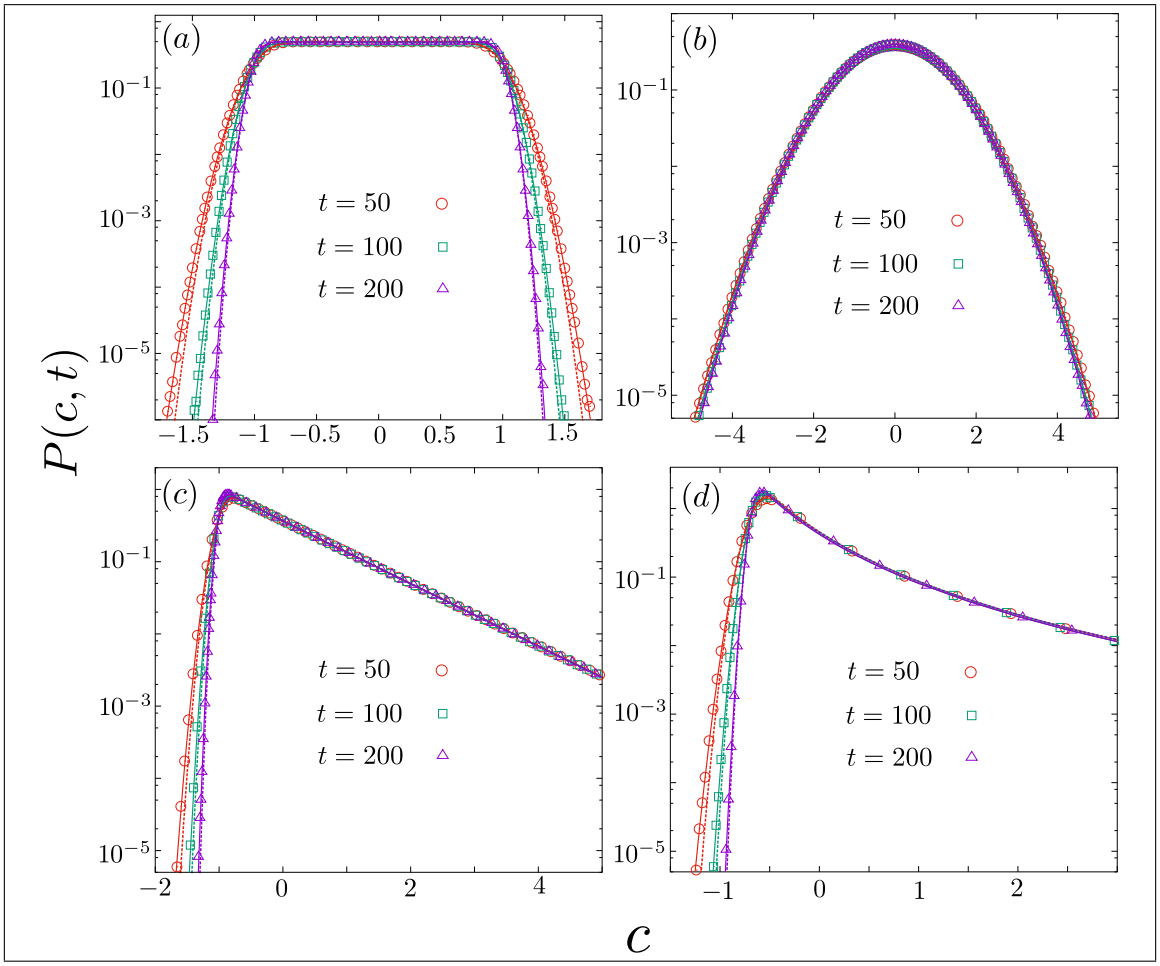

Figure 3.10: Probability density function $P(c,t)$ of the scaled net overtakings $c(t) = m(t)/t$ are plotted at three different times for case III, with four different choices of the initial velocity distribution, namely, (a) uniform (b) Gaussian (c) exponential and (d) power-law distributions. The discrete points in each plot are the simulation results. They show very good agreement with the results coming from the analysis of the large deviation form of the conditional distribution $p(c,t|v_0)$ (as shown by the bold lines). The corresponding results coming from the Gaussian approximation results are also plotted (as shown by the dashed lines), for which the agreements at the tails improve as t increases.

form of $p(c,t|v_0)$ in Eq. (3.24). Note that the tails of $P(c,t)$ comes from the large $|v_0 - \langle v \rangle|$ behavior of $p(c,t|v_0)$. For large $|v_0 - \langle v \rangle|$ the transition time $t_1^{\#}(v_0)$ is large which allows to consider the RW description of $p(c,t|v_0)$ at any finite time. Clearly, the Gaussian approximated solution in this case can be expressed as

$$P(c,t) \simeq \int_{-\infty}^{\infty} dv_0 \; \rho(v_0) \sqrt{\frac{t}{2\pi \; \sigma^2(v_0)}} \exp\left(-\frac{t\,[c + \langle v \rangle - v_0]}{2\;\sigma^2(v_0)}\right). \tag{3.27}$$

Note that the behavior of $P(c,t)$ depends on the form of $\rho(v_0)$ and, hence, we need to carry out the integral separately in each case. Figure 3.10 shows very good agreement between Eq. (3.27) and numerical simulation results for four different distributions. The agreement becomes more accurate if, instead of Gaussian approximated $p(c,t|v_0)$, one uses the exact large deviation form of Eq. (3.24) in the above equation.

Bibliography

[1] D. Chowdhury, L. Santen, and A. Schadschneider, Physics Reports **329**, 199 (2000).

[2] K. Pearson Nature. **72**, 294 (1905).

[3] P. A. Ferrari, Probab. Theo. Relat. Fields 91, 81 (1992).

[4] P. A. Ferrari and C. Kipnis, Ann. Inst. H. Poincar Probab. Statist. **31**, 143 (2005).

[5] T. Mountford and H. Guiol, Ann. Appl. Probab. **15**, 1227(2005).

[6] P. A. Ferrari, C. Kipnis, and E. Saada, Ann. Probab. **19**, 226 (1991).

[7] G. Amir, O. Angel, and B. Valk, Ann. Probab. **39**, 1205 (2011).

[8] O. Angel, A. Holroyd, and Dan Romik, Ann. Probab. **37**, 1970 (2009).

[9] M. Prhofer and H. Spohn, In V. Sidoravicius, editor, In and out of equilibrium, Prog. Probab. **51**, 185 (Birkhuser, Boston 2002).

[10] P. L. Ferrari and H. Spohn, Comm. Math. Phys. **265**, 1 (2006).

[11] J. Baik and E.M. Rains, J. Stat. Phys. **100**, 523 (2000).

[12] M. Prhofer and H. Spohn, J. Stat. Phys. **115**, 255 (2004).

[13] See M. Prhofer and H. Spohn (2003).

[14] H. van Beijeren, R. Kutner, and H. Spohn, Phys. Rev.Lett. **54**, 2026 (1985).

[15] A. L. Barabasi and H.E. Stanley, *Fractal Concepts in Surface Growth* (Cambridge University Press, Cambridge, 1995).

[16] Family, F. & Vicsek, T. Scaling of the active zone in the Eden process on percolation networks and the ballistic deposition model. J. Phys. A 18, L75L81 (1985).

[17] Karimipour V 1999 Multispecies asymmetric simple exclusion process and its relation to traffic flow Phys.Rev. E 59 20512.

[18] M.A. van der Hoef and D. Frenkel, Phys. Rev. Lett. **66**, 1591 (1991).

[19] C.P. Lowe and D. Frenkel, Physica A **220**, 251 (1995).

[20] M. Isobe, Phys. Rev. E 77, 021201 (2008).

[21] J. Krug, R. A. Neiss, A. Schadschneider, and J. Schmidt, J Stat Phys (2018).

[22] C. Landim, J. Quastel, M. Salmhofer and H.-T. Yau, Comm. Math. Phys. **244**, 455 (2004).

[23] H.-T. Yau, Ann. Math. **159**, 377 (2004).

[24] J. Quastel and B. Valk, Arch. Rational Mech. Anal. **210**, 269 (2013).

[25] B. Derrida, J. L. Lebowitz, E. R. Speer, and H. Spohn, Phys. Rev. Lett. **67**, 165 (1991); J. Phys. A **24**, 4805 (1991).

[26] P. Devillard and H. Spohn, J. Stat. Phys. **66**, 1089 (1992).

[27] M. Paczuski, M. Barma, S. N. Majumdar, and T. Hwa, Phys. Rev. Lett. **69**, 2735 (1992).

[28] H. van Beijeren, J. Stat. Phys. **63**, 47 (1991).

[29] S. N. Majumdar and M. Barma, Phys. Rev. B, **44**, 5306 (1991).

[30] A. Borodin, P. L. Ferrari, M. Pröhofer, and T. Sasamoto, J. Stat. Phys. **129**, 1055 (2007).

[31] T. Imamura and T. Sasamoto, J. Stat. Phys. **128**, 799 (2007).

[32] A. de Masi and P. A. Ferrari, J. Stat. Phys. **38**, 603 (1985).

[33] R. Kutner and H. van Beijeren, J. Stat. Phys. **39**, 317 (1985).

[34] C. Kipnis, Ann. Prob., **14**, 397 (1986).

[35] Also remarked by H. Kesten, see in F. Spitzer, Adv. Math. **5**, 246 (1970).

Chapter 4

Finite-size effects on overtaking in case of Jepsen gas on a ring

4.1 Introduction

The outcome of a stochastic observable in a system in non-equilibrium depends on how the system is being prepared, i.e., on the initial condition. It also depends on how the constituents of the system evolve at the microscopic level, i.e., on the dynamical rule of transition. The finite size of the system can also affect the results if one observes it beyond the transient limit where the boundary effects come into play.

For example, in Chapter 2, we have studied a simple non-equilibrium system of self-driven agents to investigate the statistics of a stochastic observable, namely, the net overtaking number by a tagged agent with two different initial conditions based on how the agents are distributed in space. Notably, in these two different cases, we obtain different results. By following that, in Chapter 3, we extend our investigation on a minimal model of an interacting self-driven agents to study the same quantity of interest with two different dynamical rules and got different results in those cases. Following this thread, in this Chapter, we emphasize on the boundary condition. For that, we consider the same Jepsen gas [1] in Chapter 2 with the periodic boundary condition. We aim to study this problem with two different ensembles to see how the finite system size affects the results.

Specifically, for a system of size N, in the last two Chapters, we investigate our quantities of interest in a limit where $t << N$ to ensure that there are no boundary effects in the results. In this Chapter, we investigate the same in the opposite

limit, i.e., by taking $t >> N$ to see the results with the finite system size effects. Among two different ensembles, in the 1st, we consider a fixed number of uniformly distributed agents, whereas, in the next, the number of randomly distributed agents in space is taken from a Poisson distribution of given density of agents.

In addition to all, in this Chapter, we briefly introduce the finite size scaling analysis and the dynamical exponent [2]. This exponent can estimate an approximate time at which the tagged dynamics makes a transition from system-size independent initial behavior to system-size dependent long-time behavior. In non-equilibrium systems, this exponent behaves like a critical exponent. Depending on its value, one can say the dynamical universality class on which the process belongs. Hence, this exponent has widely been studied in the context of different non-equilibrium systems, starting from well-established Edwards-Wilkilson [3] and Kardar-Parisi-Zhang (KPZ) [4] universality classes in the interface growth model to the recently studied Fibonacci universality classes in driven diffusive systems [5–7].

The rest of the chapter is organized as follows. First, in Sec. 4.2, we outline our model with two different ensembles and our quantities of interest. Next, in Sec. 4.3, we discuss our problem by considering the 1st ensemble followed by the 2nd ensemble in Sec. 4.4. In Sec. 4.3, first, we derive an approximate result of the net overtaking number by a tagged agent. By using that result, we calculate all the cumulants and the dynamical exponent associated with the process in Sec. 4.3.2. Next we discuss the conditional and the unconditional distributions associated with the tagged overtaking number in Sec. 4.3.3 and 4.3.4 respectively. In Sec. 4.4, all the results in case of 2nd ensemble are presented by following a similar sequence like the earlier section.

4.2 Model and Quantities of interest

4.2.1 The model

Consider a collection of non-interacting point particles distributed uniformly on a ring of size N. With time all these particles are moving with their constant velocities which are taken independently for each particle from an identical distribution $\rho(v)$. The space-time trajectories of the particles are given by slanted straight lines where

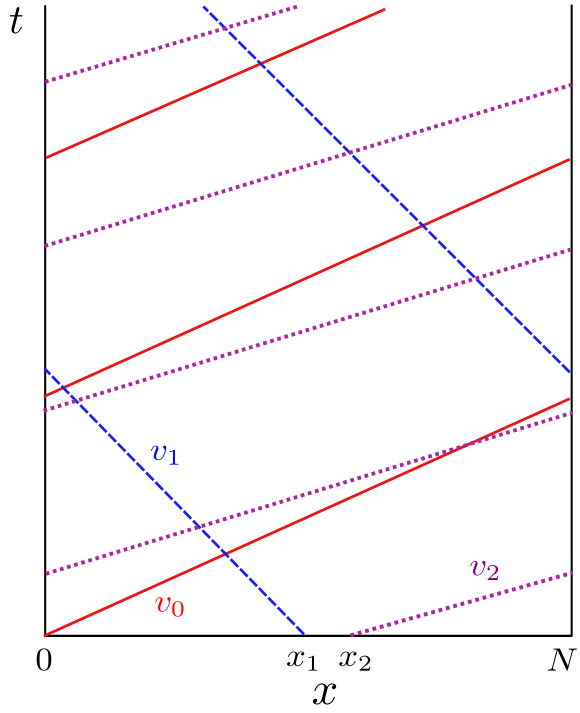

Figure 4.1: Space-time trajectories of three particles in a Jepsen gas, confined within a periodic system of size N, up to time t are shown. The red (bold) line starting at the origin ($x = 0$) represents the trajectory of a tagged particle with velocity v_0, while the blue (dashed) and the magenta (dotted) lines starting at positions x_1 and x_2 with velocities $v_1 < v_0$ and $v_2 > v_0$ represent the other two trajectories respectively. Due to the periodicity, the red line intersects the blue one four times. In the language of overtaking, the red line overtakes the blue line 4 times while being overtaken by the magenta line once. Therefore, the net number of overtake events for the red line up to time t is $4 - 1 = 3$.

the slopes with respect to the time axis represents the velocities. Notably, the periodicity in the problem allows two lines to intersect each other multiple times (as illustrated in FIG. 4.1) which is entirely different from the problem on an infinite line where any two lines can intersect each other at most once (see FIG. 2.1).

Two different ensembles:

In this chapter, we study two different ensembles. In the 1st, we take a fixed (or constant) number of agents distributed randomly within the system, whereas in the next, the number of randomly distributed agents can change from one realization to other. The probability of getting a particular number in this case is Poisson distribution.

Quantities of interest

In this chapter, we revise all the quantities we have already defined in Chapter 2 in particular in the limit where time t is much larger than the system size N. Hence, from the Sec. 2.2.2, we first recall the net overtaking number $m(t|v_0)$ by a tagged agent of velocity v_0 at time t. Our goal here is to study its mean $\langle m(t|v_0)\rangle$,

variance $\langle m^2(t|v_0)\rangle_c$, and any n-th order cumulant $\langle m^n(t|v_0)\rangle_c$. We also intend to investigate the same two probability distributions we have introduced in Sec. 2.2.2. They are the conditional and the unconditional distributions denoted by $p(m,t|v_0)$ and $P(m,t)$ respectively.

In addition to all, here we introduce a new quantity of interest, namely, the dynamical exponent [2].

4.2.2 Finite-size scaling analysis and dynamical exponent

To introduce the dynamical exponent in the context of our problem, we first define an approximate time $\tau^*(v_0)$ at which the fluctuation of $m(t|v_0)$ makes a transition from the system-size independent behavior to the system-size dependent behavior. Notably, the system-size independent behavior can be obtained by taking $N \to \infty$ first, and then $t \to \infty$, whereas the other one by reversing the limits, i.e., by taking $t \to \infty$ first, and then $N \to \infty$. The dynamical exponent relates $\tau^*(v_0)$ and the system size N via [2]

$$\tau^*(v_0) \sim N^z. \tag{4.1}$$

Now, let us consider that the fluctuation of our quantity of interest grows in time by following the relation

$$\langle m^2(t|v_0)\rangle_c \sim t^\gamma \tag{4.2a}$$

in the first limit. On the other hand, in the opposite limit the relation is

$$\langle m^2(t|v_0)\rangle_c \sim N^\alpha t^\delta. \tag{4.2b}$$

Now, combining all together we can write a scaling ansatz [2] of the variance of the net overtaking number as

$$\langle m^2(t|v_0)\rangle_c \sim N^\xi \; f\left(\frac{t}{\tau^*}\right) \sim \begin{cases} t^\gamma & \text{for } t << \tau^*(v_0) \\ N^\alpha \; t^\delta & \text{for } t >> \tau^*(v_0). \end{cases} \tag{4.3}$$

with the scaling function $f(u = t/N^z)$, and exponents α, γ, δ, and ξ. Clearly, $f(u)$ satisfies the relation $f(u) \sim u^\gamma$ for $u \to 0$ and $f(u) \sim u^\delta$ for $u \to \infty$. The behavior

of $f(u)$ in these two limits yields the following relations among the exponents (i) $\xi = \gamma z$, and (ii) $\xi - z\delta = \alpha$. Now, by combining these two relations we can find out z as

$$z = \frac{\alpha}{\gamma - \delta}. \tag{4.4}$$

For example, if we consider a biased random walk on a periodic ring, then the variance of its position on the lattice $\langle x^2(t)\rangle_c \sim t$ in the first limit and $\langle x^2(t)\rangle_c \sim N^2/12$ in the opposite limit (see Sec. 1.3). It implies $\gamma = 1$, $\alpha = 2$, and $\delta = 0$ i.e., $z = 2$ which alternatively justifies the system belonging diffusive universality class.

4.3 Ensemble I

For convenience, in this section, we consider the number of particles equal to the system size N. We study the statistics of the net overtaking number by a tagged agent moving in the environment of these N number of particles.

4.3.1 Net overtaking number

To calculate the rate of overtaking, we introduce a tagged particle of velocity v_0 at an arbitrary position which we set as origin of our periodic system. Now, let x_i, and v_i be respectively the position and the velocity of the i-th particle at the beginning. It allows us to write the net number of overtaking events by a particle with velocity v_0 up to time t as:

$$\begin{aligned} m(t|v_0) &= \underbrace{\sum_{i=1}^{N} I(v_0 > v_i) \left\lceil \frac{(v_0 - v_i)t - x_i}{N} \right\rceil}_{m_R(t|v_0)} - \underbrace{\sum_{i=1}^{N} I(v_0 < v_i) \left\lceil \frac{(v_i - v_0)t - (N - x_i)}{N} \right\rceil}_{m_L(t|v_0)} \\ &\simeq \sum_{i=1}^{N} I(v_0 > v_i) \frac{(v_0 - v_i)t - x_i}{N} - \sum_{i=1}^{N} I(v_0 < v_i) \frac{(v_i - v_0)t - (N - x_i)}{N} \\ &\simeq \left(v_0 - \frac{1}{N}\sum_{i=1}^{N} v_i \right) t \; - \; \sum_{i=1}^{N} \frac{x_i}{N} \; + \; \sum_{i=1}^{N} I(v_0 < v_i). \end{aligned} \tag{4.5}$$

On the 1st line, the first (second) term on the right hand side counts the events in which $v_0 > v_i$ ($v_0 < v_i$) with the aid of the indicator function $I(v_0 > v_i)$ ($I(v_0 < v_i)$).

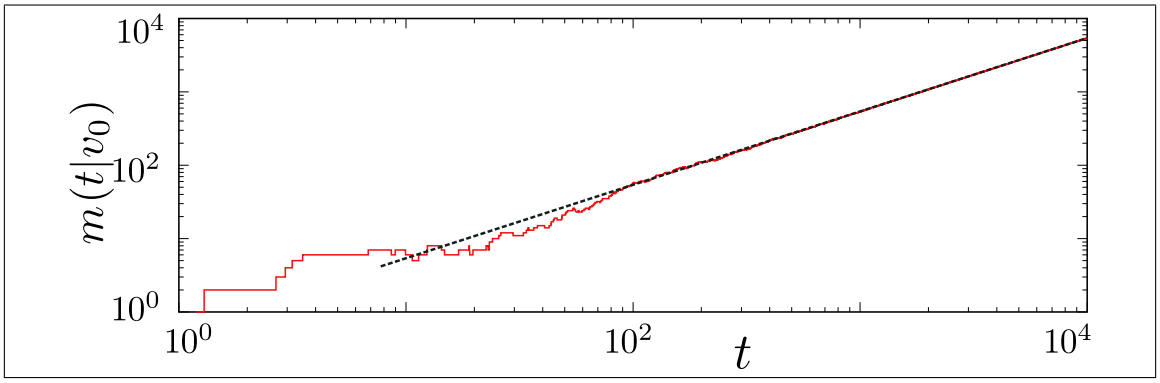

Figure 4.2: Net overtaking number $m(t|v_0)$ of a tagged particle with velocity $v_0 = 0.5$ is plotted versus time t for a system of size $N = 128$ with N number of uniformly distributed Gaussian velocities. The dotted line, plots Eq. (4.6), is showing a good agreement with $m(t|v_0)$ in the limit of $t >> N$.

Here $\lceil u \rceil$ is Ceiling function which yields the smallest integer greater than or equal to a real number u. Now using the fact that $I(v_0 > v_i) + I(v_0 < v_i) = 1$, and by assuming $m(t|v_0)$ is a large number which allows us to approximate any real variable u as $\lceil u \rceil \simeq u + \mathcal{O}(1)$. With these two assumptions, we have derived the final result in Eq. (4.5). Now, both the 2nd and 3rd terms on the right hand side in Eq. (4.5) are of the order of N, which in the limit of $t >> N$ allows to simplify the above expression as

$$m(t|v_0) \simeq \left(v_0 - \frac{1}{N} \sum_{i=1}^{N} v_i \right) t + \mathcal{O}(N) \simeq (v_0 - V)\, t \tag{4.6}$$

with a new variable $V = 1/N \sum_{i=1}^{N} v_i$, for further convenience. Notably, this V is the average valocity of N number of velocities present in the system. The derived expression in Eq. (4.6) shows a good agreement with the exact overtaking number in Eq. (4.5) as illustrated in FIG. 4.2.

4.3.2 Cumulants of the net overtaking number

As all the initial velocities are taken independently from a common distribution, one can relate the n-th order cumulant $\langle V^n \rangle_c$ of $V = N^{-1} \sum_{i=1}^{N} v_i$ with the same of the

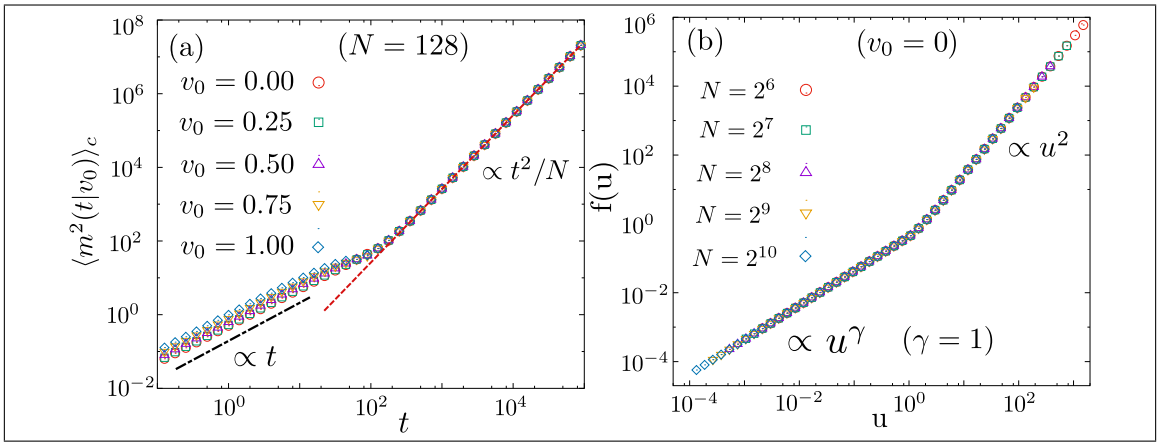

Figure 4.3: (a) Simulation results (shown by symbols), illustrating the crossover from the system-size independent initial $\propto t$ behavior to the system-size dependent long-time $\propto t^2/N$ behavior, for the variance of the net overtaking number by a tagged agent moving in a Jepsen gas. Five different tagged velocities are considered by drawing the remaining N velocities from a uniform distribution over $[-1 : 1]$ within a periodic system of size $N = 128$. (b) Numerical results of the scaling function $f(u)$ are plotted vs. $u = t/N^z$ for five different system sizes by considering the tagged velocity $v_0 = 0$ while drawing the remaining velocities from the same uniform distribution.

initial velocity distribution $\langle v^n\rangle_c$ as:

$$\langle V^n\rangle_c = \left[\frac{d^n}{ds^n}\ln\left\langle e^{sV}\right\rangle\right]_{s=0} = N\ \left[\frac{d^n}{ds^n}\ln\left\langle e^{sv/N}\right\rangle\right]_{s=0} = \frac{1}{N^{n-1}}\langle v^n\rangle_c. \tag{4.7}$$

Now using Eq. (4.6) and (4.7), we can find out the n-th order cumulant of $m(t|v_0)$ as:

$$\begin{aligned}\langle m^n(t|v_0)\rangle_c &= \left[\frac{d^n}{ds^n}\ln\left\langle e^{s\ m(t|v_0)}\right\rangle\right]_{s=0} \simeq \left[\frac{d^n}{ds^n}\ln\left\langle e^{s(v_0-V)\ t}\right\rangle\right]_{s=0}\\ &\simeq \left[\frac{d^n}{ds^n}\left(sv_0t + \ln\left\langle e^{-sVt}\right\rangle\right)\right]_{s=0} \simeq v_0\ t\ \delta_{n,1} + (-1)^n\langle V^n\ \rangle_c\ t^n\\ &\simeq v_0\ t\ \delta_{n,1} + (-1)^n\frac{1}{N^{n-1}}\langle v^n\rangle_c\ t^n. \end{aligned}\tag{4.8}$$

Note that for the power-law $\rho(v)$, depending on its exponent ν, the n-th order cumulant exist only if $n < \nu$ (see in Sec. 2.2.3).

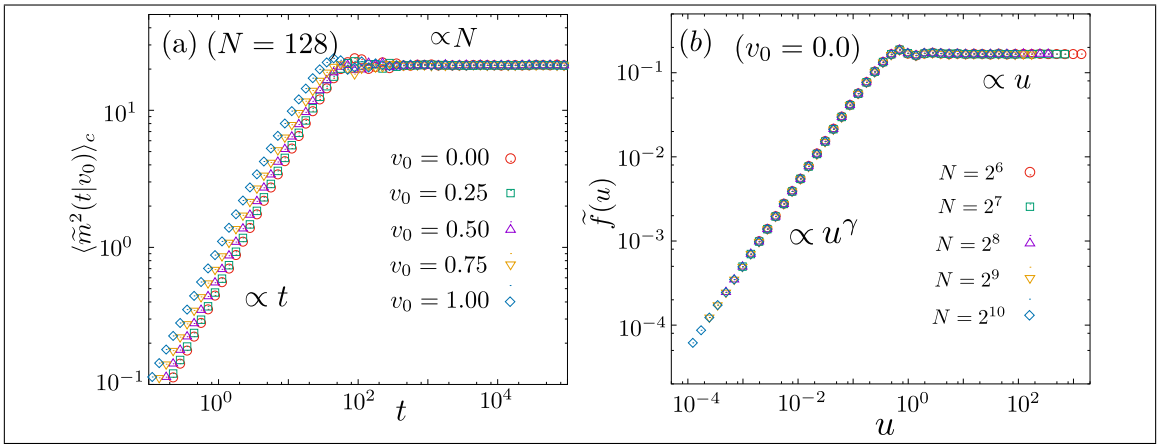

Figure 4.4: (a) Simulation results (shown by symbols), illustrating the crossover from the system-size independent initial $\propto t$ behavior to the system-size dependent long-time $\propto N$ behavior, for the variance of $\widetilde{m}(t|v_0)$ by a tagged agent moving in a Jepsen gas. Five different tagged velocities are considered by drawing the remaining N velocities from a uniform distribution over $[-1:1]$ within a periodic system of size $N = 128$. (b) Numerical results of the scaling function $\widetilde{f}(u)$ are plotted vs. $u = t/N^z$ for five different system sizes by considering the tagged velocity $v_0 = 0$ while drawing the remaining velocities from the same uniform distribution.

Dynamical exponent

For a Jepsen gas on an infinite line $\langle m^2(t|v_0)\rangle_c$ grows linearly with time t (see Eq. (2.16)), which makes $\gamma = 1$. Now, the scaling ansatz of the form of Eq. (4.3), and then Eq. (4.8) allow us to identify $\alpha = -1$ and $\delta = 2$. By putting all these in Eq. (4.4) we can easily find out $z = 1$. We verify this result via numerical simulation by plotting the scaling function $f(u = t/N^z)$ in FIG. 4.3(b). The collapsed data-points of $f(u)$ for different N, supports our analytical $z = 1$. Arguably, the obtained result is quite intuitive. The logic behind it is as follows: The individual particles are moving ballistically without interacting with each other. It makes the gap between two successive intersecting time equals to $N/|v_1 - v_2| \propto N$ for two velocities v_1 and v_2. This intersecting time is directly proportional to the transition time τ^*, i.e., $\tau^* \propto N$ which yields $z = 1$.

Note that, in terms of the new variable $\widetilde{m}(t|v_0) = m(t|v_0) - \sum_{i=1}^{N} v_i/N$ we have found $\langle \widetilde{m}^2(t|v_0)\rangle_c \propto t$ in the limit $t << N$ and $\propto N$ in the limit $N << t$ (see FIG. 4.4(a)). In this case we can easily identify $\gamma = 1$, $\alpha = 1$, and $\delta = 0$. It also yields the dynamical exponent $z = 1$. The corresponding scaling function $\widetilde{f}(u) \propto u$

for $u << 1$ and goes to a constant for $u >> 1$. We have plotted it in FIG. 4.4(b)

4.3.3 Conditional distribution

In this subsection we describe the conditional distribution $p(m, t|v_0)$ for four different initial velocity distributions, one by one.

Gaussian $\rho(v)$:

First for the Gaussian distribution, employing Eq. (2.7) in Eq. (4.8), we can find out the conditional distribution in terms of a scaled variable $y = \sqrt{N}(m - v_0 t)/t$ as

$$p(y) \simeq \frac{1}{\sqrt{2\pi}} \text{Exp}\left(-\frac{y^2}{2}\right). \tag{4.9}$$

We verify this result with the numerical simulation results as shown in FIG. 4.5(a).

Uniform $\rho(v)$:

For uniform distribution of the form Eq. (2.4), we know that all odd moments/cumulants are zero. It implies, from Eq. (4.8), that all the odd cumulants (and hence, all odd moments) of the conditional distribution are zero except the mean $\langle m(t|v_0)\rangle = v_0 t$. Clearly, the distribution is symmetric around the mean with variance $\langle m^2(t|v_0)\rangle_c \simeq t^2/3N$. Now to measure the non-Gaussianity of the distribution we calculate the excess kurtosis as

$$g = \frac{\langle m^4(t)\rangle_c}{\langle m^2(t)\rangle_c^2} \simeq \frac{1}{N}\frac{\langle v^4\rangle_c}{\langle v^2\rangle_c^2} \simeq -\frac{6}{5N} \sim \mathcal{O}(N^{-1}). \tag{4.10}$$

For a sufficiently large, but finite system of size N, we can see that $g \to 0$. It makes the conditional distribution Gaussian of the form Eq. (4.9) in terms of a scaled variable $y = \sqrt{3N}(m - v_0 t)/t$ as verified by numerical simulation in FIG. 4.5(b).

Exponential $\rho(v)$:

For the exponential $\rho(v)$ of the form of Eq. (2.5), we can calculate the characteristic function by employing Eq. (2.9) and (4.8), and then writing it in terms of $c = m/t$,

and a reduced variable $\widetilde{k} = kt/N$ as

$$\begin{aligned}\left\langle e^{i\widetilde{k}N\, c(v_0)} \right\rangle &\simeq \text{Exp}\left[i\widetilde{k}N(v_0 - \langle v\rangle) + N\sum_{n=2}^{\infty} \frac{1}{n}\left(-i\widetilde{k}\right)^n \right] \\ &\simeq \text{Exp}\left[i\widetilde{k}Nv_0 - N\,\log\left(1 + i\widetilde{k}\right)\right].\end{aligned} \tag{4.11}$$

Now, inverting the Fourier transform, and then expressing it in terms of $\bar{c}(v_0) = v_0 - \langle v\rangle = v_0 - 1$, we can write

$$p(c|\bar{c}) = \frac{N}{2\pi}\int_{-\infty}^{\infty} d\widetilde{k}\; e^{-N\varphi(\widetilde{k},c)} \tag{4.12a}$$

$$\text{with}\;\; \varphi(\widetilde{k},c) = i\widetilde{k}(c - \bar{c} - 1) + \ln(1 + i\widetilde{k}). \tag{4.12b}$$

By evaluating this integration with the method of saddle point (see Sec. 1.3 for details), we can write

$$p(c|\bar{c}) \simeq \sqrt{\frac{N}{2\pi}}\; \frac{e^{-N\varphi(\widetilde{k}^*,c)}}{\sqrt{\varphi''(\widetilde{k}^*,c)}} \tag{4.13a}$$

$$\text{with} \qquad \varphi(\widetilde{k}^*,c) = -(c - \bar{c}) - \ln(\bar{c} + 1 - c) \tag{4.13b}$$

$$\text{and} \qquad \varphi''(\widetilde{k}^*,c) = (\bar{c} + 1 - c)^2 \tag{4.13c}$$

$$\text{at the saddle point} \qquad \widetilde{k}^* = i(c - \bar{c})/(c - \bar{c} - 1). \tag{4.13d}$$

From here, we can easily simplify it as

$$p(c|\bar{c}) \simeq \sqrt{\frac{N}{2\pi}}\; e^{N(c-\bar{c})}\; (\bar{c} + 1 - c)^{N-1}. \tag{4.14}$$

In terms of a scaled variable $y = \sqrt{N}(c - \bar{c})$, it further reduces to

$$p(y) \simeq \frac{1}{\sqrt{2\pi}} e^{\sqrt{N}y}\left(1 - \frac{y}{\sqrt{N}}\right)^{N-1}. \tag{4.15}$$

The obtained result shows good agreement with the numerical simulation result as displayed in FIG. 4.5(c). It is also clear that in the limit $N \to \infty$ it yields the Gaussian distribution of the form of Eq. (4.9), as shown in the same figure alongside

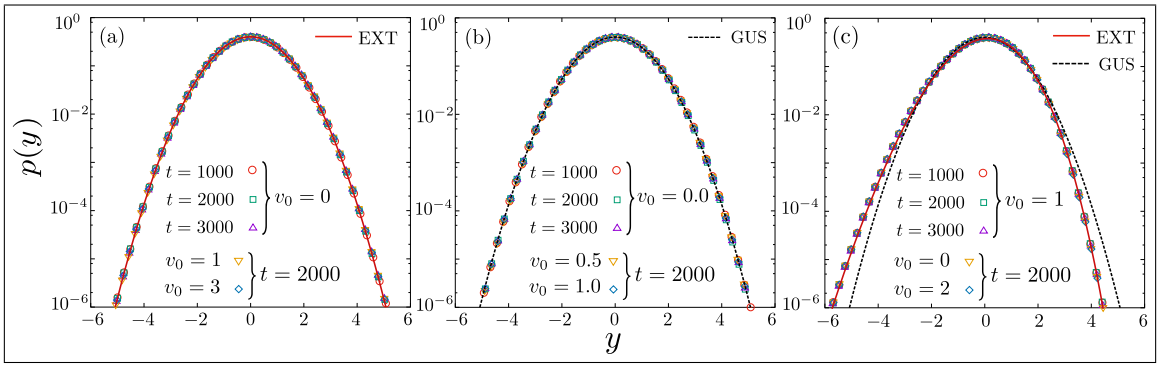

Figure 4.5: Conditional PDF of the scaled net overtakings $y = \sqrt{N}(m - \langle m(t|v_0)\rangle)/\sqrt{\langle m^2(t|v_0)\rangle_c}$ are plotted in the case of a Jepsen gas enclosed within a ring of size $N = 128$ with N number of velocities which are taken initially from (a) Gaussian, (b) uniform, and (c) exponential distributions. The discrete points are numerical simulation results which are showing good agreement with the exact analytical result (EXT) or/and the Gaussian approximated result (GUS) as shown by the solid and the dashed lines respectively.

the exact result.

Power-law $\rho(v)$:

To calculate the conditional distribution of the power-law distribution of the form Eq. (2.6), we first simplify the characteristic function in terms of $c = m/t$, and a reduced variable $\widetilde{k} = kt/N$ as

$$\begin{aligned}\left\langle e^{i\widetilde{k}N\, c(v_0)}\right\rangle &\simeq e^{i\widetilde{k}Nv_0}\left\langle e^{-i\widetilde{k}NV}\right\rangle \simeq e^{i\widetilde{k}Nv_0}\left\langle e^{-i\widetilde{k}v}\right\rangle^N \\ &\simeq \mathrm{Exp}\left[N\left(i\widetilde{k}v_0 + \log(\langle e^{-i\widetilde{k}v}\rangle)\right)\right].\end{aligned} \tag{4.16}$$

In the limit of large time, the number of overtake events are expected to be large, and hence, the expansion of this characteristic function around $\widetilde{k} \to 0$, is assumed to lead a well-approximated result. From here, by inverting the above equation via inverse Fourier transform, we can get the final result as

$$p(c|v_0) \simeq \frac{N}{2\pi}\int_{-\infty}^{\infty} d\widetilde{k}\ \mathrm{Exp}[N(-i\widetilde{k}(c - v_0) + \log(\langle e^{-i\widetilde{k}v}\rangle))]. \tag{4.17}$$

Now, depending on the expansion of $\log(\langle e^{-i\widetilde{k}v}\rangle)$ around $\widetilde{k} \to 0$ we discuss five different cases. They are respectively (a) $0 < \nu < 1$ (all the moments diverging), (b)

$\nu = 1$ (2nd and all the higher moments diverging with the logarithmic divergence of the 1st moment), (c) $1 < \nu < 2$ (finite 1st moment only), (d) $\nu = 2$ (finite 1st moment only and the logarithmic divergence of the 2nd moment with all diverging higher moments), and (e) $\nu > 2$ (finite 1st and 2nd moments).

(a) For $0 < \nu < 1$:

For the power-law distribution with $0 < \nu < 1$, we can write

$$\left\langle e^{-i\widetilde{k}v} \right\rangle = {}_1F_2\left(-\frac{\nu}{2}; \frac{1}{2}, 1-\frac{\nu}{2}; -\frac{\widetilde{k}^2}{4}\right) - i\widetilde{k}\left(\frac{\nu}{\nu-1}\right) {}_1F_2\left(\frac{1}{2}-\frac{\nu}{2}; \frac{3}{2}, \frac{3}{2}-\frac{\nu}{2}; -\frac{\widetilde{k}^2}{4}\right) - \Gamma(1-\nu)\,|\widetilde{k}|^\nu \,\mathrm{Exp}\left(\frac{i\pi\nu}{2}\,\mathrm{sgn}(\widetilde{k})\right), \quad (4.18)$$

with the generalized hypergeometric function ${}_pF_q(\{a_1, .., a_p\}; \{b_1, .., b_q\}; z)$, and the sign function $\mathrm{sgn}(x)$ which yields 1 for $x > 1$, 0 for $x = 0$, and -1 for $x < 1$. Now, by expanding the above expression around $\widetilde{k} \to 0$ for $\nu < 1$ we can write approximately

$$\langle e^{-i\widetilde{k}v} \rangle \simeq 1 - \Gamma(1-\nu)|\widetilde{k}|^\nu \,\mathrm{Exp}\left(\frac{i\pi\nu}{2}\,\mathrm{sgn}(\widetilde{k})\right) + \mathcal{O}(\widetilde{k}), \quad (4.19a)$$

$$\text{and hence, } \log(\langle e^{-i\widetilde{k}v} \rangle) \simeq -\Gamma(1-\nu)|\widetilde{k}|^\nu \,\mathrm{Exp}\left(\frac{i\pi\nu}{2}\,\mathrm{sgn}(\widetilde{k})\right) + \mathcal{O}(\widetilde{k}). \quad (4.19b)$$

Using this result in Eq. (4.17) we can derive an approximate result in terms of a scaled variable $y = N^{1-1/\nu}(c - v_0)$ and $s = \widetilde{k}N^{1/\nu}$ as as follows:

$$p(y) \simeq \frac{1}{2\pi}\int_{-\infty}^{\infty} ds\, \mathrm{Exp}\left[-isy - \Gamma(1-\nu)|s|^\nu \,\mathrm{Exp}\left(\frac{i\pi\nu}{2}\,\mathrm{sgn}(s)\right)\right] \simeq \frac{1}{\pi}\int_0^{\infty} ds\ \mathrm{Exp}\left[-\Gamma(1-\nu)s^\nu \,\mathrm{Cos}\left(\frac{\pi\nu}{2}\right)\right] \times \mathrm{Cos}\left[sy + s^\nu\,\Gamma(1-\nu)\,\mathrm{Sin}\left(\frac{\pi\nu}{2}\right)\right]. \quad (4.20)$$

One can evaluate this integration numerically, and find out that it is showing a good agreement with the result obtained from the numerical simulation as shown in FIG. 4.6(a).

(b) For $\nu = 1$:

For $\nu = 1$, as we know, all the moments of $\rho(v)$ diverge. Notably, the divergence of the 1-st moment is logarithmic. It makes this case completely different from the previous one. For example, the analogue of Eq. (4.18) in this case can be written as

$$\left\langle e^{-i\widetilde{k}v} \right\rangle = e^{-i\widetilde{k}} - i\widetilde{k}\,\Gamma(0, i\widetilde{k}) \simeq 1 - i\widetilde{k}\left(1 - \gamma - \frac{i\pi}{2}\mathrm{sgn}(\widetilde{k}) - \log(\widetilde{|k|})\right) + \mathcal{O}(\widetilde{k}^2) \quad (4.21)$$

with upper incomplete gamma function defined by $\Gamma(s,x) = \int_x^\infty du\ e^{-u}\ u^{s-1}$ and Euler's constant $\gamma = 0.5772156...$ Notably, the approximate result in Eq. (4.21) obtained by expanding around $\widetilde{k} \sim 0$. It further allows us to obtain

$$\log(\langle e^{-i\widetilde{k}v}\rangle) \simeq -i\widetilde{k}\left(1 - \gamma - \frac{i\pi}{2}\mathrm{sgn}(\widetilde{k}) - \log(\widetilde{|k|})\right) + \mathcal{O}(\widetilde{k}^2). \quad (4.22)$$

By using this result we can finally write and simplify the PDF in terms of a scaled variable $y = (c - v_0 + \log(N))$ and $s = \widetilde{k}N$ as

$$\begin{aligned} p(y) &\simeq \frac{1}{2\pi}\int_{-\infty}^{\infty} ds\ \mathrm{Exp}\left[-is\left(y + 1 - \gamma - \frac{i\pi}{2}\ \mathrm{sgn}(s) - \log(s)\right)\right] \\ &\simeq \frac{1}{\pi}\int_0^\infty ds\ \mathrm{Exp}\left[-\frac{s\pi}{2}\right]\ \mathrm{Cos}\left[s\left(y + 1 - \gamma - \log\left(s\right)\right)\right]. \end{aligned} \quad (4.23)$$

The obtained expression of $p(y)$ is showing a good agreement with the numerical simulation result as displayed in FIG. 4.6(b).

(c) For $1 < \nu < 2$:

In this domain the general expression of $\langle e^{-i\widetilde{k}v}\rangle$ would be similar as of Eq. (4.18), but while expand it around $k \to 0$ it yields

$$\langle e^{-i\widetilde{k}v}\rangle \simeq 1 - i\widetilde{k}\langle v\rangle - \ \Gamma(1-\nu)|\widetilde{k}|^\nu\ \mathrm{Exp}\left(\frac{i\pi\nu}{2}\ \mathrm{sgn}(\widetilde{k})\right) + \mathcal{O}(\widetilde{k}^{1+\nu}). \quad (4.24a)$$

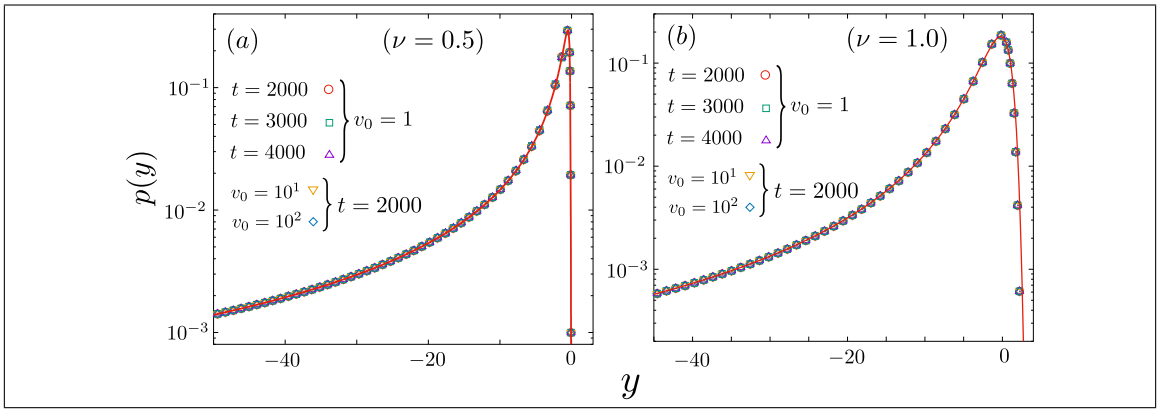

Figure 4.6: Conditional PDF of the scaled net overtakings y are plotted in the case of a Jepsen gas enclosed in a ring of size $N = 128$ and comprised of N number of velocities which are taken initially from a power-law distribution of exponents (a) $\nu = 0.5$, and (b) 1.0. The discrete points are numerical simulation results, which are showing a good agreement with the analytical result as shown by solid (red) lines.

From here we can write approximately

$$\log(\langle e^{-i\widetilde{k}v}\rangle) \simeq -i\widetilde{k}\langle v\rangle + \frac{1}{2}\widetilde{k}^2\langle v\rangle^2 - \ \Gamma(1-\nu)|\widetilde{k}|^\nu \ \mathrm{Exp}\left(\frac{i\pi\nu}{2}\ \mathrm{sgn}(\widetilde{k})\right) + \mathcal{O}(\widetilde{k}^{1+\nu}). \tag{4.24b}$$

By inserting it in Eq. (4.17) we have found that the imaginary part of the integrand is an odd function around $\widetilde{k}$, and the real part of that integrand is an even function around the same point. This allow us to simplify Eq. (4.17) in terms of scaled variables $y = N^{1-1/\nu}(c - \bar{c})$, and $s = \widetilde{k}N^{1/\nu}$, and a constant $u_1 = 1/2\ N^{1-2/\nu}\langle v\rangle^2$ as

$$\begin{aligned} p(y) &\simeq \frac{1}{\pi}\int_0^\infty ds\ \mathrm{Exp}\left[u_1 s^2 - \Gamma(1-\nu)s^\nu\ \mathrm{Cos}\left(\frac{\pi\nu}{2}\right)\right] \\ &\qquad \times \mathrm{Cos}\left[sy + s^\nu\ \Gamma(1-\nu)\ \mathrm{Sin}\left(\frac{\pi\nu}{2}\right)\right] \\ &\simeq \frac{1}{\pi}\int_0^\infty ds\ \mathrm{Exp}\left[-\Gamma(1-\nu)s^\nu\ \mathrm{Cos}\left(\frac{\pi\nu}{2}\right)\right] \\ &\qquad \times \mathrm{Cos}\left[sy + s^\nu\ \Gamma(1-\nu)\ \mathrm{Sin}\left(\frac{\pi\nu}{2}\right)\right]\left(1 + u_1 s^2\right). \end{aligned} \tag{4.25}$$

Note that in the first line of Eq. (4.25) the second term ($\propto s^\nu$) within the exponential dominates over the first term ($\propto s^2$) in the limit of $s \to 0$. It allows us to approximately write $\mathrm{Exp}(u_1 s^2) \simeq 1 + u_1 s^2$, and hence, get the last line. One can

evaluate this integration numerically, and find out that it shows a good agreement with the numerical simulation result as shown in FIG. 4.7(a).

(d) For $\nu = 2$:

For $\nu = 2$, as we know, all the higher moments of $\rho(v)$ except the first one diverge. More importantly, the divergence of the second moment is logarithmic. In this case the analogue of Eq. (4.18) can be written as

$$\begin{aligned}\left\langle e^{-i\widetilde{k}v}\right\rangle &= e^{-i\widetilde{k}}(1-i\widetilde{k}) - \widetilde{k}^2\int_1^\infty dv\frac{e^{-i\widetilde{k}v}}{v} = e^{-i\widetilde{k}}(1-i\widetilde{k}) - \widetilde{k}^2\,\Gamma(0,i\widetilde{k}) \\ &\simeq 1 - i\widetilde{k}\langle v\rangle + \left(\gamma - \frac{3}{2} + \frac{i\pi}{2}\mathrm{sgn}(\widetilde{k}) + \log|\widetilde{k}|\right)\widetilde{k}^2 + \mathcal{O}(\widetilde{k}^3)\end{aligned} \tag{4.26a}$$

with the upper incomplete gamma function $\Gamma(0, i\widetilde{k})$. The expression in the final line is obtained by expanding around $\widetilde{k} \to 0$. From here we can write approximately

$$\log(\langle e^{-i\widetilde{k}v}\rangle) \simeq -i\widetilde{k}\langle v\rangle + \left(\gamma + \frac{1}{2} + \log(|\widetilde{k}|) + \frac{i\pi}{2}\,\mathrm{sgn}(\widetilde{k})\right)\widetilde{k}^2 + \mathcal{O}(\widetilde{k}^3). \tag{4.26b}$$

Following the similar procudure like above, we can write Eq. (4.17) in terms of scaled variables $y = N^{1/2}(c - \bar{c})$, and $s = \widetilde{k}N^{1/2}$ including a new constant $u_2 = 1/2\,\log(N/e) - \gamma$ as follows:

$$\begin{aligned}p(y) &\simeq \frac{1}{2\pi}\int_{-\infty}^{\infty} ds\; e^{-isy}\;\mathrm{Exp}\left[(-u_2 + \frac{i\pi}{2}\mathrm{sgn}(s) + \log(|s|))s^2\right] \\ &\simeq \frac{1}{\pi}\int_0^\infty ds\;\mathrm{Exp}\left[-(u_2+\log(s))s^2\right]\mathrm{Cos}\left(sy - \frac{\pi s^2}{2}\right) \\ &\simeq \frac{1}{\pi}\int_0^\infty ds\; e^{-u_2 s^2}\mathrm{Cos}\left(sy - \frac{\pi s^2}{2}\right)\left(1 + s^2\log(s)\right).\end{aligned} \tag{4.27}$$

On the 2nd line of Eq. (4.27) the 1st term ($\propto s^2$) within the exponential becomes larger than the 2nd term ($\propto s^2\,\log(s)$) in the limit of $s \to 0$. It allows us to approximately write the last line. We numerically compute this integration and find out that it shows a good agreement with the numerical simulation result as displayed in FIG. 4.7(b).

(e) For $\nu > 2$:

In case of $\nu > 2$ we can exapnd Eq. (4.18) around $\widetilde{k} \to 0$, and hence write approximtely

$$\langle e^{-i\widetilde{k}v}\rangle \simeq 1 - i\widetilde{k}\langle v\rangle - \frac{1}{2}\widetilde{k}^2\langle v^2\rangle - \Gamma(1-\nu)\,|\widetilde{k}|^\nu\,\mathrm{Exp}\left[\frac{i\pi\nu}{2}\,\mathrm{sgn}(\widetilde{k})\right] + \mathcal{O}(\widetilde{k}^3) \tag{4.28a}$$

$$\log(\langle e^{-i\widetilde{k}v}\rangle) \simeq -i\widetilde{k}\langle v\rangle - \frac{1}{2}\widetilde{k}^2\langle v^2\rangle_c - \Gamma(1-\nu)\,|\widetilde{k}|^\nu\,\mathrm{Exp}\left[\frac{i\pi\nu}{2}\,\mathrm{sgn}(\widetilde{k})\right] + \mathcal{O}(\widetilde{k}^3) \tag{4.28b}$$

Here we can write the distribution in terms of the scaled variable $y = N^{1-1/\nu}(c-\bar{c})$, $s = \widetilde{k}N^{1/\nu}$ and a constant $u_3 = 1/2\; N^{1-2/\nu}\langle v^2\rangle_c$ as follows:

$$p(y) \simeq \frac{1}{2\pi}\int_{-\infty}^{\infty} ds\;\mathrm{Exp}\left[-isy - u_3 s^2 - \Gamma(1-\nu)\,|s|^\nu\,\mathrm{Exp}\left(\frac{i\pi\nu}{2}\,\mathrm{sgn}(s)\right)\right]. \tag{4.29}$$

It can further reduce to

$$\begin{aligned} p(y) &\simeq \frac{1}{\pi}\int_0^{\infty} ds\;\mathrm{Exp}\left[-u_3\,s^2 - \Gamma(1-\nu)s^\nu\,\mathrm{Cos}\left(\frac{\pi\nu}{2}\right)\right] \\ &\qquad\qquad \times \mathrm{Cos}\left[sy + s^\nu\,\Gamma(1-\nu)\,\mathrm{Sin}\left(\frac{\pi\nu}{2}\right)\right] \\ &\simeq \frac{1}{\pi}\int_0^{\infty} ds\;\mathrm{Exp}[-u_3\,s^2]\;\left(1 - \Gamma(1-\nu)s^\nu\,\mathrm{Cos}\left(\frac{\pi\nu}{2}\right)\right) \\ &\qquad\qquad \times \mathrm{Cos}\left[sy + s^\nu\,\Gamma(1-\nu)\,\mathrm{Sin}\left(\frac{\pi\nu}{2}\right)\right]. \end{aligned} \tag{4.30}$$

Note that, on the first line of Eq. (4.30) the 1st term ($\propto s^2$) within the exponential is larger than the 2nd term ($\propto s^\nu$) in the limit of $s \to 0$. It enable us to reach in the final result which we have computed numerically and found that it shows a good match with the numerical simulation result as displayed in FIG. 4.7(c).

Approximate result for the left tail of the conditional distribution

In case of power-law $\rho(v)$ of the form Eq. (2.6), we can approximately calculate the behavior of the left tail of $p(m,t|v_0)$ by starting from Eq. (4.6). For that, we first recall that the contribution of the left tail comes from the largest velocities

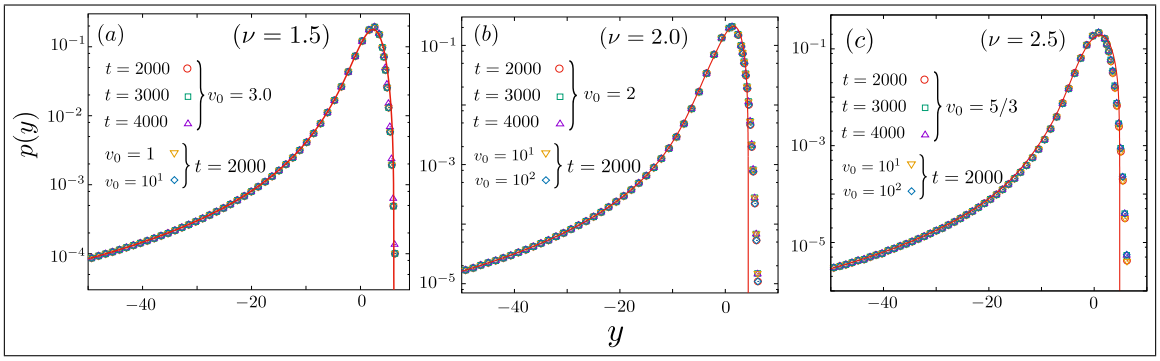

Figure 4.7: Conditional PDF of the scaled net overtakings y are plotted in the case of a Jepsen gas enclosed in a ring of size $N = 128$ and comprised of N number of velocities which are taken initially from a power-law distribution of exponents (a) 1.5, (b) 2.0, and (c) 2.5. The discrete points are numerical simulation results, which are showing a good agreement with the analytical result as shown by bold (red) lines.

present in the system. We denote the maximum velocity by v_{max}. Now, by using the formalism of order statistics [9,10], we can write the distribution of v_{max} among N number of velocities chosen independently from $\rho(v)$ as follows:

$$\mathcal{P}_1(v_{max}|N) = N\left(F_v(v_{max})\right)^{N-1}\rho(v_{max}), \tag{4.31a}$$

with the cumulative distribution function (CDF)

$$F_v(u) = \int_1^u dv \frac{\nu}{v^{1+\nu}} = (1-u^{-\nu}). \tag{4.31b}$$

Notably, in the limit of $N >> 1$ we can approximately write

$$\left(F_v(u)\right)^N \simeq \text{Exp}\left[-\frac{N}{u^\nu}\right], \tag{4.31c}$$

which is nothing but the CDF of the Fréchet distribution in extreme value statistics [11,12] with the scale and shape parameters $N^{1/\nu}$ and ν respectively. Using this result with the approximation of $N >> 1$ we can calculate

$$\mathcal{P}_1(v_{max}|N) \simeq \frac{\nu\, N}{v_{max}^{\nu+1}}\,\text{Exp}\left(-\frac{N}{v_{max}^\nu}\right). \tag{4.32a}$$

Note that, in the limit $N >> 1$, this distribution is normalized.

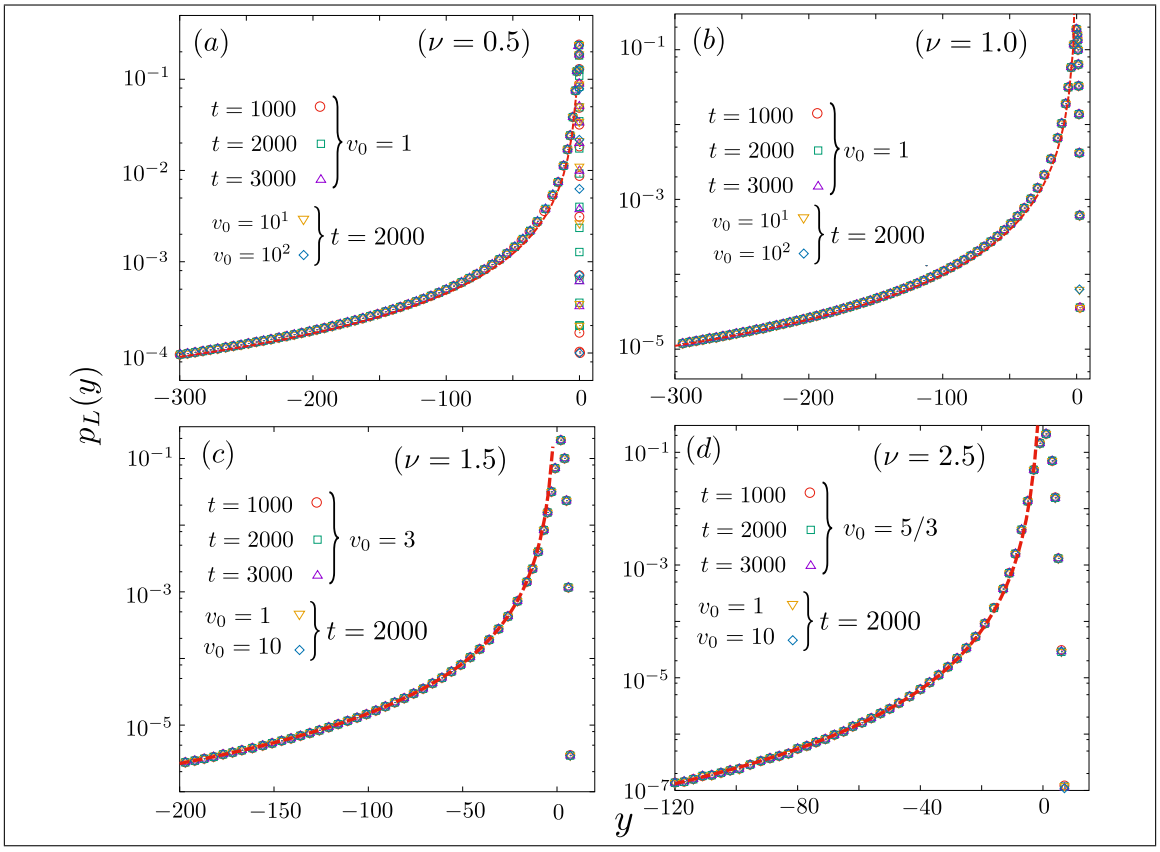

Figure 4.8: PDF of the scaled net overtakings are plotted in the case of a Jepsen gas within a ring of size $N = 128$ and comprised of N number of velocities which are taken initially from a power-law distribution of exponents (a) $\nu = 0.5$, (b) 1.0, (c) 1.5, and (d) 2.5. All the numerical results at the left tail are showing good agreement with the corresponding analytical result in Eq. (4.35).

Now we can split Eq. (4.6) in terms of $c = m/t$ as

$$c(v_0) = v_0 - \frac{1}{N} v_{max} - \frac{1}{N} \sum_{i=1}^{N-1} v_{(i)}. \tag{4.33}$$

Here, $v_{(i)}$ denotes the jth order velocity. For example, $v_{(1)} = min(v_1, v_2, ..., v_N)$, $v_{(2)} = min(\{v_1, v_2, ..., v_N\} \backslash \{v_{(1)}\})$, $v_{(3)} = min(\{v_1, v_2, ..., v_N\} \backslash \{v_{(1)}, v_{(2)}\})$, and so on. Now, ignoring all other terms except v_{max} we can approximately write the scaling variable

$$y \simeq -\frac{1}{N^{1/\nu}} v_{max}. \tag{4.34}$$

Following a similar procedure like previous case, we can proceed here as

$$p_L(y) \simeq \int_1^\infty dv_{max}\, \mathcal{P}_1(v_{max}|N)\, \delta\left(y + N^{-1/\nu}\, v_{max}\right)$$
$$\simeq N^{1/\nu}\, \mathcal{P}_1(-yN^{1/\nu}|N)\, \Theta\left(-yN^{1/\nu} - 1\right) \simeq \frac{\nu}{(-y)^{\nu+1}}\, e^{-(-y)^{-\nu}} \quad (4.35)$$

where y is bound within $-\infty$ and $-N^{-1/\nu}$. The obtained result is nothing but a stretched exponential distribution which is showing a good agreement with the result obtained from numerical simulation as displayed in FIG. 4.8.

4.3.4 Unconditional distribution

In this subsection, we describe the unconditional distribution $P(c)$ for our four different initial velocity distributions. To find out the unconditional distribution, it is convenient to re-express Eq. (2.2) in terms of $\bar{c} = v_0 - \langle v \rangle$ as

$$P(c) = \int_{-\infty}^{\infty} d\bar{c}\, p(c|\bar{c})\, \rho(\bar{c} + \langle v \rangle). \quad (4.36)$$

Gaussian and uniform $\rho(v)$:

Now, in the cases of Gaussian and uniform distributions, writing Eq. (4.9) in terms of c and $\bar{c}$ in Eq. (4.36), we can calculate respectively

$$P(c) \simeq \frac{1}{\sqrt{2\pi}} \sqrt{\frac{N}{N+1}} \text{Exp}\left[-\frac{c^2 N}{2(N+1)}\right] \simeq \frac{e^{-c^2/2}}{\sqrt{2\pi}} \left(1 + \frac{c^2 - 1}{2N}\right) + \mathcal{O}(N^{-2}), \quad (4.37)$$

$$P(c) \simeq \frac{1}{4} \left(\text{Erf}\left[\sqrt{\frac{3N}{2}}(1+c)\right] + \text{Erf}\left[\sqrt{\frac{3N}{2}}(1-c)\right] \right). \quad (4.38)$$

The obtained analytical results are showing good agreement with numerical simulation results as shown in FIG. 4.9 (a) and (b) respectively. From here it is easy to see that both the distributions in the limit of $N \to \infty$ converge to the initial velocity distributions.

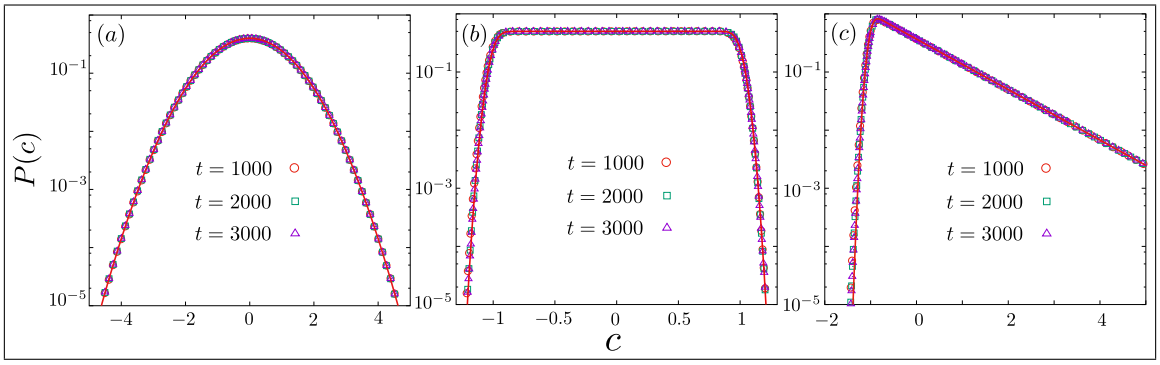

Figure 4.9: PDF of the scaled net overtakings $c = m(t)/t$ are plotted at three different times, in the case of a Jepsen gas, confined within a ring of size $N = 128$, and comprised of N number of velocities which are taken initially from (a) Gaussian, (b) uniform, and (c) exponential distributions. The symbols are numerical simulation results which are showing a good match with the analytical results as shown by the solid lines.

Exponential $\rho(v)$:

Next, for the exponential distribution we can calculate an approximate result by using $p(c|\bar{c})$ from in Eq. (4.14) first, and then proceed as follows

$$\begin{aligned} P(c) = \int_{-1}^{\infty} d\bar{c}\, e^{-(\bar{c}+1)}\, p(c|\bar{c}) &\simeq \sqrt{\frac{N}{2\pi}} e^{Nc-1} \int_{-1}^{\infty} d\bar{c}\, e^{-(N+1)\bar{c}}\, (1+\bar{c}-c)^{N-1} \\ &\simeq \sqrt{\frac{N}{2\pi}}\, e^{-c+N}\, (1+N)^{-N}\, \Gamma(N, -c(N+1)) \end{aligned} \tag{4.39}$$

with the upper incomplete gamma function defined by $\Gamma(s,x) = \int_x^{\infty} dy\ e^{-y}\ y^{s-1}$. Using this definition we can write

$$P(c) \simeq \sqrt{\frac{N}{2\pi}}\, \frac{e^{N-c}}{(1+N)^N} \int_{-c(N+1)}^{\infty} dy\, e^{\varphi_2(y)} \tag{4.40}$$

with $\varphi_2(y) = -y + (N-1)\,\ln(y)$. For large N, one can expand $\varphi_2(y)$ around the saddle point $y^* = N-1$ as follows $\varphi_2(y) \simeq -(N-1) + (N-1)\,\ln(N-1) - 1/(2N -$

2) $(y-N+1)^2+\mathcal{O}(N^{-2})$. Inserting this result on the above Eq. (4.40) we can get

$$P(c) \simeq \frac{1}{2}\sqrt{\frac{N}{N-1}}\left(\frac{N-1}{N+1}\right)^N e^{(1-c)}\left(1+\text{Erf}\left[\frac{N-1+c(N+1)}{\sqrt{2(N-1)}}\right]\right)$$
$$\simeq e^{-(1+c)}\left(1-\frac{1}{2}\,\text{Erfc}\left[\sqrt{\frac{N}{2}}(c+1)\right]\right). \quad (4.41)$$

Now, instead of the exact result of $p(c,t|v_0)$ in Eq. (4.14), if we use it Gaussian approximated solution in Eq. (4.36), then also we recover the same result in the limit of large N as follows

$$P(c) = \frac{1}{2}\,\text{Exp}\left[-1-c+\frac{1}{2N}\right]\left(1+\text{Erf}\left[\frac{cN+N-1}{\sqrt{2N}}\right]\right)$$
$$\simeq e^{-(1+c)}\left(1-\frac{1}{2}\,\text{Erfc}\left[\sqrt{\frac{N}{2}}(c+1)\right]\right). \quad (4.42)$$

The above analytical results are showing good agreements with the data obtained from the numerical simulation as shown in FIG. 4.9(c).

Power-law $\rho(v)$:

Finally, for the power-law distribution, we numerically solve the Eq. (4.36) by using the numerical results of $p(c|\bar{c})$ from the previous Sec. 4.3.3. The obtained numerical results are showing a good agreement with the data obtained from the numerical simulation as displayed in FIG. 4.16.

Approximate result for the left tail for $\nu = 1$:

In case of $\nu = 1$ we know that the scaled variable is $y = c - v_0 + \log(N)$. Using this relation in Eq. (4.35) we can get

$$p_L(c|v_0) \simeq \frac{1}{(v_0+\log(N)-c)^2}\,\text{Exp}\left[-\frac{1}{(v_0+\log(N)-c)}\right]. \quad (4.43a)$$

Now, averaging it over v_0 we can write

$$P_L(c) \simeq \int_1^\infty \frac{dv_0}{v_0^2} \frac{1}{(v_0+\log(N)-c)^2} \text{Exp}\left[-\frac{1}{(v_0+\log(N)-c)}\right] \simeq \int_0^{1+\log(N)-c} du\, e^{-u} \left(\frac{1}{u}-\log(N)+c\right)^{-2} \tag{4.43b}$$

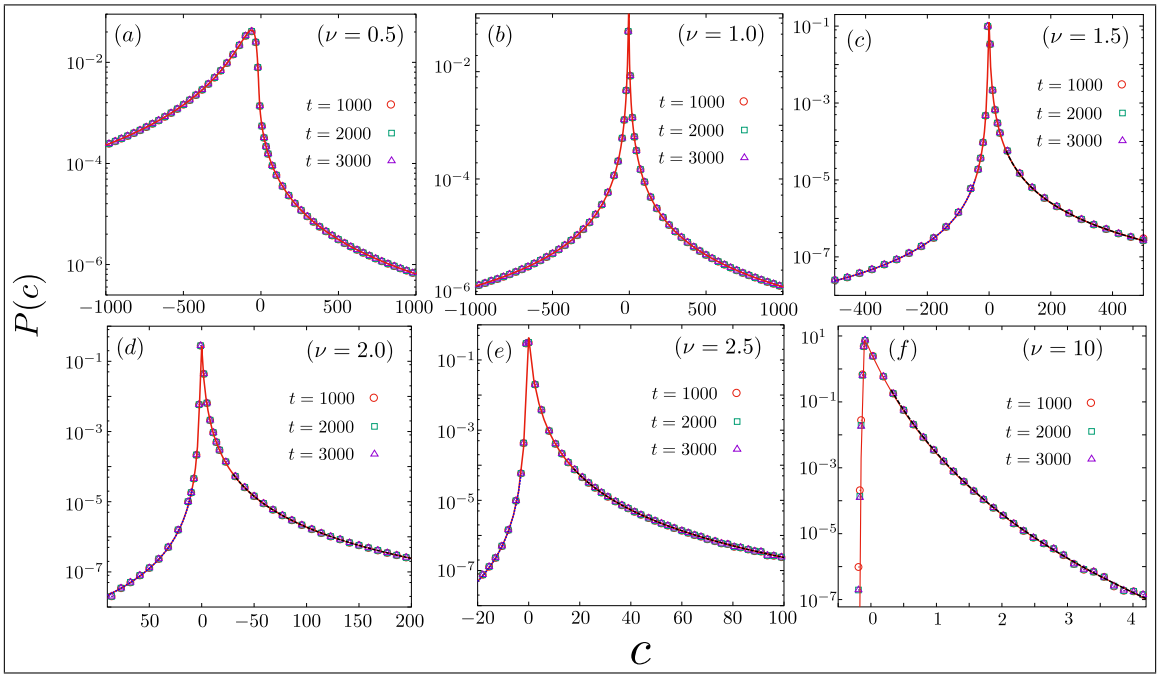

Figure 4.10: PDF of the scaled net overtakings $c = m(t)/t$ are plotted at three different times, in the case of a Jepsen gas, confined within a ring of size $N = 128$ and comprised of N number of velocities which are taken initially from a power-law distribution of exponent (a) $\nu = 0.5$, (b) 1.0, (c) 1.5, (d) 2.0, (e) 2.5, and (f) 10. The discrete points are numerical simulation results which are showing a good agreement with the analytical result as shown by (red) bold lines.

Approximate result for the left tail for $\nu > 1$:

An approximate result for the left tail (L) in case of power-law $\rho(v)$ can be obtained by rewriting Eq. (4.36) as

$$P_L(c) \simeq \int_{1-\langle v\rangle}^\infty d\bar{c}\, \rho(\bar{c}+\langle v\rangle)\, p_L(c|\bar{c}), \tag{4.44a}$$

and then, using the approximate result for the left-tail of the conditional distribution by writing it in terms of c and $\bar{c}$ from Eq. (4.35) as

$$p_L(c|\bar{c}) \simeq \frac{\nu\ N^{1-\nu}}{(\bar{c}-c)^{1+\nu}}\ \text{Exp}\left[-\frac{N^{1-\nu}}{(\bar{c}-c)^{\nu}}\right]. \tag{4.44b}$$

Using the variable transform we further reduce it as

$$P_L(c) \simeq \int_0^{\frac{N^{1-\nu}}{(1-c-\langle v\rangle)^{\nu}}} \frac{\nu\ du\ e^{-u}}{\left(c+\langle v\rangle+\frac{1}{N}\left(\frac{N}{u}\right)^{\frac{1}{\nu}}\right)^{1+\nu}}. \tag{4.45}$$

From the upper limit of this integration we can say that c is bound within $-\infty$ and $(1-\langle v\rangle)$. It can also be said that $P(c)$ for power-law $\rho(v)$ contains two different tails, namely the right and the left, which are intersect close to the point $1-\langle v\rangle$ for $\nu > 1$. This integration can not be solved exactly. Hence, we evaluate it numerically which matches quite well with the data obtained from the numerical simulation as shown in FIG. 4.16. Note that in the limit $N \to \infty$ or $\nu >> 1$ the spread of the left tail shrink to zero as $P_L(c) \to 0$ in that limit. To verify this behavior, we have plotted $P(c)$ for $\nu = 10$ in FIG. 4.16(f).

Approximate result for the right tail for $\nu > 1$:

To obtain a qualitative behavior of the right (R) tail of $P(c)$, we argue as follows: as the contribution of $P_L(c)$ comes from the large velocities present in the system, hence the rest of the velocities, which are mostly around the mean of $\rho(v)$, contributes to $P_R(c)$. It allows us to write approximately Eq. (4.17) as

$$p_R(c|v_0) \simeq \frac{N}{2\pi}\int_{-\infty}^{\infty} d\widetilde{k}\ e^{-i\widetilde{k}N\ (c-\bar{c})} \sim N\delta(N(c-\bar{c})) \sim \delta(c-\bar{c}). \tag{4.46}$$

By inserting it in Eq. (4.36) we can easily calculate $P_R(c) \sim \rho(c+\langle v\rangle)$.

4.4 Ensemble II

Instead of a fixed number of particles, we consider this number a random variable in this case. We consider the probability of getting a particular particle number

l within a system of size N is $\mathcal{P}(l, \varrho N) = e^{-\varrho N}(\varrho N)^l/l!$ where ϱN is the average number of particles within the system. Notably, this kind of ensemble of particles we can build as follows: first introduce a tagged particle at $x = 0$. Then, a random distance is chosen from an exponential distribution of the form $\varrho\ e^{-\varrho x}$ to put first neighbor the tagged particle. The position of the second neighbor and all the other particles are chosen one by one by drawing the random gaps independently from the same exponential distribution. We repeat this procedure as long as the position of the last particle remain within the system size N.

4.4.1 Rates of overtaking by a tagged velocity

To calculate the rates of overtaking, we consider the tagged particle at $x = 0$ with a given velocity v_0. Now, for a particle starting at position $x > 0$ with velocity v to be overtaken by a tagged particle that starts at the origin ($x = 0$) with velocity v_0, between time t and $t+dt$, one must have $t < (x+N\lfloor(v_0 - v)t/N\rfloor)/(v_0-v) < t+dt$ with $v_0 > v$. Since, x can be anywhere in $[0, N]$ with a probability density ϱ, and v, drawn from $\rho(v)$, can take any value less than v_0, the probability of this two trajectories crossing between t and $t + dt$ is

$$\rho_R(v_0)dt = \int_0^N \varrho\ dx \int_{-\infty}^{v_0} dv\ \rho(v)\ \delta\left(t - \frac{x + N\left\lfloor\frac{(v_0-v)t}{N}\right\rfloor}{v_0 - v}\right) dt. \tag{4.47}$$

Using, $\delta\left(t - \frac{x+N\lfloor(v_0-v)t/N\rfloor}{v_0-v}\right) = (v_0 - v)\ \delta(x - (v_0 - v)t + N\lfloor(v_0 - v)t/N\rfloor)$ and then carrying out the integration over x, with the fact that $0 \leq (v_0 - v)t - N\lfloor(v_0 - v)t/N\rfloor < N$, gives the rate of crossing the tagged particle from the right to the left at time t as

$$\rho_R(v_0) = \varrho \int_{-\infty}^{v_0} dv\ \rho(v)\ (v_0 - v). \tag{4.48}$$

Similarly, to find out the rate of crossing the tagged particle from the left at time t we can write

$$\rho_L(v_0)dt = \int_0^N \varrho\ dx \int_{v_0}^{\infty} dv\ \rho(v)\ \delta\left(t - \frac{x - N\left\lceil\frac{(v-v_0)t}{N}\right\rceil}{v - v_0}\right) dt \tag{4.49}$$

with the Ceiling function $\lceil u \rceil = 1 + \lfloor u \rfloor$. Following the above procedure in this case also we can derive

$$\rho_L(v_0) = \varrho \int_{v_0}^{\infty} dv\ \rho(v)\ (v - v_0). \tag{4.50}$$

Clearly, these rates are the same as that for a Jepsen gas distributed on an infinite line with the same density ϱ (see Sec. 2.3.1). More importantly, the intersecting rates of the underlying process, in this case, become non-Poissonian unlike the system of infinite size. Since, only the initial positions and velocities are chosen independently, all the intersecting times associated with two given trajectories become dependent. For example, in FIG. 4.1, all the four intersecting times of v_0 and v_1 are dependent which is quite clear from their values $x_1/(v_0-v_1)$, $(x_1+N)/(v_0-v_1)$, $(x_1+2N)/(v_0-v_1)$, $(x_1+3N)/(v_0-v_1)$. These correlated sequences of times make the underlying process non-Poissonian.

4.4.2 Cumulants of the net overtaking number

To proceed here, first we note that for a given l number of particles, we can modify Eq. (4.5) by replacing the upper limit of the sum, i.e., N, by l. Then, by following a similar procedure in Sec. 4.3.1 we can calculate approximately

$$m_l(t|v_0) \simeq \frac{t}{N} \sum_{j=1}^{l} (v_0 - v_j) \tag{4.51}$$

in the limit $t >> N$. The subscript l denotes for l number of particles in the system. As l is taken from a Poisson distribution, the process of overtaking becomes a compound Poisson process [8]. Using the above result, we calculate cumulants of the net overtaking number for a given ϱ and N.

First, we can calculate the mean number as

$$\langle m_\varrho(t|v_0)\rangle = \sum_{l=1}^{\infty} \mathcal{P}(l, \varrho N)\ \langle m_l(t|v_0)\rangle \simeq \varrho\ t(v_0 - \langle v\rangle). \tag{4.52}$$

Here, the subscript ϱ denotes the density. Now, we can find out the variance by

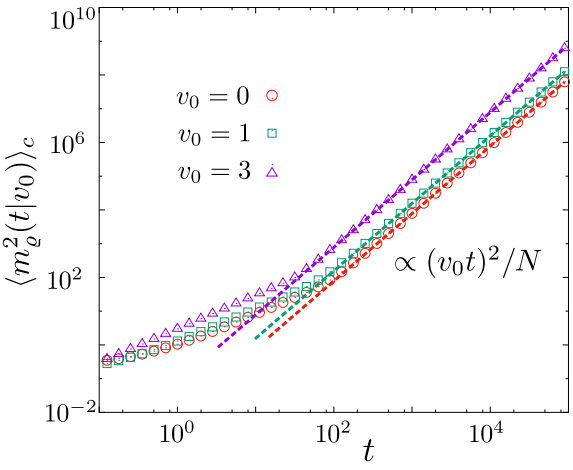

Figure 4.11: The variance of the net overtaking number by a tagged agent of velocity v_0 is plotted for different v_0. Clearly, it is showing a transition from a system-size independent initial behavior to the system-size dependent long-time behavior $\propto v_0^2 t^2/N$. In the plot, we consider a periodic system of size $N = 128$ with $\varrho = 1$ and velocities of the rest of the particles chosen independently from the Gaussian distribution.

using Eq. (4.51) and (4.52) as follows:

$$\langle m_\varrho^2(t|v_0)\rangle_c = \langle m_\varrho^2(t|v_0)\rangle - \langle m_\varrho(t|v_0)\rangle^2 \simeq \sum_{l=1}^{\infty} \mathcal{P}(l,\varrho N)\ \langle m_l^2(t|v_0)\rangle - \varrho^2\ t^2 (v_0 - \langle v\rangle)^2$$
$$\simeq \frac{\varrho\ t^2}{N}\left[\langle v^2\rangle_c + (v_0 - \langle v\rangle)^2\right] \simeq \frac{\varrho\ t^2}{N}\left\langle (v_0 - v)^2\right\rangle . \tag{4.53}$$

Note that, this obtained result is quite different from the result of the same for constant number of particles (see Eq. (4.8)). The variance, in this case, depends on v_0 and $\langle v\rangle$ unlike Eq. (4.8). This result is verified by the numerical simulation, as shown in FIG. 4.11. Since $\langle m_\varrho^2(t|v_0)\rangle_c \propto t^2/N$, in this case also we can compute the dynamical exponent $z = 1$ by following a similar formalism like Sec. 4.3.2.

Not only the mean and the variance, but we can also calculate all the higher-order cumulants of $m_\varrho(t|v_0)$. For that, first we calculate the characteristic function of $m_\varrho(t|v_0)$ in terms of $c_\varrho(v_0) = m_\varrho(t|v_0)/t$ and $\widetilde{k} = kt/N$, and with the assumption of $\varrho N >> 1$ as follows:

$$\left\langle e^{i\widetilde{k}Nc_\varrho(v_0)}\right\rangle = \sum_{l=1}^{\infty} \mathcal{P}(l,\varrho N)\left\langle e^{i\widetilde{k}\sum_{j=1}^{l}(v_0 - v_j)}\right\rangle \simeq e^{-\varrho N}\sum_{l=1}^{\infty}\frac{(\varrho N)^l}{l!}\left\langle e^{i\widetilde{k}(v_0 - v)}\right\rangle^l$$
$$\simeq \mathrm{Exp}\left[\varrho N\left\langle e^{i\widetilde{k}(v_0 - v)}\right\rangle - \varrho N\right]. \tag{4.54}$$

From Eq. (4.54) we can find out the nth order cumulant by using the relation

between cumulant and cumulant generating function as

$$\langle m_\varrho^n(t|v_0)\rangle_c = t^n \langle c_\varrho^n(v_0)\rangle_c \simeq \varrho N \left(\frac{t}{N}\right)^n \langle (v_0 - v)^n\rangle \,. \tag{4.55}$$

Now, using the explicit form of $\rho(v)$ from Sec. 2.2.3 we can calculate $\langle (v_0 - v)^n\rangle$ for the Gaussian, uniform, exponential, and power-law distributions as follows:

$$\text{Gaussian:}\quad \langle (v_0 - v)^n\rangle = \begin{cases} \frac{2^{(n-1)/2}}{\sqrt{\pi}}\, n v_0\, \Gamma(n/2)\, {}_1F_1\left(\frac{1-n}{2}; \frac{3}{2}; -\frac{v_0^2}{2}\right) & \text{for odd n,} \\ \frac{2^{n/2}}{\sqrt{\pi}}\, \Gamma((n+1)/2)\, {}_1F_1\left(-\frac{n}{2}; \frac{1}{2}; -\frac{v_0^2}{2}\right) & \text{for even n,} \end{cases} \tag{4.56}$$

$$\text{Uniform:}\quad \langle (v_0 - v)^n\rangle = \frac{1}{2(n+1)} \left((v_0+1)^{1+n} - (v_0-1)^{n+1}\right), \tag{4.57}$$

$$\text{Exponential:}\quad \langle (v_0 - v)^n\rangle = (-1)^n e^{-v_0}\, \Gamma(1+n, -v_0), \tag{4.58}$$

$$\text{Power-law:}\quad \langle (v_0 - v)^n\rangle = (-v_0)^{n-\nu}\, \nu\, B_{1/v_0}(-\nu, 1+n) \quad \text{for } n < \nu. \tag{4.59}$$

Here, $\mathrm{B}_z(a,b)$ is the incomplete beta function defined by $\mathrm{B}_z(a,b) = \int_0^z dx\, x^{a-1}\, (1-x)^{b-1}$. From the above results it is clear that, not only the variance, but in fact, all the higher order cumulants also depend on v_0 unlike the case of constant number of particles in Sec. 4.3.

4.4.3 Conditional and Unconditional distributions

We can also calculate the full probability distribution of $m_\varrho(t|v_0)$ by writing down the conditional distribution of constant ϱ with the same of fixed l through the relation

$$p_\varrho(m, t|v_0) = \sum_{l=1}^{\infty} \mathcal{P}(l, \varrho N)\, p_l(m, t|v_0). \tag{4.60}$$

Now, by using the inverse Fourier transform with Eq. (4.54) we can write the conditional distribution in terms of a scaled variable $y = \sqrt{N/\varrho}\, (c - \varrho(v_0 - \langle v\rangle))/\sqrt{\langle (v_0 - v)^2\rangle}$

as follows (see Sec. 2.4.1 for details):

$$p_\varrho(y|v_0) \simeq \frac{1}{2\pi}\int_0^\infty ds\; e^{-isy-s^2/2}\;\text{Exp}\left[\sum_{n=3}^{\infty}\frac{(is)^n}{n!}(\varrho N)^{1-n/2}\;\frac{\langle(v_0-v)^n\rangle}{\langle(v_0-v)^2\rangle^{n/2}}\right]$$
$$\simeq \frac{1}{\pi}\int_0^\infty ds\; e^{-s^2/2}\;\text{Cos}\left(sy+\frac{s^3}{3!\sqrt{\varrho N}}\frac{\langle(v_0-v)^3\rangle}{\langle(v_0-v)^2\rangle^{3/2}}\right)\left(1+\frac{s^4}{4!\;\varrho N}\frac{\langle(v_0-v)^4\rangle}{\langle(v_0-v)^2\rangle^2}\right). \tag{4.61}$$

In the final line of the above expression we have written approximately the distribution by taking its contribution up to $n = 4$. In the limit $N >> 1$ the contribution of $n > 4$ terms become negligible. Using the relation between y and c with Eq. (2.2), we can express the unconditional distribution as follows:

$$P_\varrho(c) \simeq \frac{1}{\pi}\int_{-\infty}^{\infty} dv_0\;\rho(v_0)\;\int_0^\infty ds\;\frac{\sqrt{N}\;e^{-s^2/2}}{\sqrt{\varrho\;\langle(v_0-v)^2\rangle}}\left(1+\frac{s^4}{4!\;\varrho N}\frac{\langle(v_0-v)^4\rangle}{\langle(v_0-v)^2\rangle^2}\right)$$
$$\times\;\text{Cos}\left(\frac{s\sqrt{N}\;(c-\varrho v_0+\varrho\langle v\rangle)}{\sqrt{\varrho\;\langle(v_0-v)^2\rangle}}+\frac{s^3}{3!\sqrt{\varrho N}}\frac{\langle(v_0-v)^3\rangle}{\langle(v_0-v)^2\rangle^{3/2}}\right). \tag{4.62}$$

Now, using results from Eq. (4.56), (4.57), and (4.58) we can numerically evaluate the final result as displayed in FIG. 4.12 and FIG. 4.13 respectively. In the same figures we have also shown a Gaussian approximated result which one can obtain by considering the contribution up to $\mathcal{O}(s^2)$ term in Eq. (4.61) and (4.62).

Power-law $\rho(v)$

Now, in case of power-law $\rho(v)$ we can follow a similar formalism like Sec. 4.3.3. In this case we start from Eq. (4.54).

For $0 < \nu < 1$ **:**

First, in case of $0 < \nu < 1$, using result of Eq. (4.19) in Eq. (4.54), in the limit of $\widetilde{k} \to 0$ we can approximately write

$$\left\langle e^{i\widetilde{k}Nc_\varrho(v_0)}\right\rangle \simeq \text{Exp}\left[\varrho N\left(i\widetilde{k}v_0-\;\Gamma(1-\nu)|\widetilde{k}|^\nu\;\text{Exp}\left(\frac{i\pi\nu}{2}\;\text{sgn}(\widetilde{k})\right)\right)\right]. \tag{4.63a}$$

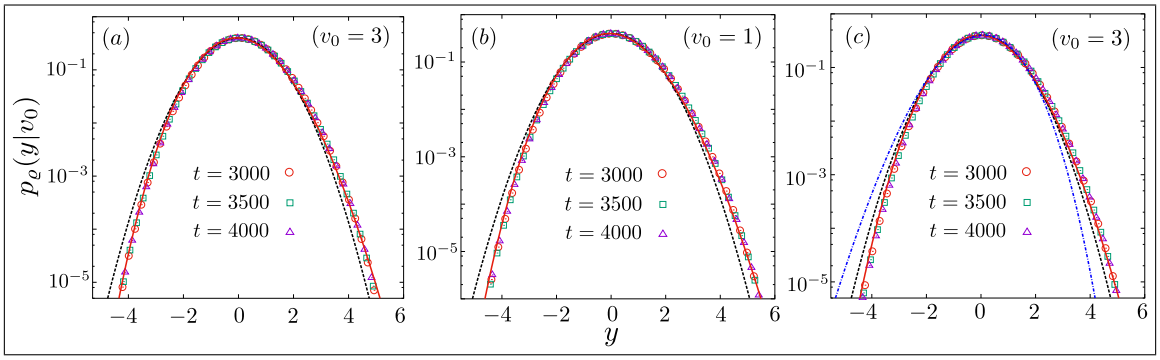

Figure 4.12: PDF of scaled net overtakings $y = \sqrt{N/\varrho}\ (c - \varrho(v_0 - \langle v\rangle))/\sqrt{\langle (v_0 - v)^2\rangle}$ are respectively plotted by considering $v_0 = 3$, 1, and 3 in case of (a) Gaussian, (b) uniform, and (c) exponential velocity distributions of the remaining particles which are distributed with density $\varrho = 1$ in a system of size $N = 128$. Discrete points are numerical simulation results which are showing a good agreement with the result coming from Eq. (4.61). A Gaussian approximated result is also plotted as shown by the dotted lines. These Gaussian approximated result in (a) and (b) are the exact result in case of constant $N = 128$ number of particles, whereas in (c) it is shown by (blue) dotdashed line.

By using this result we further get

$$p(c_\varrho|v_0) \simeq \frac{N}{2\pi} \int_{-\infty}^{\infty} d\widetilde{k}\ \mathrm{Exp}\left[-i\widetilde{k}N(c - \varrho v_0) - \Gamma(1-\nu)|\widetilde{k}|^\nu\ \mathrm{Exp}\left(\frac{i\pi\nu}{2}\ \mathrm{sgn}(\widetilde{k})\right)\right]. \tag{4.63b}$$

From here, in terms of a scaling variable $y = N\ (\varrho N)^{-1/\nu}\ (c_\varrho - \varrho v_0)$ and $s = (\varrho N)^{1/\nu}\widetilde{k}$ we can derive the identical expression like Eq. (4.20). Hence, for $\nu < 1$, the results in two ensembles are identical.

For $\nu = 1$:

Now, in case of $\nu = 1$, using Eq. (4.21) in Eq. (4.54) we can approximately write

$$p(c_\varrho|v_0) \simeq \frac{N}{2\pi} \int_{-\infty}^{\infty} d\widetilde{k}\ \mathrm{Exp}\left[-i\widetilde{k}N(c - \varrho v_0) - i\widetilde{k}\varrho N\left(1 - \gamma - i\pi\ \mathrm{sgn}(\widetilde{k})/2 - \log|\widetilde{k}|\right)\right]. \tag{4.64}$$

From here, in terms of a scaling variable $y = (c_\varrho - \varrho v_0 - \varrho\ \log(\varrho N))/\varrho$ and $s = (\varrho N)\widetilde{k}$ we can get result identical to Eq. (4.23). The obtained result is showing a good agreement with the data obtained from numerical simulation as displayed

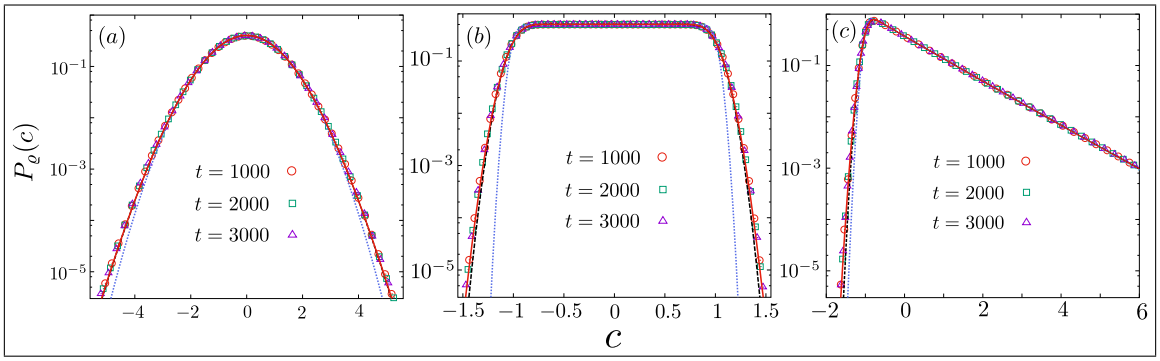

Figure 4.13: PDF of scaled net overtakings $c = m(t)/t$ are plotted at three different times for a Jepsen gas enclosed in a periodic system of size $N = 128$ with particle density $\varrho = 1$. The velocities of the particles are taken independently from (a) Gaussian, (b) uniform, and (c) exponential distributions. Discrete points are numerical simulation results which are showing good agreements with the result coming from Eq. (4.62). A Gaussian approximated result in each case is also plotted as shown by the dashed lines. For comparison, the result of the same in case of fixed N number of particles are also plotted by a (blue) dotted line.

in FIG. 4.15(b).

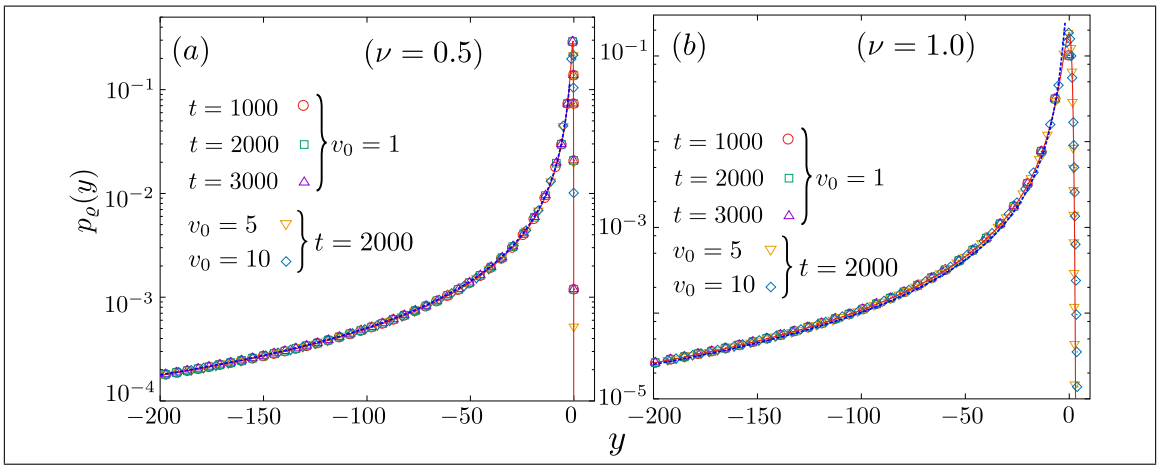

Figure 4.14: PDF of scaled net overtakings are plotted in the case of a Jepsen gas enclosed within a ring of size $N = 128$ with particle density $\varrho = 1$. The remaining velocities are taken independently from a power-law distribution of exponent (a) $\nu = 0.5$, and (b) 1.0. The discrete points are numerical simulation results, which are showing a good agreement with the analytical results as shown by bold (red) lines. An approximate numerical result (Eq. (4.35)) for the left tail is also plotted by (blue) dashed lines

For $1 < \nu < 2$:

Using Eq. (4.24a) and (4.54) here we can calculate

$$\left\langle e^{i\widetilde{k}Nc_{\varrho}(v_0)} \right\rangle \simeq \text{Exp}\left[\varrho N \left(i\widetilde{k}(v_0 - \langle v\rangle) - \frac{\widetilde{k}^2}{2}(v_0^2 - 2v_0\langle v\rangle) \right.\right.$$
$$\left.\left. - \Gamma(1-\nu)\,|\widetilde{k}^{\nu}|\,\text{Exp}\left[\frac{i\pi\nu}{2}\text{sgn}(\widetilde{k})\right] + \mathcal{O}(\widetilde{k}^{1+\nu})\right)\right]. \quad (4.65)$$

From here, the distribution of the scaled variable $y = N(\varrho N)^{-1/\nu}(c - \varrho v_0 + \varrho\langle v\rangle)$ in terms of $s = (\varrho N)^{1/\nu}\ \widetilde{k}$ and $u_1(v_0) = 1/2\ (\varrho N)^{1-2/\nu}(2v_0\langle v\rangle - v_0^2)$ comes out as idential as Eq. (4.25). Notably, the scaled distribution in this case depends on v_0 through $u_1(v_0)$.

For $\nu = 2$:

Using Eq. (4.26a) and (4.54) here we can calculate

$$\left\langle e^{i\widetilde{k}Nc_{\varrho}(v_0)} \right\rangle \simeq \text{Exp}\left[\varrho N \left(i\widetilde{k}(v_0 - \langle v\rangle) - \frac{\widetilde{k}^2}{2}(v_0^2 - 2v_0\langle v\rangle) \right.\right.$$
$$\left.\left. + \left(\gamma - \frac{3}{2} + \frac{i\pi}{2}\text{sgn}(\widetilde{k}) + \log(|\widetilde{k}|)\right)\widetilde{k}^2 + \mathcal{O}(\widetilde{k}^3)\right)\right] \quad (4.66)$$

From here, the distribution of the scaled variable $y = N(\varrho N)^{-1/2}(c - \varrho v_0 + \varrho\langle v\rangle)$ in terms of $s = (\varrho N)^{1/2}\ \widetilde{k}$ and $u_2(v_0) = 1/2\ (v_0^2 - 2v_0\langle v\rangle - 2\gamma + 3 + \log(\varrho N))$ becomes similar to Eq. (4.27). The scaled distribution in this case also depends on v_0 through $u_2(v_0)$.

For $\nu > 2$:

Using Eq. (4.28) and (4.54) here we can calculate

$$\left\langle e^{i\widetilde{k}Nc_{\varrho}(v_0)} \right\rangle \simeq \text{Exp}\left[\varrho N \left(i\widetilde{k}(v_0 - \langle v\rangle) - \frac{\widetilde{k}^2}{2}(v_0 - \langle v\rangle)^2 \right.\right.$$
$$\left.\left. - \Gamma(1-\nu)\,|\widetilde{k}^{\nu}|\,\text{Exp}\left[\frac{i\pi\nu}{2}\text{sgn}(\widetilde{k})\right] + \mathcal{O}(\widetilde{k}^3)\right)\right]. \quad (4.67)$$

From here, the distribution of scaled variable $y = N(\varrho N)^{-1/\nu}(c - \varrho v_0 + \varrho\langle v\rangle)$ in terms of $s = (\varrho N)^{1/\nu}\widetilde{k}$ and $u_3(v_0) = 1/2\ (\varrho N)^{1-2/\nu}(v_0 - \langle v\rangle)^2$ comes out as idential to Eq. (4.30). The scaled distribution in this case also depends on v_0 through $u_3(v_0)$.

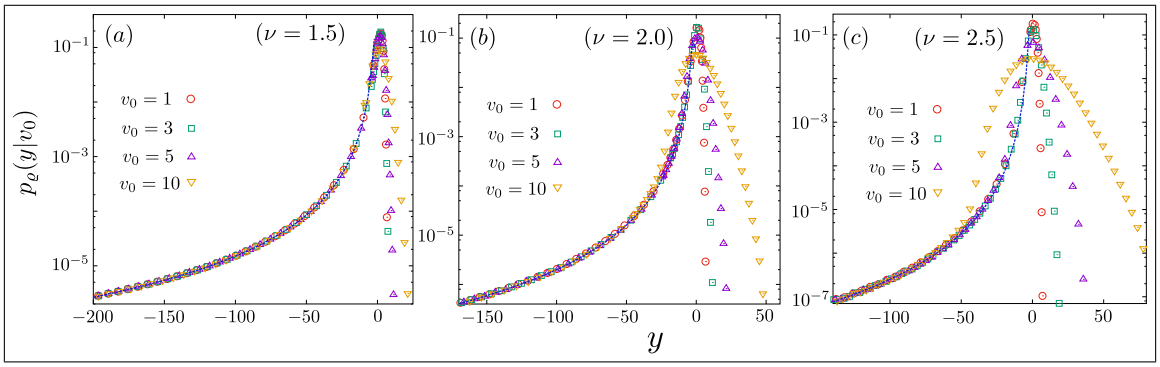

Figure 4.15: PDF of scaled net overtakings are plotted for tagged velocities in the case of a Jepsen gas enclosed within a ring of size $N = 128$ with particle density $\varrho = 1$. The remaining velocities are taken independently from a power-law distribution of exponent (a) $\nu = 1.5$, (b) $\nu = 2.0$, and (c) 2.5. The discrete points are numerical simulation results, which is v_0-independent at the left tail and showing good agreements with the approximate result in Eq. (4.35) as plotted by (blue) dashed lines.

Notably, from the above discussion it is clear that the scaled distribution remains v_0-independent in case of $\nu \leq 1$. It depends on v_0 for $\nu > 1$ which we have verified from the numerical results in FIG. 4.15. Using relation between the scaled variable y and $m(t|v_0)$ in case of $\nu > 1$ we can find out v_0-independent behavior of the left tail in the next.

Approximate result for the left tail

Following the procedure in Sec. 4.3.3, we can calculate the behavior of the left tail here also. For that, first we calculate the distribution of v_{max} for a given density of particle ϱ in a system of size N. Now, using Eq. (4.31), we can proceed here as follows:

$$\begin{aligned}\mathcal{P}_1(v_{max}|\varrho, N) &= \sum_{n=1}^{\infty} e^{-\varrho N}\frac{(\varrho N)^n}{n!} n\,(F_v(v_{max}))^{n-1}\,\rho(v_{max}) \\ &= \varrho N\ \rho(v_{max})\ \mathrm{Exp}\left[-\varrho N(1 - F_v(v_{max}))\right] \simeq \frac{\nu\varrho N}{v_{max}^{\nu+1}}\mathrm{Exp}\left[-\frac{\varrho N}{v_{max}^{\nu}}\right].\end{aligned} \tag{4.68a}$$

Now, in terms of v_{max} we can approximately write the scaling variable as

$$y \simeq -(\varrho N)^{-1/\nu} v_{max}. \tag{4.68b}$$

Finally, by following a similar procedure in Sec. 4.3.3 we can get same results in Eq. (4.35). The obtained result is showing a good matching with simulation result as displayed in FIG. 4.15.

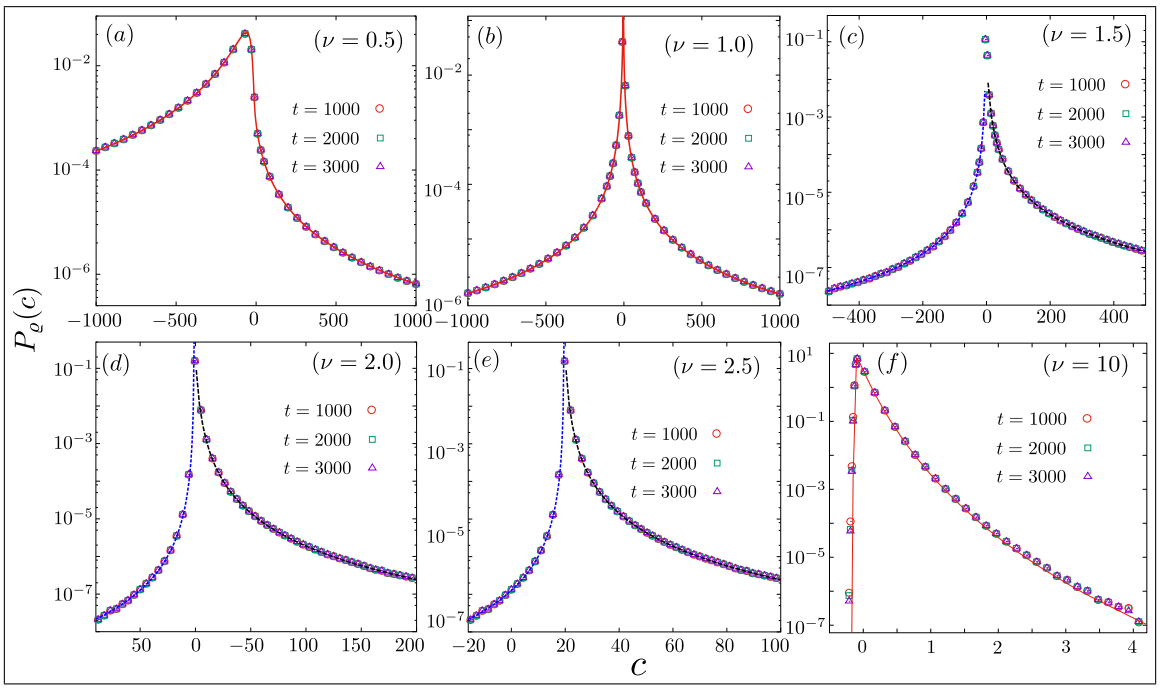

Figure 4.16: PDF of scaled net overtakings $c = m(t)/t$ are plotted at three different times, in the case of a Jepsen gas, confined within a ring of size $N = 128$ with particle density $\varrho = 1$ and their velocities are taken independently from a power-law distribution of exponent (a) $\nu = 0.5$, (b) 1.0, (c) 1.5, (d) 2.0, (e) 2.5, and (f) 10. The discrete points are numerical simulation results which are showing good agreements with the numerically obtained results as shown by (red) bold lines in (a), (b), and (f). In (c), (d), and (e) we have plotted approximate results for the left and the right tails as shown by dashed lines.

Bibliography

[1] D. W. Jepsen, J. Math. Phys. (N.Y.) **6**, 405 (1965).

[2] A.-L. Barabsi and H. E. Stanley, *Fractal concepts in surface growth* (Cambridge university press, England, 1995), J. Krug, Adv. Phys. **46**, 139 (1997).

[3] S. Edwards, Proc. R. Soc. London, Ser. A **381**, 17 (1982).

[4] M. Kardar, G. Parisi, and Y.-C. Zhang, Physical Review Letters **56**, 889 (1986).

[5] V. Popkov, A. Schadschneider, J. Schmidt, and G. M. Schtz, Proceedings of the National Academy of Sciences **112**, 12645 (2015).

[6] V. Popkov, J. Schmidt, and G. Schtz, Physical review letters **112**, 200602 (2014).

[7] V. Popkov, J. Schmidt, and G. Schtz, Journal of statistical physics **160**, 835 (2015).

[8] W. Feller, *An introduction to probability theory and its applications*, Vol. 2 (John Wiley Sons, 2008).

[9] H. A. David and H. N. Nagaraja, Encyclopedia of Statistical Sciences (2004).

[10] B. C. Arnold, N. Balakrishnan, and H. N. Nagaraja, *A first course in order statistics*, Vol. 54 (Siam, 1992).

[11] R.A. Fisher and L.H.C. Tippett, Cambridge Philos. Soc. **28**, 180 (1928).

[12] E.J. Gumbel, *Statistics of Extremes*, Columbia Univer-sity Press, 1958.

Chapter 5

Finite-size effects on overtaking for a finite number of interacting agents on a ring

5.1 Introduction

In Chapter 3, we have proposed and studied a simple one-dimensional (1D) model of overtaking in the limit where the system size N is much larger than observation time t. In this chapter we study the same problem in the limit $t >> N$ to investigate the finite-size effects on the statistics of the net overtaking number by a tagged agent. For convenience, we consider our system to be periodic. We aim to investigate all quantities of interest which we have studied in Chapter 3 including the finite-size scaling analysis to compute the dynamical exponent associated with the tagged dynamics.

The rest of the chapter is organized as follows. In Sec. 5.2, we outline our model of overtaking with its dynamical rules and quantities of interest. Similar to Chapter 3, here also we investigate three different cases depending on the dynamical rules. First, in Sec. 5.3, we study case I followed by Case II and III in Sec. 5.4 and 5.5 respectively. After that, in Sec. 5.6, we study the finite-size scaling analysis in detail.

5.2 Model, Transition rule, and Quantities of interest

5.2.1 The Model

Consider a 1D lattice of N sites ($i = 0, 1, 2, ..., N-1$) with periodic boundary conditions (PBC) $N + i \equiv i$. Initially, each site i on this lattice is occupied by an agent. Each agent is assigned with a real scalar variable v_i by drawing them independently from an identical distribution $\rho(v)$. Notably, this assign variable associated with each agent characterizes the self-driven property of singly-seated agent on that site, and for further convenience, we name this variable *velocity*. We assume each agent retaining their velocity in time. With time each neighboring pair $(i, i+1)$ of the left (L) and the right (R) velocities, v_L and v_R respectively, are exchanged their sites at the rate r, which depends on their corresponding velocities i.e., $r \equiv r(v_L, v_R)$. Clearly, v_L and v_R associated with a pair are time-dependent variables. They instantaneously take the velocities of agents seated on the respective sites. The site exchange rule of the neighboring pair mimics overtaking. A successful exchange of an adjacent pair increases (decreases) the net overtaking number by an amount $+1$ (-1) for the left (right) agent of a selected pair as illustrated in FIG. 5.1.

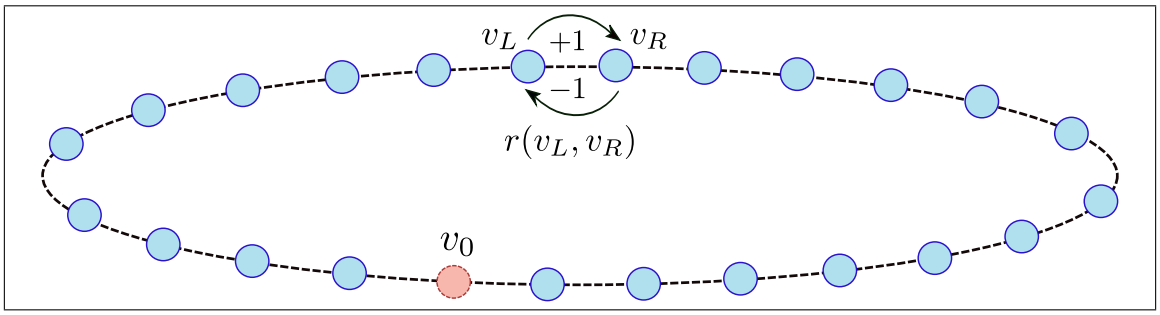

Figure 5.1: Schematic of a periodic system of 24 sites with singly-seated agents of random but constant initial velocities. As a dynamics, each neighboring pair of the left (L) and the right (R) velocities, v_L and v_R respectively, exchange their sites at the rate $r(v_L, v_R)$. A successful exchange increases (decreases) the net overtaking number by an amount $+1$ (-1) for the left (right) agent. The agent in red with velocity v_0 is tagged to study how the finite system-size (or the finite number of agents) affects its net overtaking number with time.

5.2.2 Three different dynamical rules

In this subsection, we recall three different dynamical rules in Chapter 3 which we constructed on the bais of exchange (overtaking) rate $r(v_L, v_R)$ of nearest neighboring pairs of velocities v_L and v_R. From Sec. 3.2.1 we can write these three different cases as

$$r(v_L, v_R) = \begin{cases} 1 & \text{as case I} \\ \Theta(v_L - v_R) & \text{as case II} \\ (v_L - v_R)\Theta(v_L - v_R) & \text{as case III} \end{cases} \tag{5.1}$$

where $\Theta(v) = 1$ for $v > 0$ and 0 for $v \leq 0$, is the Heaviside theta function.

5.2.3 Quantities of interest

In this chapter, we investigate all the quantities we have already defined in Chapter 2 in particular in the limit where time $t >> N$. Therefore, from Sec. 2.2.2, we first recall our main quantity of interest, namely, the net overtaking number $m(t|v_0)$ by a tagged agent of velocity v_0 upto time t. We study its mean $\langle m(t|v_0)\rangle$, variance $\langle m^2(t|v_0)\rangle_c$, and the same two probability distributions which we have defined in Sec. 2.2.2. The distributions are namely the conditional and the unconditional distributions which are denoted by $p(m, t|v_0)$ and $P(m, t)$ respectively.

Besides that, we also discuss here the finite-size scaling analysis to numerically compute the dynamical exponent and the relevant quantities associated with it [1]. Note that, we introduced and studied this concept in Sec. 4.2.2 and 4.3.2 in the context of the same problem in Jepsen gas on a ring.

5.3 Case I : $r(v_L, v_R) = 1$

The velocity independent stochastic updation rule makes the tracer dynamics simple in this case. Here two bonds associated with any site or equivalently with any particle are independently selected with the rate one. It effectively makes any tagged agent to execute a symmetric random walk on the lattice with the left (l) and the right (r) hopping rates $p_l = p_r = 1$. Notably, in a periodic system, the displacement of a random walker remains unaffected by the finite system size. Hence, it yields the

same result, which we have discussed in Sec. 3.3.

5.4 Case II : $r(v_L, v_R) = \Theta(v_L - v_R)$

In this case an agent with a given velocity, higher than its right neighbor (or lower than its left neighbor) can make an exchange. More importantly, all the allowed exchanges are executed at an equal rate one. These two criteria make this process similar to the totally asymmetric simple exclusion process (TASEP) with infinitely many classes of particles [2–7]. But, from the viewpoint of a tagged v_0, it dynamics becomes equivalent to the dynamics of a *second class particle* in TASEP [2](see Sec. 3.4.1 for details) with the density of particle $\rho_+(v_0)$. $\rho_+(v_0)$ and $\rho(v_0)$ are related through Eq. (3.2) in Sec. 3.4.1. Now, using Eq. (3.2) in the next, we discuss the mean and the variance of $m(t|v_0)$.

5.4.1 Mean and variance of the net overtaking number

For a system of size N, excluding a *2nd class particle*, the Bernoulli product measure initial distribution of velocities implies that the probability of having $n \in [0, N-1]$ number of particles for a given $\rho_+(v_0)$ is a binomial distribution of the form

$$\mathcal{P}_B(n|v_0, N) = \binom{N-1}{n} \rho_+(v_0)^n \, (1 - \rho_+(v_0))^{N-n-1}. \tag{5.2}$$

For a particular n, the average speed $\bar{c}(n)$ is equal to the probability of having a hole at the right-neighboring-site of v_0 minus the probability of having a particle at the left-neighboring-site of the same i.e.,

$$\bar{c}(n) = \frac{N-1-n}{N-1} - \frac{n}{N-1} = \left(1 - \frac{2n}{N-1}\right). \tag{5.3}$$

Taking average over all particle numbers, the mean speed $\bar{c}(v_0)$ for a given v_0 can be calculated as

$$\bar{c}(v_0) = \sum_{n=0}^{N-1} \mathcal{P}_B(n|v_0, N) \; \bar{c}(n) = 1 - 2\rho_+(v_0). \tag{5.4}$$

Notably, $\langle m(t|v_0)\rangle = \bar{c}(v_0)\, t$ remain unchanged under the periodic boundary condition.

Now, to discuss the variance, from Chapter 3, we first recall that, on taking the limit $N \to \infty$ first, and then $t \to \infty$, the variance of the net overtaking number comes out diffusive ($\propto t$) followed by super-diffusion ($\propto t^{4/3}$) with a velocity dependent crossover time $t_1^*(v_0)$ [8] i.e.,

$$\langle m^2(t|v_0)\rangle_c \propto \begin{cases} t & \text{for } t << t_1^*(v_0) \\ \chi^{2/3}(v_0)\, t^{4/3} & \text{for } t >> t_1^*(v_0). \end{cases} \tag{5.5}$$

The crossover time $t_1^*(v_0) \propto \chi^{-2}(v_0)$ with $\chi(v_0) = \rho_+(v_0)(1-\rho_+(v_0))$ [8]. Now, using the relation $\rho_+(v_0) = \int_{v_0}^{\infty} dv\ \rho(v)$ it can be said that for $v_0 \sim \langle v\rangle$, the behavior at finite but large time is super-diffusive as it yields $t_1^*(v_0) \sim \mathcal{O}(1)$. On the other hand, in the opposite limit ($v_0 \to \pm\infty$) $t_1^*(v_0) \to \infty$, which brings out a diffusive behavior at any finite time.

Now to discuss the variance in the opposite limit (i.e., in the limit $t >> N$) we first use the result from [10,11]. Using matrix formulation Derrida *et al.* [10,11] calculated the size dependent diffusivity $\mathcal{D}(n|N)$ of a *2nd class particle* in the presence of n number of particles within a system of size N as

$$\mathcal{D}(n|N) = \frac{2\ (2N-3)!}{(2n+1)!(2N-2n-1)!}\left(\frac{n!(N-n-1)!}{(N-1)!}\right)^2 \times \left((N-5)(N-n-1)n + (N-1)(2N-1)\right). \tag{5.6}$$

Clearly, this expression supports two intuitive results in two extreme limits i.e., $\mathcal{D}(0|N) = \mathcal{D}(N-1|N) = 1$. Taking average over all particle numbers the diffusivity $D(v_0|N)$ for a given v_0 can be calculated as

$$D(v_0|N) = \sum_{n=0}^{N-1} \mathcal{P}_B(n|v_0, N)\ \mathcal{D}(n|N). \tag{5.7}$$

Notably, in the limit of $N >> 1$, we can define a new variable $\rho_0 = n/N$. Using the Stirling approximation $x! = \sqrt{2\pi x}\ (x/e)^n$ in Eq. (5.2) and (5.6), can be written

as [11]

$$\mathcal{P}_B(\rho_0, v_0|N) \simeq \frac{1}{\sqrt{2\pi\rho_0(1-\rho_0)N}} \left(\frac{\rho_+(v_0)}{\rho_0}\right)^{\rho_0 N} \left(\frac{1-\rho_+(v_0)}{1-\rho_0}\right)^{(1-\rho_0)N}. \tag{5.8}$$

$$\mathcal{D}(\rho_0|N) \simeq \frac{1}{4}[N\pi\rho_0(1-\rho_0)]^{1/2} \tag{5.9}$$

Now, taking $\rho_0 \in [0:1]$ as a continuum variable we can write

$$\begin{aligned} D(v_0|N) &\simeq N \int_0^1 d\rho_0 \, \mathcal{P}_B(\rho_0|v_0, N) \, \mathcal{D}(\rho_0|N) \\ &\simeq \frac{N}{4\sqrt{2}} \int_0^1 d\rho_0 \left(\frac{1-\rho_+(v_0)}{1-\rho_0}\right)^{N-N\rho_0} \left(\frac{\rho_+(v_0)}{\rho_0}\right)^{N\rho_0} \\ &\simeq \frac{N}{4\sqrt{2}} \int_0^1 d\rho_0 \, e^{N\varphi(\rho_0,\, \rho_+(v_0))} \end{aligned} \tag{5.10a}$$

with

$$\varphi(\rho_0,\ \rho_+(v_0)) = (1-\rho_0)\log\left[\frac{1-\rho_+(v_0)}{1-\rho_0}\right] + \rho_0\ \log\left[\frac{\rho_+(v_0)}{\rho_0}\right]. \tag{5.10b}$$

By solving this integration with the method of saddle point, we can write

$$D(v_0|N) \simeq \frac{1}{4}\sqrt{\pi N}\ \frac{e^{N\ \varphi(\rho_0^*,\, \rho_+(v_0))}}{\sqrt{|\varphi''(\rho_0^*,\ \rho_+(v_0))|}} \simeq \frac{\sqrt{\pi}}{4}\sqrt{N\ \chi(v_0)} \tag{5.11}$$

with $\varphi'(\rho_0^*,\ \rho_+(v_0)) = 0$ and $\chi(v_0) = (|\varphi''(\rho_0^*,\ \rho_+(v_0))|)^{-1} = \rho_+(v_0)(1-\rho_+(v_0))$ at the saddle point $\rho_0^* = \rho_+(v_0)$. Now, we can say that on taking $t \to \infty$ first, and then $N \to \infty$, the behavior of the variance comes out linear in time i.e., $\langle m^2(t|v_0)\rangle_c = D(v_0|N)\ t$. Using this relation and Eq. (5.5) we can estimate the crossover time $t_2^*(v_0)$ of size-independent super-diffusive behavior to the size-dependent diffusive one as

$$t_2^*(v_0) \propto N^{3/2}\chi^{-1/2}(v_0). \tag{5.12}$$

Note that this size-dependent diffusivity appears only around $v_0 \sim \langle v\rangle$, because the opposite limit ($v_0 \to \pm\infty$) corresponds $\rho_+(v_0) \to 0$ or 1, which further yields $\chi(v_0) \to 0$, or equivalently $t_2^*(v_0) \to \infty$. In this limit the behavior of $\langle m^2(t|v_0)\rangle_c$ remains same as that of size-independent behavior which is equal to t [8]. So, in

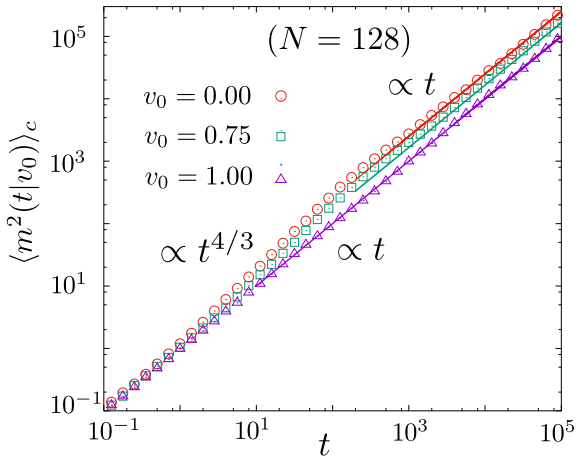

Figure 5.2: Discrete points are simulation results, illustrating the crossover from the system-size independent initial behavior to the system-size dependent long-time $\propto t$ behavior, for the variance of the net overtaking number by a tagged agent in case II. Three different tagged velocities $v_0 = 0.0$, 0.75, and 1.0 are considered by drawing the remaining velocities from a uniform distribution over $[-1 : 1]$ for a periodic system of size $N = 128$. The bold lines plot the analytical results which show a good agreement with the corresponding numerical results. For $v_0 = 0.0$ and 0.75, transition from an initial anomalous growth $\propto t^{4/3}$ to the long-time diffusive one $\propto t$ is clearly noticeable, while $v_0 = 1.0$ shows only a linear growth $\propto t$ in time, which implies a size-independent behavior in the whole regime.

brief, we can write

$$\langle m^2(t|v_0)\rangle_c \simeq \begin{cases} D(v_0|N)\, t & \text{for } v_0 \sim \langle v\rangle \\ t & \text{for } v_0 \sim \pm\infty. \end{cases} \tag{5.13}$$

as shown and illustrated in FIG. 5.2.

5.4.2 Conditional Distribution

From the above discussion, it is clear that there are two different cases for which we expect two different behaviors of the conditional distribution. These cases are respectively $v_0 \sim \pm\infty$ and $v_0 \sim \langle v\rangle$.

In the first case, we know [8] that the the tagged v_0 execute a biased random walk with right (r) and left (l) jumping rates $p_r(v_0) \equiv \rho_+(v_0)$ and $p_l(v_0) \equiv 1 - \rho_+(v_0)$ respectively. By using the fact of $p_r(v_0) + p_l(v_0) = 1$, an approximate result of the

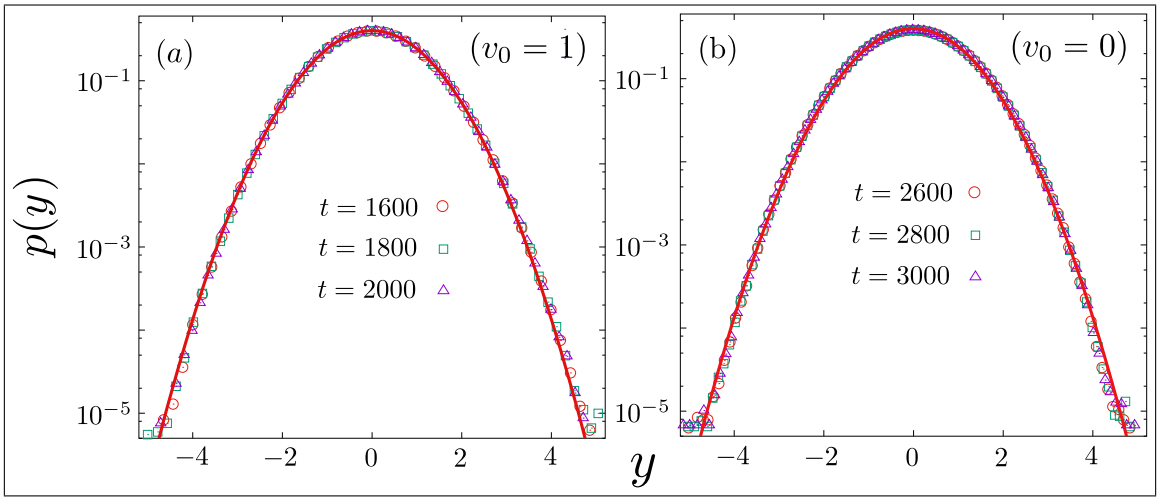

Figure 5.3: Conditional PDF of the net overtaking number $m(t|v_0)$ by a tagged agent of velocity v_0 are plotted at three different times in two different limits (a) $v \to \pm\infty$ and (b) $v \sim \langle v \rangle$ in case II by considering a periodic system of $N = 128$ sites. To satisfy those limits we conveniently consider $v_0 = 1$ and $v_0 = 0$, respectively, by drawing the remaining velocities from a uniform distribution over $[-1 : 1]$. In both figures, the simulation results, denoted by points, for the PDF of the scaled net overtaking number $y \propto (m - \bar{c}t)/\sqrt{t}$, are plotted in log-linear scale together with the respective analytical results as denoted by the bold lines.

conditional PDF can be written as:

$$p(c, t|\bar{c}) \simeq \sqrt{\frac{t}{2\pi}} \frac{e^{-t\,\phi(c,\bar{c})}}{\sqrt{|\phi''(c,\bar{c})|}} \tag{5.14}$$

with the large deviation function [9] $\phi(c, \bar{c}) = c \log\left[(c + \sqrt{c^2 + 1 - \bar{c}^2})/(\bar{c} + 1)\right] + 1 - \sqrt{c^2 + 1 - \bar{c}^2}$, and $|\phi''(c, \bar{c})| = \sqrt{c^2 + 1 - \bar{c}^2}$. In the limit of large t, expanding c around $\bar{c}$, and then, write it in terms of a scaled variable $y = \sqrt{t}(c - \bar{c})$, we can find out the well-known Gaussian distribution of the form $p(y) \simeq 1/\sqrt{2\pi}\, \exp(-y^2/2)$ as verified by numerical simulation and shown in FIG. 5.3(a).

To discuss behavior of $v_0 \sim \langle v \rangle$, we first use result from ref [10]. From this reference, we can say that the displacement distribution of a second class particle for a given number of particles (or alternatively for a given ρ_0) is Gaussian with variance $D(\rho_0|N)$. It simply makes the distribution of $p(m, t|v_0)$ Gaussian with the variance $D(v_0|N)$ as we verified it by the numerical simulation as shown in FIG. 5.3(b).

5.4.3 Unconditional Distribution

From two different results of the conditional distribution, it is quite obvious to predict that the unconditional distribution $P(c,t)$ also has two different behaviors. First, we describe the behavior in the limit of $t \to \infty$. Using Eq. (5.4) and (5.13) we can say that the speed varies at the large time as $c \sim \bar{c} + \mathcal{O}(t^{-\frac{1}{2}})$. More importantly, it remains unaffected by the finite system size. Hence, from Sec. 3.4.4 we can recall that the variable c is random within $[-1:1]$ by ignoring the fluctuations around $\bar{c}$ in the limit $t \to \infty$, as $c \simeq \bar{c}(v_0) \simeq (1 - 2\rho_+(v_0))$. Now, using $dc/dv_0 = -2\rho'_+(v_0) = 2\rho(v_0)$, we get

$$P(c) \simeq \frac{\rho(v_0(c))}{|dc/dv_0|} \simeq \frac{1}{2}. \tag{5.15}$$

Thus, $c = m(t)/t$, in the limit $t \to \infty$, is uniformly distributed over $[-1:1]$, for all continuous distribution $\rho(v)$.

Now, to get finite but large time behaviors of $P(c,t)$, we can proceed as follows: If we treat the tagged agent as a second class particle, then the number of particles in the system can vary from 0 to $(N-1)$. For a particular v_0, probability of n number of particles present in the system is $\mathcal{P}_B(n|v_0, N)$. We denote the conditional distribution for a given n by $p(c,t|n)$ to write

$$\begin{aligned}
P(c,t) &= \int_{-\infty}^{\infty} dv_0\ \rho(v_0)\ p(c,t|v_0) = \int_{-\infty}^{\infty} dv_0\ \rho(v_0)\ \sum_{n=0}^{N-1} \mathcal{P}_B(n|v_0,N)\ p(c,t|n) \\
&= \sum_{n=0}^{N-1} p(c,t|n) \int_{-\infty}^{\infty} dv_0\ \rho(v_0)\ \mathcal{P}_B(n|v_0,N) \\
&= \sum_{n=0}^{N-1} p(c,t|n) \binom{N-1}{n} \int_{-\infty}^{\infty} dv_0\ \rho(v_0)\ \rho_+(v_0)^n\ (1-\rho_+(v_0))^{N-n-1} \\
&= \sum_{n=0}^{N-1} p(c,t|n) \binom{N-1}{n} \int_0^1 dz\ z^n\ (1-z)^{N-1-n} = \frac{1}{N} \sum_{n=0}^{N-1} p(c,t|n).
\end{aligned} \tag{5.16}$$

In the last line we have made a variable transformation $z = \rho_+(v_0)$ and used the relation $\rho_+(v_0) = \int_{v_0}^{\infty} dv\ \rho(v)$.

First to discuss the behavior of the tails of $P(c,t)$ we can say its contribution comes from $v_0 \to \pm\infty$. In this limit, writing the Gaussian approximated solution of

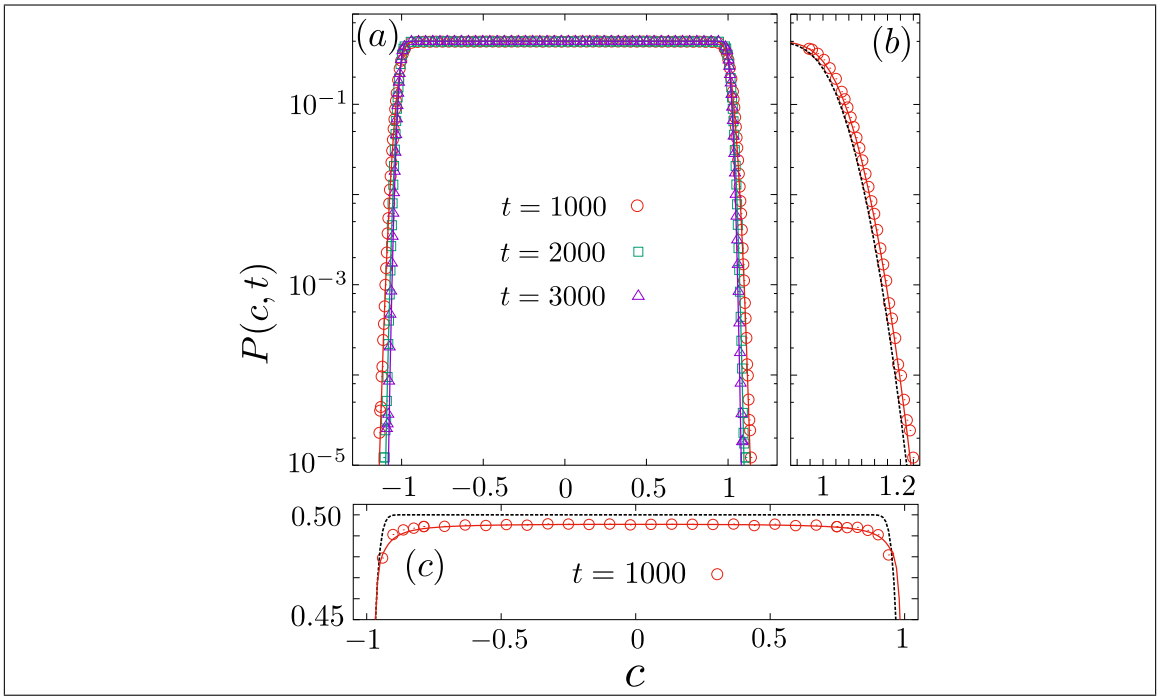

Figure 5.4: (a) PDF of the scaled net overtakings $c(t) = m(t)/t$ are plotted at three different times in case II by considering a periodic system of size $N = 128$ with it's initial velocities taken independently from a uniform distribution over $[-1 : 1]$. The discrete points are the simulation results, which at the tails of $P(c,t)$, are showing good agreements with the result in Eq. (5.17), as shown by the bold lines. In (b): Simulation results of $P(c,t)$ at $t = 1000$ plotted alongside the analytical results in Eq. (5.17) and (5.18) as displayed by (red) bold line and black (dashed) line respectively. The bulk of $P(c,t)$ is highlighted in (c) to show it holds a good agreement with Eq. (5.19) as plotted by (red) solid line. A dashed line of Eq. (5.17) is also included to make a comparison.

$p(c,t|n)$ we can proceed as follows:

$$P(c,t) \simeq \frac{1}{N}\sum_{n=0}^{N-1}\sqrt{\frac{t}{2\pi}}\,\mathrm{Exp}\left[-\frac{t}{2}(c-\bar{c}(n))^2\right]$$
$$\simeq \frac{1}{N}\sqrt{\frac{t}{2\pi}}\sum_{n=0}^{N-1}\mathrm{Exp}\left[-\frac{t}{2}\left(c-1+\frac{2n}{N-1}\right)^2\right]. \quad (5.17)$$

The obtained result is showing good agreements with the simulation result as shown in FIG. 5.4(a). Notably if we consider $x = n/(N-1)$ a continuous variable within $[0 : 1]$, then we can convert the above sum into integration and calculate $P(c,t)$ as

follows:

$$P(c,t) \simeq \left(1-\frac{1}{N}\right)\sqrt{\frac{t}{2\pi}}\int_0^1 dx\ \mathrm{Exp}\left[-\frac{t}{2}\left(c-1+2x\right)^2\right]$$
$$\simeq \frac{1}{4}\left(1-\frac{1}{N}\right)\left(\mathrm{Erf}\left[\sqrt{\frac{t}{2}}\left(c+1\right)\right]-\mathrm{Erf}\left[\sqrt{\frac{t}{2}}\left(c-1\right)\right]\right). \quad (5.18)$$

Clearly, in the limit of $N \to \infty$ it yields the result of Eq. (3.17). But, for any finite N, the conversion of the sum into integration gives rise to a clear difference as shown in FIG. 5.4(b).

Now, to get result around the bulk, using the same argument like Eq. (5.17), we can write

$$P(c,t) \simeq \frac{1}{N}\sum_{n=0}^{N-1}\sqrt{\frac{t}{2\pi\ D(n|N)}}\ \mathrm{Exp}\left[-\frac{t}{2\ D(n|N)}(c-\bar{c}(n))^2\right] \quad (5.19)$$

with $D(n|N) \simeq (\pi n(1-n/N))^{1/2}/4$. Notably, this $D(n|N)$ we get by putting $\rho = n/N$ in Eq. (5.9). The obtained numerical result shows a good agreement with the data obtained from the numerical simulation as we displayed in FIG. 5.4(c).

5.5 Case III : $r(v_L, v_R) = (v_L - v_R)\,\Theta(v_L - v_R)$

The relative velocity-dependent exchange rule, in this case, make the process completely different from the earlier one. This velocity-dependent exchange corresponds to an infinite-species Karimipour model [12, 13] as we discussed in Chapter 3. In the next, we derive an approximate expression of the net overtaking number by a tagged agent.

5.5.1 The net overtaking number

In the limit of $t >> N$, two trajectories on the lattice intersect each other multiple times due to the periodic boundary condition.It allows us to apply a similar formalism we have already used in Sec. 4.3.1 in case of a Jepsen gas enclosed in a ring.

First, using Eq. (4.5) we can write

$$m(t|v_0) = m_R(t|v_0) - m_L(t|v_0) \tag{5.20}$$

with $m_R(t|v_0)$ and $m_L(t|v_0)$, counting the number of jump events of v_0 to the right and the left upto time t respectively. Now, in a system of N given velocities v_0, v_1,....,v_{N-1}, we can write the average displacement of v_0 and v_i as $\left(v_0 - \frac{1}{N-1}\sum_{j=1}^{N-1} v_j\right) t$ and $\left(v_i - \frac{1}{N-1}\sum_{\substack{j=0 \\ j\neq i}}^{N-1} v_j\right) t$. If we denote x_i as the distance between v_0 and v_i at time $t = 0$, then, we can calculate an approximate $m_R(t|v_0)$ as follows:

$$\begin{aligned} m_R(t|v_0) &\simeq \sum_{i=1}^{N-1} I(v_0 > v_i) \frac{\left(v_0 - \frac{1}{N-1}\sum_{j=1}^{N-1} v_j\right) t - \left(v_i - \frac{1}{N-1}\sum_{\substack{j=0 \\ j\neq i}}^{N-1} v_j\right) t - x_i}{N} \\ &\simeq \sum_{i=1}^{N-1} I(v_0 > v_i) \left(\frac{(v_0 - v_i)t}{N-1} - \frac{x_i}{N}\right). \end{aligned} \tag{5.21}$$

Following a similar procedure we can get

$$m_L(t|v_0) \simeq \sum_{i=1}^{N-1} I(v_0 < v_i) \left(\frac{(v_i - v_0)t}{N-1} - \frac{N - x_i}{N}\right). \tag{5.22}$$

Inserting Eq. (5.21) and (5.22) into Eq. (5.23) we finally get

$$m(t|v_0) \simeq \left(v_0 - \frac{1}{N-1}\sum_{i=1}^{N-1} v_i\right) t + \mathcal{O}(N) \simeq (v_0 - U)\, t \tag{5.23}$$

in the limit of $t >> N$ in terms of a new variable $U = (N-1)^{-1}\sum_{i=1}^{N-1} v_i$.

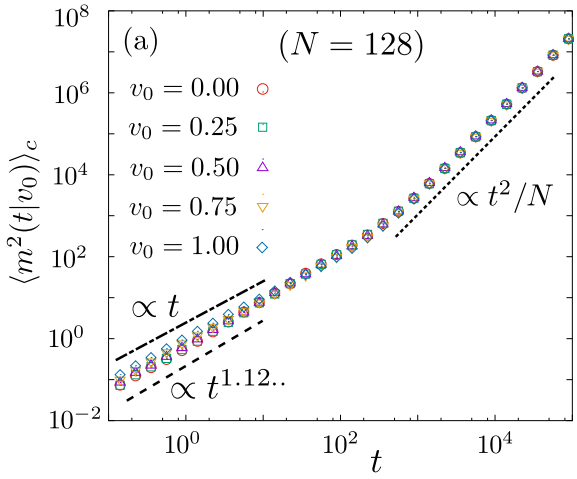

Figure 5.5: Discrete points are simulation results, illustrating the crossover from system-size independent initial behavior to the system-size dependent long-time $\propto t^2/N$ behavior, for the variance of the net overtaking number by a tagged agent in case II. Five different velocities are tagged by drawing the remaining velocities from uniform distribution within a periodic system of size $N = 128$.

5.5.2 Cumulants of the net overtaking number

Using Eq. (5.23) we first see it return the mean $\langle m(t|v_0)\rangle \simeq (v_0 - \langle U\rangle)t \simeq (v_0 - \langle v\rangle)t \simeq \bar{c}(v_0)t$. Now, the variance can be calculated as

$$\langle m^2(t|v_0)\rangle_c \simeq \langle (v_0 - U)^2\rangle_c \, t^2 \simeq \langle (v_0 - U)^2\rangle \, t^2 - \langle (v_0 - U)\rangle^2 \, t^2 \simeq \langle U^2\rangle_c \, t^2 \simeq \frac{1}{N}\langle v^2\rangle_c \, t^2 \simeq \frac{\sigma^2}{N-1} \, t^2 \quad (5.24)$$

with σ^2, the variance of the initial velocity distribution. Note that this variance becomes independent of the exact value of the tagged v_0 as shown in FIG. 5.5. In fact, we can calculate all the higher order cumulants in terms of the same of initial velocity distribution as

$$\langle m^n(t|v_0)\rangle_c \simeq v_0 \, t \, \delta_{n,1} + \frac{(-1)^n}{(N-1)^{n-1}}\langle v^n\rangle_c \, t^n \quad (5.25)$$

(see Sec. 4.3.2 for details).

5.5.3 Conditional and Unconditional Distributions

Compare Eq. (5.23) with Eq. (4.6), we can say that the process of overtaking by a given v_0 becomes identical to the same process in case of a Jepsen gas with uniformly distributed $(N-1)$ particles within a periodic system of size N. In the limit $N >> 1$, we can expect that the results for the conditional and the unconditional

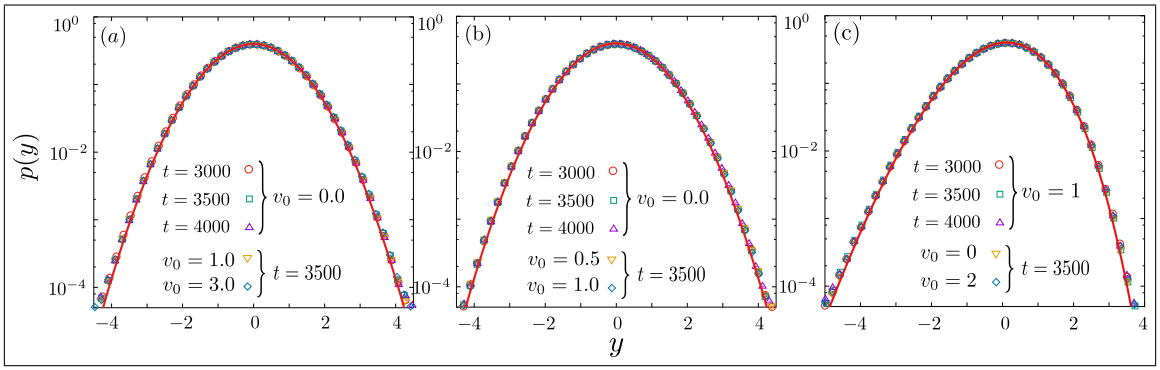

Figure 5.6: Conditional PDF of scaled net overtakings $y = \sqrt{N/\langle v^2 \rangle_c}(c - \bar{c}(v_0))$ are plotted for a given tagged v_0 in case III by considering a periodic system of 64 sites with it velocities taken independently from (a) Gaussian, (b) uniform, and (c) exponential distributions. The symbols are obtained from the numerical simulations, which are showing good agreements with the analytical results (Eq. (4.9) for (a) & (b) and Eq. (4.15) for (c)) as plotted by solid lines.

distributions, in this case, come out same as that of Jepsen gas with $(N-1) \simeq N$ particles in a system of size N. We verify these by numerical simulations and shown in FIG. 5.6 and FIG. 5.7.

5.6 Finite-size scaling analysis and the dynamical exponent

5.6.1 Case II

Following the definition in Eq. (4.1) with Eq. (5.12) we can say the dynamical exponent $z = 3/2$ in this case. The reason of getting $z = 3/2$ is as follows: the dynamics of a tagged v_0 in this case is equivalent to the dynamics of a second class particle in TASEP with density of particles $\rho_+(v_0)$ (see Sec. 3.4.1). More importantly, this second class particle follows the coarse-grained density fluctuation in TASEP (see Sec. 3.4.2 and Sec. 1.4.1). This coarse-grained density fluctuation in TASEP follows the fluctuating hydrodynamics equation (see Sec. 1.4.2) which can be converted into KPZ equation of interface growth model [14] by a varible transformation (see Sec. 1.4.3). It relates the dynamics of tagged v_0 with the KPZ universality class, and hence brings out $z = 3/2$, which characterize the corresponding universality class.

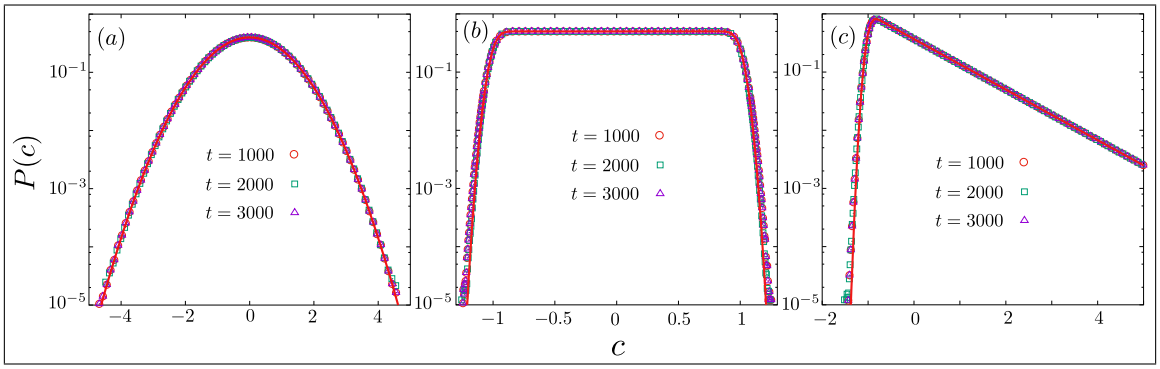

Figure 5.7: PDF of scaled net overtakings $c = m(t)/t$ are plotted at different times by considering a periodic system of size $N = 128$ in case III. Initial velocities of the agents are taken independently from (a) Gaussian, (b) uniform, and (c) exponential distributions. The symbols are obtained from the numerical simulations, which are showing good agreements with analytical results (Eq. (4.38) for (a) & (b) and Eq. (4.42) for (c)) as plotted by solid lines.

Notably, all the other exponents $\alpha, \gamma, \delta, \xi$ (see Sec. 4.2.2) in this case can be written in terms of z. First, in case of KPZ universality class it is known that $\alpha + z = 2$ [1], i.e.,

$$\alpha = 2 - z. \tag{5.26}$$

For γ, using the relation in Eq. (3.11) first, then by writing $\beta = \alpha/z$ for KPZ universality class [1] we can get

$$\gamma = 2\beta + \frac{1}{z} = \frac{5}{z} - 2. \tag{5.27}$$

Finally, by using Eq. (4.4) and $\xi = \gamma z$ (see Sec. 4.2.2) we can get

$$\delta = \gamma - \frac{\alpha}{z} = \frac{3}{z} - 1, \tag{5.28}$$

and

$$\xi = 5 - 2z. \tag{5.29}$$

In FIG. 5.8 we plot the scaling function $f(u)$ for different system sizes. The collapse data-points supports all the results we have shown above.

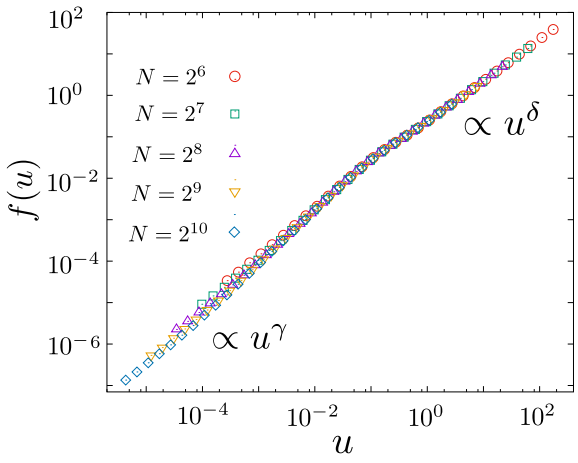

Figure 5.8: Numerical results of the scaling function $f(u)$ are plotted vs $u = t/N^z$ for five different system sizes N by considering the tagged $v_0 = 0.0$ in the environment of random but independently taken velocities from a uniform distribution over $[-1 : 1]$. The collapse datapoints of $f(u)$ for different N are obtained by using the dynamical exponent $z = 3/2$ with $\alpha = 1/2$, $\gamma = 4/3$, $\delta = 1$, and $\xi = 2$.

5.6.2 Case III

In this section, first, we study a systematic transition from case II to case III to get some cues from the earlier. Notably, we study this transition in the limit $N >> t$. For that, in the next, we briefly introduce the discrete velocity distribution.

Discrete velocity distribution:

Let consider a velocity distribution of the form

$$\rho_n(v) = \sum_{j=1}^{n} p_j \, \delta\left(v - v_j\right). \tag{5.30}$$

A randomly chosen velocity from this distribution can take n distinct values with assigned probabilities. Notably, if one choose

$$v_j = v_{min} + \left(j - \frac{1}{2}\right) \frac{(v_{max} - v_{min})}{n}, \tag{5.31a}$$

$$\text{and} \;\; p_j = \int_{v_{j-1/2}}^{v_{j+1/2}} dv \; \rho(v), \tag{5.31b}$$

then, $\rho_n(v)$, in the limit $n \to \infty$, converges to a continuous probability distribution $\rho(v)$ which is bound within $[v_{min} : v_{max}]$. For example, here, we consider three different $\rho(v)$, which are namely, uniform, Gaussian, and exponential distributions.

First, for uniform $\rho(v)$ bound within $[-1:1]$, we can get

$$v_j = -1 + \frac{2}{n}\left(j - \frac{1}{2}\right) \qquad \text{with} \qquad p_j = \frac{1}{n}. \tag{5.32}$$

Next, to discretize the Gaussian distribution ($\rho(v) = (2\pi)^{-1/2}\, e^{-v^2/2}$), we first bound $\rho(v)$ within $[-v_g : v_g]$. Notably, this finite bound yields a negligible error in the limit $v_g >> 1$. For $v_g = 4$, the relative error is $\mathcal{O}(10^{-4})$. Using this approximate bound we can calculate

$$v_j \simeq -v_g + \frac{2v_g}{n}\left(j - \frac{1}{2}\right) \text{ and } p_j \simeq \frac{1}{2\ \mathrm{Erf}[v_g/\sqrt{2}]} \times \left(\mathrm{Erf}\left[\frac{v_g}{\sqrt{2}n}(2+n-2j)\right] - \mathrm{Erf}\left[\frac{v_g}{\sqrt{2}n}(n-2j)\right]\right). \tag{5.33}$$

Finally, for exponential distribution ($\rho(v) = e^{-v}$), instead of it exact bound $[0:\infty]$, if we consider it within $[0 : v_e]$, then we get

$$v_j \simeq \frac{v_e}{n}\left(j - \frac{1}{2}\right) \text{ and } p_j \simeq e^{-jv_e/n}\left(\frac{e^{v_e/n} - 1}{1 - e^{-v_e}}\right). \tag{5.34}$$

Notably, if one consider $v_e = 8$, then the relative error in this case becomes $\mathcal{O}(10^{-4})$. Now, using these $\rho_n(v)$, we discuss a systematic transition from case II to case III.

Transition from case II to case III :

Let consider a tagged $v_0 = \langle v \rangle$ in a periodic system of size N. All the remaining velocities in the system are taken independently from $\rho_n(v)$ of the form of Eq. (5.30). For example, consider $\rho_n(v)$ from Eq. (5.30) with p_j and v_j are from Eq. (5.32). In this case, if we choose $n = 2$ with $v_0 = 0$, then all the allowed transitions in the system can be written as

$$\begin{aligned} v_2 v_1 &\to v_1 v_2 \quad \text{at rate } 1, \\ v_2 v_0 &\to v_0 v_2 \quad \text{at rate } 1/2, \\ v_0 v_1 &\to v_1 v_0 \quad \text{at rate } 1/2. \end{aligned}$$

These allowed transitions are quite similar to that of a *second class particle* in TASEP (see Sec. 3.4.1). In fact, the qualitative behavior of the displacement vari-

ance of v_0, in this case, remains same as that of the *second class particle* in TASEP. Moreover, with the increase of n, $\langle m^2(t|v_0)\rangle_c$ converges to the same which we obtained from $\rho(v)$. We illustrate this transition in FIG. 5.9(a).

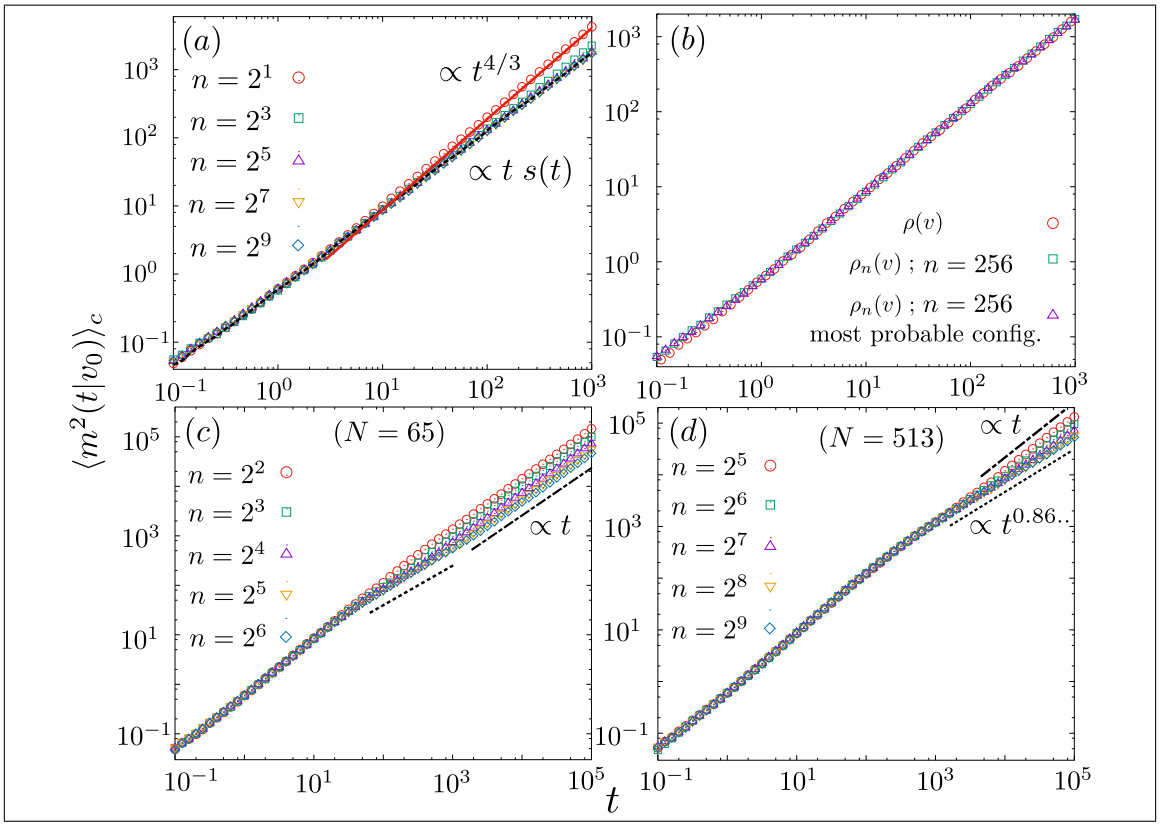

Figure 5.9: Simulation results of the variance of the net overtaking number by a tagged particle of velocity $v_0 = 0$ are plotted vs. time. Excluding v_0, all the remaining velocities are chosen independently from $\rho_n(v)$ of the form of Eq. (5.30) with Eq. (5.32). In (a): We show a systematic transition from case II to case III in a periodic system of size $N = 5121$. The black dotted line plots the result in case III. In (b): we plot the same quantity for $\rho(v)$, $\rho_n(v)$ with the number of different velocities $n = 256$, and the most probable configurations of $\rho_n(v)$ with $n = 256$ in a system of size $N = 5121$. In (c) and (d) we show an intermediate regime as displayed by (black) dotted line between the limits $t << N$ and $t >> N$ by considering the of system size $N = 65$ and $N = 513$ respectively. In the case of $N = 513$ it is clear that the length of this intermediate regime increases with the increment of n.

Instead of $\rho_n(v)$, if one initialized the system with the most probable configurations of $\rho_n(v)$, then also it yields the same result of $\langle m^2(t|v_0)\rangle_c$. In the most probable configurations, excluding the tagged v_0, the number of particles with velocity v_j are $p_j(N-1)$ in a system of size N. We plot $\langle m^2(t|v_0)\rangle_c$ with the most probable config-

uration in FIG. 5.9(b). In case of the most probable configurations, one can simplify U in Eq. (5.23) as

$$U = \frac{1}{N-1}\sum_{i=1}^{N-1} v_i = \sum_{j=1}^{n} v_j p_j. \tag{5.35}$$

In the limit of large n, as $\rho_n(v)$ converges to $\rho(v)$, we can expect $\sum_{j=1}^{n} v_j p_j$ converges to the mean of $\rho(v)$ i.e., $\langle v \rangle$. It makes $m(t|v_0) \simeq (v_0 - \langle v \rangle)t$, a constant number at a given time t. It also makes $\langle m^2(t|v_0)\rangle_c \simeq 0$ in Eq. (5.24). More importantly, these most probable configurations allow us to go beyond the average description of the net overtaking number by a tagged v_0, which we have given in Sec. 5.5. Hence, from here onwards, we consider only the most probable configurations of $\rho_n(v)$ to investigate the finite-size effects in the limit of $t >> N$.

Conserved quantities present in the system :

In case II (or alternatively for $n = 2$), we already knew that there is one conserved quantity in the system. Local fluctuations of this conserved quantity brings out $t^{4/3}$ behavior of $\langle m^2(t|v_0)\rangle_c$. Taking cues from this, we can say that for a given n, the number of conserved quantity in the system is $(n-1)$. The super-diffusive behavior in the limit of large n (or alternatively in case III) is due to the large conserved quantities present in the system.

From the numerical simulation, we have found few important results in the limit $t >> N$, which we discuss here before going to the finite-size scaling analysis. In the limit of $t >> N$ we obtain a diffusive behavior of $\langle m^2(t|v_0)\rangle_c$. With the increase of n, we can see an intermediate regime in between the limits $t << N$ and $t >> N$. More importantly, the length of this intermediate regime increases with increase of both N and n (see in FIG. 5.9(c) and (d)). From this point, it is quite clear that this intermediate regime appears in the limit of a large number of conserved quantities present in the system. We have already argued that the super-diffusive behavior of $\langle m^2(t|v_0)\rangle_c$ in the limit of $N \to \infty$ first, and then $t \to \infty$ is due to a large number of conserved quantities. Hence, for the finite-size scaling analysis, we focus on this intermediate regime.

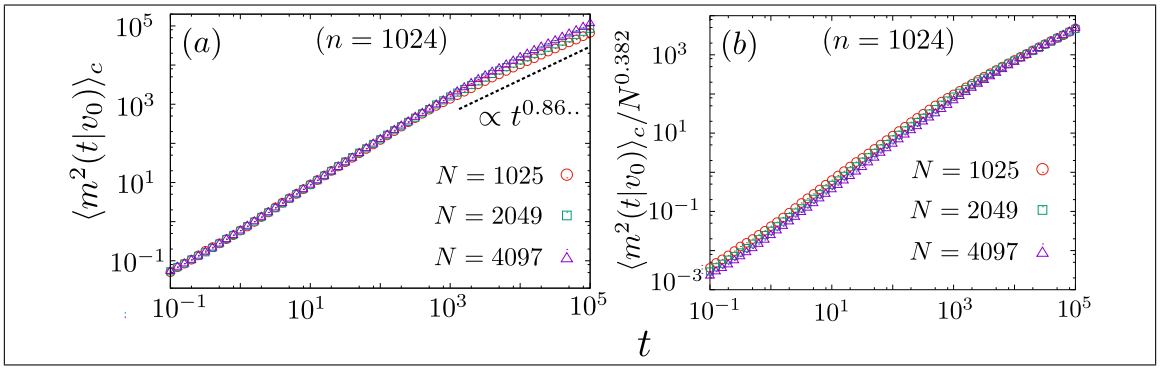

Figure 5.10: Simulation results of the variance $\langle m^2(t|v_0)\rangle_c$ of the net overtaking number by a tagged particle of velocity $v_0 = 0$ are plotted vs. time. Excluding v_0, all the remaining velocities are chosen independently from $\rho_n(v)$ of the form of Eq. (5.30) with Eq. (5.32). In (a) & (b): we compute $\delta \simeq 0.86..$ and $\alpha \simeq 0.38$ respectively by taking different system sizes with the number of different velocities $n = 1024$.

Finite-size scaling analysis:

In the presence of a large number of conserved quantities, it is recently studied by nonlinear fluctuating hydrodynamics that the dynamical exponent converges to Golden mean value $(1+\sqrt{5})/2 \simeq 1.618$ [15]. Taking cues from this, we can expect that the dynamical exponent $z \simeq 1.618$ in our case III as it results out from a large number of conserved quantities present in the system. From the numerical simulation we have computed $\alpha \simeq (3-\sqrt{5})/2 \simeq 0.382$, i.e., the relation $\alpha + z = 2$ [16, 17] is hold in this case (see FIG. 5.10(b)). Using the numerical simulation we also get $\delta \simeq 0.86..$ (see FIG. 5.10(a) and (b)). Now, using z, α, and δ, in Eq. (4.4) we can compute $\gamma = \alpha/z + \delta \simeq 1.1..$, and from there $\xi = \gamma z \simeq 1.77...$ The predicted values of all these exponents by assuming Golden mean z and $\alpha + z = 2$ yields a good data collapse in computing the scaling function $f(u = t/N^z)$ which we have displayed in FIG. 5.11.

The first point we can mention from here is the exponent $\gamma \simeq 1.1...$ It ensures the super-diffusive behavior of $\langle m^2(t|v_0)\rangle_c$ we obtained in Chapter 3 is power-law in nature. As a second point, if we consider the dynamical rules as $r(v_L, v_R) = (v_L - v_R)^\lambda \Theta(v_L - v_R)$ with $\lambda > 0$ instead of $r(v_L, v_R) = (v_L - v_R)\Theta(v_L - v_R)$ in case III, then also we also we get good data collapse in computation of scaling function with the same values of the exponents (see FIG. 5.11). It implies the result

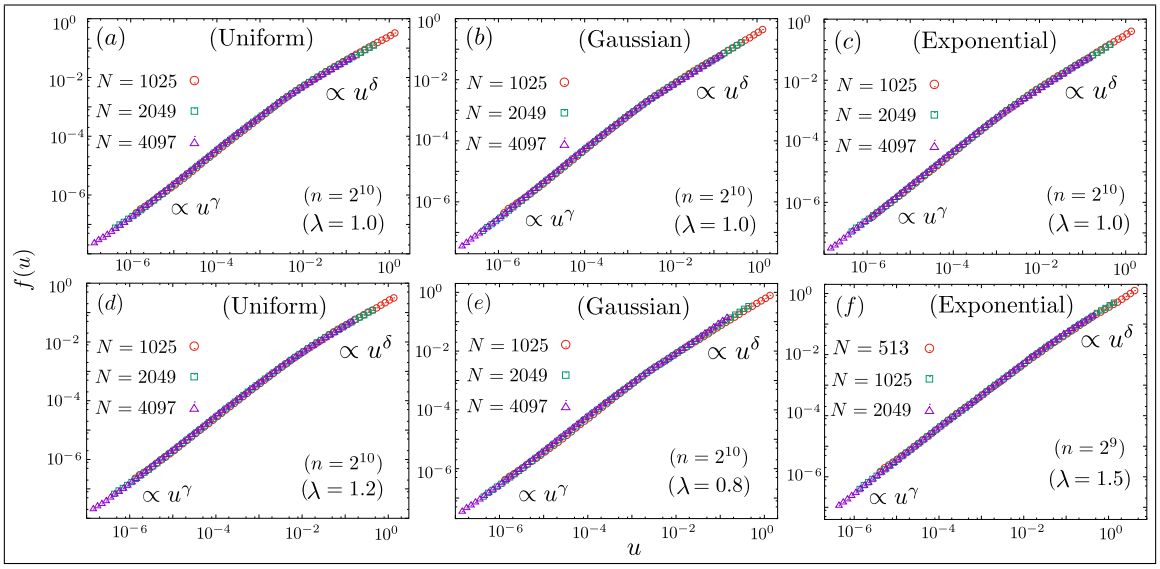

Figure 5.11: Simulation results of the scaling function $f(u)$ are plotted vs $u = t/N^z$ for three different system sizes by considering the tagged $v_0 = \langle v \rangle$ and drawing the remaining velocities from the most probable configurations of the discretized uniform (a) & (d), Gaussian (b) & (e), and exponential (c) & (f) velocity distributions. Collapsed data-points of $f(u)$ for different system size N, supports the predicted exponents $z = (1+\sqrt{5})/2$, $\alpha = (3-\sqrt{5})/2$, $\delta \simeq 0.86..$ and $\gamma \simeq 1.1..$ indirectly.

is universal as it is independent of initial velocity distribution and the dynamical rules. It arises because of large number of conserved quantities present in the system and it is related to Golden mean z.

Bibliography

[1] A.-L. Barabsi and H. E. Stanley, *Fractal concepts in surface growth* (Cambridge university press, England, 1995), J. Krug, Adv. Phys. **46**, 139 (1997).

[2] P. A. Ferrari, Probability Theory and Related Fields **91**, 81 (1992).

[3] P. A. Ferrari, L. P. Pimentel, *et al.*, The Annals of Probability **33**, 1235 (2005).

[4] T. Mountford, H. Guiol, *et al.*, The Annals of Applied Probability **15**, 1227 (2005).

[5] P. Ferrari, C. Kipnis, E. Saada, *et al.*, The Annals of Probability **19**, 226 (1991).

[6] G. Amir, O. Angel, B. Valk, *et al.*, The Annals of Probability **39**, 1205 (2011).

[7] O. Angel, A. Holroyd, D. Romik, *et al.*, The Annals of Probability *37*, 1970 (2009).

[8] S. Das, D. Dhar, and S. Sabhapandit, Physical Review E **98**, 052122 (2018).

[9] H. Touchette, Phys. Rep. **478**, 1 (2009).

[10] B. Derrida and M. Evans, Journal of Physics A: Mathematical and General **32**, 4833 (1999).

[11] B. Derrida and M. Evans, in *Probability and Phase Transition* (Springer, 1994) pp. 116.

[12] V. Karimipour, Physical Review E **59**, 205 (1999).

[13] V. Karimipour, EPL (Europhysics Letters) **47**, 304 (1999).

[14] M. Kardar, G. Parisi, and Y.-C. Zhang, Physical Review Letters **56**, 889 (1986).

[15] V. Popkov, A. Schadschneider, J. Schmidt, and G. M. Schtz, Proceedings of the National Academy of Sciences **112**, 12645 (2015).

[16] P. Cipriani, S. Denisov, and A. Politi, From Anomalous Energy Diffusion to Levy Walks and Heat Conductivity in One-Dimensional Systems, Phys. Rev. Lett. 94, 244301 (2005).

[17] V. Zaburdaev, S. Denisov, and J. Klafter, Lvy walks, Rev. Mod. Phys. 87, 483 (2015).

Chapter 6

Conclusion

In this thesis, we have studied the phenomenon of "overtaking", ubiquitous in self-driven systems. To quantify, analyze and understand this phenomenon in details, we consider different models of overtaking. Both the non-interacting and interacting models of self-driven agents are investigated with different initial and boundary conditions. With different dynamical rules of evolution we have investigated the interacting systems of self-driven agents. In each model, we assumed all the particles are moving with a certain "velocity" chosen at random from a common distribution. We have studied the net overtaking number $m(t|v_0)$ by a tagged agent of velocity v_0 up to time t. Two different probability distributions associated with $m(t|v_0)$ are investigated in details. They are the conditional and unconditional distributions. Investigation of the dynamical exponent z has been done in details in the second part of this thesis (chapter 4 and 5).

6.1 Outline of the Result

6.1.1 Chapter 2

This chapter is about studying a simple non-interacting model of self-driven agents, namely the Jepsen gas, to get an introductory essence of overtaking statistics. We divided this chapter into two segments depending on two different initial conditions we consider. These conditions are the constant density and constant separation of particles.

In case of the constant density of particles, we have found that $m(t|v_0)$ is the

outcome of two independent Poisson process. Using this result, we have derived the mean, variance, all the higher-order cumulants of $m(t|v_0)$, and hence the conditional distribution $p(m, t|v_0)$. The behavior of this distribution at the tail is sensitive to v_0. However, in case of constant separation between all neighboring agents, the same distribution comes out v_0 independent.

In case of unconditional distribution, denoted by $P(c = m/t, t)$, we have found that it converges to the initial velocity distribution with a Galilean shift by the mean of the velocity distribution in the limit of $t \to \infty$. Although these results in the asymptotic limit are the same for both cases, their approach to this behavior is different.

6.1.2 Chapter 3

In this chapter, we consider a simple model of interacting self-driven agents on an infinite lattice to study the statistics of $m(t|v_0)$. The model is 1D lattice with each site occupied of singly-seated agents with their fixed but random initial velocities. With time, each neighboring pair can exchange their sites with a specified rate that depends on their velocities. This site exchange mimics the event of overtaking in this system. Three different cases are considered depending on the exchange rules.

In the first case exchange of neighboring pair is independent of their velocities and it occurs at a unit rate. In this case $m(t)$ is nothing but the displacement of the simple random walk on the lattice. Here we obtained $m(t) \propto \sqrt{t}$ at large time t and $m/\sqrt{t}$, in the limit $t \to \infty$, is distributed according to the Gaussian distribution.

In the next case, the left and the right velocities, v_L and v_R, of an adjacent pair are exchanged their sites at the rate one if the velocity at the left is higher than the same at the right, i.e., $v_L > v_R$. In this case, we have found the dynamics of a tagged agent of velocity v_0 is equivalent to the dynamics of a second class particle in TASEP with the density of particle $\rho_+(v_0)$. Using this mapping we have derived the mean $m(t|v_0)$ of a tagged agent of velocity v_0 grows linearly with time whereas the corresponding variance $\langle m^2(t|v_0)\rangle_c$ shows a linear increment $\propto t$ followed by a super-diffusive growth $\propto t^{4/3}$ with a velocity dependent transition time $t_1^*(v_0)$. The scaled distribution of $p(m, t|v_0)$ we have found in the limits $t \ll t_1^*(v_0)$ and $t \gg t_1^*(v_0)$. In the same case, the unconditional distribution $P(c, t)$ in the limit of $t \to \infty$,

is distributed uniformly on $[-1 : 1]$ which is independent of the initial velocity distribution. We also discuss the large time approach to this limiting behavior in details.

In the third case, where we consider the exchange rate of a neighboring pair is equal to their relative velocity $v_L - v_R$ with the additional condition of $v_L > v_R$. The qualitative behavior of $\langle m(t|v_0)\rangle$, $\langle m^2(t|v_0)\rangle_c$ in this case, remain same as that of the earlier case except a new super-diffusive behavior of $\langle m^2(t|v_0)\rangle_c$ observed above the velocity dependent transition time $t_1^{\#}(v_0)$. Although the exact nature of the super-diffusion is unclear in this case, we have seen from the numerical simulation that this behavior and the corresponding scaling distribution is quite robust in a sense that, that it is independent of the initial velocity distribution. In case of unconditional distribution in the limit $t \to \infty$, we have found it converges to the distribution of velocity itself, with a Galilean shift by the mean velocity. The finite but large time behavior of the same distribution is also discussed in case of four different initial velocity distributions.

6.1.3 Chapter 4

In this chapter, we have studied how the finite size N of the system affects $m(t|v_0)$ in the non-interacting model of the Jepen gas. We have introduced here the concept of the dynamical exponent z in the context of our problem. This exponent yields an approximate time-scale over which the fluctuation of $m(t|v_0)$ showing a transition from the initial N-independent behavior to the N-dependent behavior. We divided this chapter in two segments depending on two different ensembles of particles. In the 1st case we fixed the number of particle in the periodic system, whereas, in the next, this number is chosen from a Poisson distribution.

With a constant number of particles, we have derived an approximate expression of $m(t|v_0)$. Using this result, we have calculated all the cumulants of $m(t|v_0)$. We have found that only the mean of $m(t|v_0)$ depends on v_0 and it remains same as that of infinite system. However the variance and all the higher-order cumulants become independent of v_0, but depends on N. When the initial velocity distribution $\rho(v)$ is Gaussian or uniform or exponential the scaled distribution of $m(t|v_0)$ is same and depends only on N. In case of power-law distribution, the power-law exponent also

enters into the distribution. The distribution $P(c = m/t)$ of a randomly chosen agent is also investigated in all cases of $\rho(v)$. We have found $P(c)$ attains stationary distribution that depends on N.

In the case when the particle number is allowed to fluctuate, we have calculated all the cumulants of $m(t|v_0)$. Unlike the earlier case, here we have found all the higher-order cumulants of $m(t|v_0)$ depend on v_0. The scaled distribution $m(t|v_0)$ in this case also depends on v_0.

We also computed the dynamical exponent $z = 1$ associated with the fluctuation of $m(t|v_0)$.

6.1.4 Chapter 5

In this chapter we have discussed the same problem of the chapter 3 with a periodic lattice, but in a different limit where finite-size effects on $m(t|v_0)$ become relevant.

In the 1st case where the site exchange of a pair is independent of their velocities, $m(t|v_0)$ becomes equivalent to the displacement of the simple random walker on the lattice which never affected by the finite size of the system.

In the 2nd case where the tagged particle behaves like a second class particle in TASEP we have calculated the mean and the variance of $m(t|v_0)$ in the limit $t \gg N$. We find that the variance $\langle m^2(t|v_0)\rangle_c$ has two different behaviors, which depend on v_0. The first one is in the regime $v_0 \sim \pm\infty$, where v_0 executes a biased random walk on the lattice without being affected by the finite system size. On the other hand, for $v_0 \sim \langle v\rangle$, the system size-dependence comes into the tagged dynamics via the diffusion constant $D(N|v_0)$. In this regime, we have shown the dynamical exponent associated with the tagged dynamics is $z = 3/2$, the well-known dynamical exponent of the KPZ universality class. Moreover, these two different behaviors of $\langle m^2(t|v_0)\rangle_c$ yield the same scaled Gaussian distribution for $p(m, t|v_0)$. But it brings out two different results in case of unconditional distribution $P(c, t)$. The tails of this distribution comes from $v_0 \sim \pm\infty$ whereas the bulk is from $v_0 \sim \langle v\rangle$.

In the final case, where the exchange rate is proportional to the relative velocity, we have found by the numerical simulation that the variance of $m(t|v_0)$ follows a linear growth at late time. In particular, in case of $v_0 \sim \langle v\rangle$, in the intermediate regime of time, we have found that the dynamical exponent associated with the

fluctuation of $m(t|v_0)$ is same as the golden mean. This exponent is result out from the large number of conserved velocities present in the system and we have predicted this exponent by taking cues from the non-linear fluctuating hydrodynamics. It also allows us to conclude that the super-diffusive behavior $\langle m^2(t|v_0)\rangle_c$ we obtain in the limit of $N \gg t$ (in chapter 3) is power-law in nature, and it is $\propto t^{1.11..}$.

6.2 Future Direction

There are several interesting open directions for future research. First and foremost one is of course to analyze real data. Another question is whether there are other classes, and if any, how to identify them. Third, here we have studied only a single time property. However, one can study correlations between overtakes at different times or the overtaking dynamics itself as a process. Here, it is somewhat assumed that the density of agents is homogeneous in the real space, so that velocity is the only relevant variable for overtaking. One can explore the effect of inhomogeneity by considering a dilute case, where a finite number of sites, chosen randomly with a given density, are not occupied by agents (equivalently, occupied by agents having zero velocity). The model on a finite line is also of interest. In this case, there are important end effects, and there are shock waves that start at the ends and travel inwards, and determine the qualitative behavior in the region deep inside for times of order of the system size. Instead of continuous distribution of velocity, one can consider the velocities taken from the discrete velocity distribution with the neighboring pair site exchange rate $r(v_L, v_R) = (v_L - v_R)^\lambda \Theta(v_L - v_R)$ with $\lambda \geq 0$. In the limit of a large number of conserved velocities we can study different correlation functions in this system. For example, the density-density correlation function of a particular species of velocity and the density-density cross-correlation function between two different species of velocities. It will be interesting to study the behavior of $m(t|v_0)$ in the limit of $t \gg N$ with an arbitrary $0 \leq \lambda \leq 1$. Changing the number of conserved velocities from a small number (say, for example, 2) to the large number, one can investigate how the dynamical exponent associated with the fluctuation of $m(t|v_0)$ gradually makes a transition from $z = 3/2$ to $z = (1+\sqrt{5})/2$, scaling behaviors of the distribution of $m(t|v_0)$, etc. In a nutshell these simple models of overtaking presented in the above chapters can serve as a stepping stone

for further research of this phenomenon.